Constrained crystallization and depletion in the polymer medium for transdermal drug delivery system

A Thesis

Presented to

The Academic Faculty

by

Jianming Zeng

In Partial Fulfillment

of the Requirements for the Degree

Doctor of Philosophy in Polymers

Georgia Institute of Technology

July 2004

Constrained crystallization and depletion in the polymer medium for transdermal drug delivery system

Approved:

Dr. Karl I. Jacob, Advisor

Dr. Satish Kumar

Dr. Iwona M. Jasiuk

Dr. Malcolm B. Polk

Dr. C. P. Wong

Date Approved: July 9, 2004

ACKNOWLEDGEMENTS

First I would like to thank Dr. K.I. Jacob for his guidance, patient, understanding and persistent dedication during the course of this research. His support and friendship made the completion of this work possible. I must also thank Dr. M. B. Polk, Dr. S. Kumar, Dr. I. Jasiuk and Dr. C. P. Wong for serving as my reading committee members as well as providing technical support.

I also appreciate Dr. Park for assisting with fluorescence microscopy, Dr. Shuying Yang with Raman, Dr. Hongming Ma with FTIR, Dr. C. Burda with fluorescence spectroscopy and Ms. B. Yolanda with SEM (EDS).

Special thanks are extended to Center for Computational Molecular Science & Technology for providing computing time for simulation.

I also would like to thank Dr. M. Sharaf and Mr. Hai Dong for discussion and providing suggestion on simulation.

Finally, a special gratitude is expressed to the author's family for the never-ending encouragement and confidence.

TABLE OF CONTENTS

LIST OF TABLES

LIST OF FIGURES

SUMMARY

Transdermal drug delivery systems (TDS) are pharmaceutical devices that are designed to deliver specific drugs to the human body by diffusion through skin. The TDS effectiveness suffers from crystallization in the patch when they are kept in storage for more than two years. It has been reported that there are two types of crystals in the patch: needle and aggregate, and growth of drug crystals in TDS generally occurs only in the middle third of the polymer layer. In our study, fluorescence microscopy, EDS (SEM) and Raman microspectroscopy were used to further characterize the crystals. The results show that the needle crystals most probably contain estradiol and acrylic resin conjugate. The FTIR spectrum of the model sample proved the occurrence of a reaction between estradiol and acrylic resin. Crystal growth in an unstressed matrix of a dissolved crystallizable drug component was simulated using a kinetic Monte Carlo model. Simulation using Potts model with proper boundary condition gives the crystals in the middle of matrix in the higher temperature. Bond fluctuation model is also being implemented to study representative dense TDS polymer matrix. This model can account for the size effect of polymer chain on the crystal growth. The drug release profile from TDS was also studied by simulating the diffusion of drug molecules using Monte Carlo techniques for different initial TDS microstructure. The release rate and profile of TDS depend on the dissolution process of the crystal. At low storage temperature, the grains are evenly distributed throughout the thickness of the TDS patch, thus the release rate and profile is similar to the randomly initiated system. Further work on stress induced crystallization is currently under development. Although the study was specifically done

for drug in a polymer medium, the techniques developed in this investigation is in general applicable to any constrained crystallization in a polymer medium.

Chapter 1

Introduction

Transdermal drug delivery systems (TDS) are pharmaceutical devices that can deliver a drug to the blood stream through permeation. A typical TDS consists of a polymer patch with dissolved drug, which diffuses into the skin when it is in contact with the skin. TDS can maintain the drug concentration within a certain therapeutic range for the drug to act properly. Drugs become toxic above a certain level and are ineffective under the lower level. As shown in Figure 1.1, for conventional drug delivery the drug concentration in blood varies significantly with time, but the concentration remains reasonably constant with a TDS approach. There are several advantages for TDS over conventional drug delivery. The transdermal system avoids the chemically hostile gastrointestinal (GI) environment and first-pass effect[1,2,3] compared to oral administration of drugs. Meanwhile, it allows effective use of drug supply in a narrow therapeutic window and provides controlled plasma transport for very potent drugs. By avoiding the undesirable sensation of a needle as much as by decreasing the frequency of drug application with TDS, the transdermal system can increase patient compliance. Another important advantage for this system is that drug input can promptly be interrupted if any toxicity occurs. However, drugs that require high concentrations in the blood cannot be administered due to the permeation limitation of skin, which functions as a barrier to protect the human body. Unlike traditional oral delivery in which a full dosage of drug is supplied resulting in a high concentration of drug in the blood which gradually decreases, TDS can supply a relatively constant dosage of drug. There are many factors to be

considered for the successful design of a drug delivery system. Aspects such as drug stability, physical stability of formulation, skin irritation and sensitization properties are all critical parameters to be considered when designing a TDS. Chemical and physical characteristics of the polymeric materials in which the drug is dissolved will also be critical in determining the performance of the overall system.

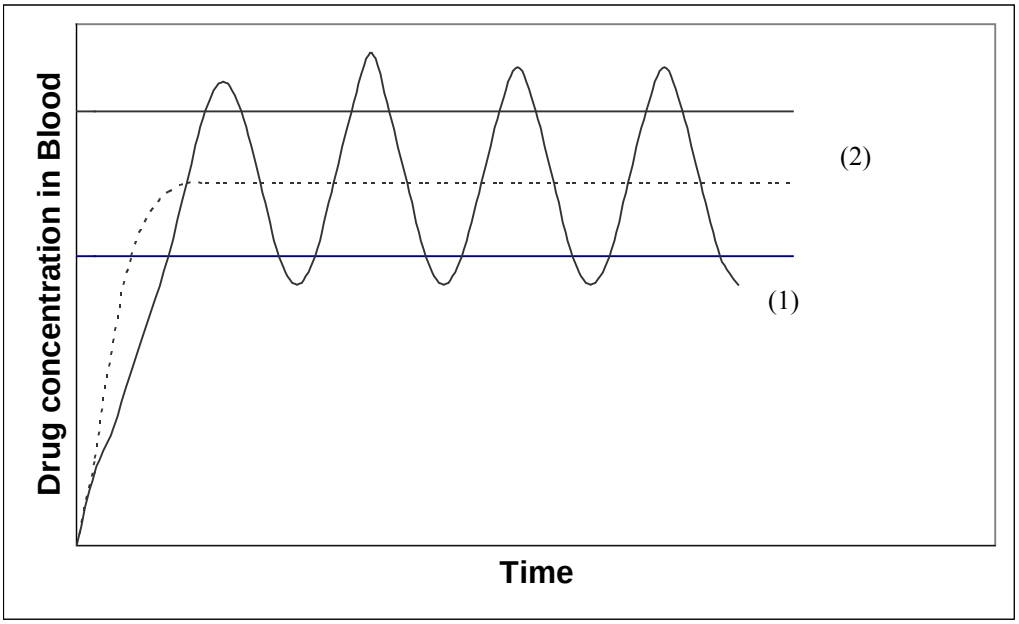

Figure 1.1. Hypothetical blood level pattern from (1) a conventional multiple dosing schedule, and (2) a idealized pattern from a transdermal controlled-release system. (Reference 4)

The drug properties can influence release characteristics for its delivery system. From conventional drug delivery systems, the rate limiting step in drug availability is usually absorption of drug across a biological membrane. In the TDS, one aims for release of drug at a specific dosage below the rate-limiting step level. Thus, drug availability is

controlled by the kinetics of drug release rather than absorption. Consequently, the associated rate constants for drug release from a specific dosage are smaller than the absorption rate constant. Therefore, the interplay between physiochemical properties of a drug and characteristics of its delivery system determines the temporal release pattern that is observed.

The chemical and physical properties of the components of TDS influence the rate of drug release to the skin and the adhesive properties of the device to the skin. The main components of the transdermal delivery system are: polymer adhesive, a drug, permeation enhancer and plasticizers or tackifing agents. In order to improve the adhesion between skin and TDS and to facilitate easy application and removal of the transdermal patch, pressure-sensitive adhesives are commonly used which are based on natural or synthetic rubbers, polyacrylates or silicones.

The choice of drugs to be delivered transdermally is the most difficult one, and careful consideration should be given to each application before large expenditures are committed to clinical testing. Table 1.1 shows the important criteria that should be considered in the drug selection process. Based on these criteria, currently there are many drugs available in transdremal devices. Among these are scopolamine to treat motion sickness[5], nitroglycerin for angina[6], estradiol for postmenopausal syndrome and perhaps eventually to prevent osteoporosis[7], and clonidine as an antihypertensive[8]. New drug applications have been filed for transdermal administration of nicotine for smoking cessation[9, 10, 11], fentanyl for analgesia and in anesthesia for relief of moderate to severe surgical pain for an extended duration[12, 13, 14], and testosteone for male hormonal insufficiencies. The regimen for these transdermal systems varies from 1 day to 1 week,

although skin tolerability is a concern for the long-duration patches. Among these are hormones, cardiovascular drugs, analgesics, antihistamines and drug for central nervous system. The drug generally is dissolved in the matrix and diffuses from the matrix through the skin and into the capillary plexus. These drugs may be applied directly in their natural form or as derivatives.

Table 1.1 Important Criteria in the Drug Selection process

1. Adequate skin permeability:
Drug with low molecular weight
Drugs with low melting point
Drugs with moderate oil and water solubility
Potency of drugs
2. Adequate skin acceptability:
Nonirritating drugs
Nonsensitizing drugs
Nonmetabolizing drugs
3.Adequate clinical need
Need to prolong administration
Need to increase patient compliance
Need to reduce side effects on nontarget tissue

Transdermal drug absorption can be enhanced by various chemical and physical methods. Chemical enhancers exert their influence on lipids in the stratum corneum as well as on lower dermal layers, and possible capillary beds. Surfactants may alter the structure of fluidized lipids as reflected by the discontinuous increase in skin permeation with surfactant concentration from the FTIR spectra with and without these surfactants[15, 16]. Absorption of polar compounds may be enhanced by surfactants with a head group of great hydrophilicity, or nonpolar and polar compounds when surfactants are mixed with other solvents, such as diols or ethanol[17, 18]. Ethanol can increase permeation of nonpolar

species by increasing their solubility in the stratum corneum without altering their diffusion constants[19,20, 21]. Ethanol is the only solvent used in a commercial transdermal system where the relationship between the flux of the drug, estradiol, and that of the solvent has been characterized[22, 23]. Sometimes a plasticizer is used to improve adhesive properties of this system.

Devices have been successfully developed to provide better rate control over the release and transdermal permeation of the drug. These devices can be divided into three broad types as showed in Figure 1.2. The first system just consists of a drug-containing adhesive protected by a backing layer and a release liner which is taken out before usage. In this system, the adhesive serves as a matrix of the drug and a binding layer to the skin, but not as a rate controller of the drug delivery. This is the simplest TDS system. The second system consists of the three layers: a backing layer, rate-controlling matrix containing drug and an adhesive layer. The most significant factor in this device is the use of polymer matrix for controlling release rate. The controlled drug concentration (usually supersaturation) in the polymer matrix can give a more consistent drug release rate during its application. The third type reservoir system is one where the drug is contained in the polymeric reservoir and the release rate of drug is controlled by a membrane. The adhesive in the last two devices only provide the bonding of transdermal devices to the skin. The design and selection of a specific TDS system depend on many factors. The efficiency and simplicity of devices during their application are among the most important factors for consideration. In our investigation, we focused on the behavior of the adhesive layer with the dissolved drug.

Adhesive Device

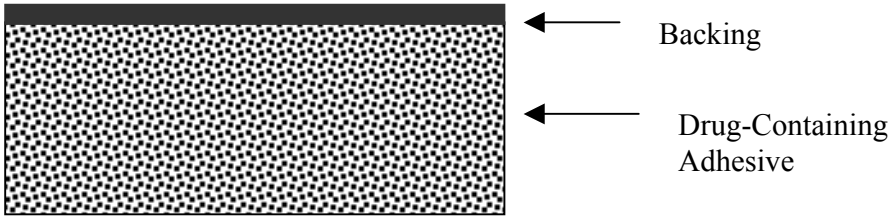

Monolithic Device

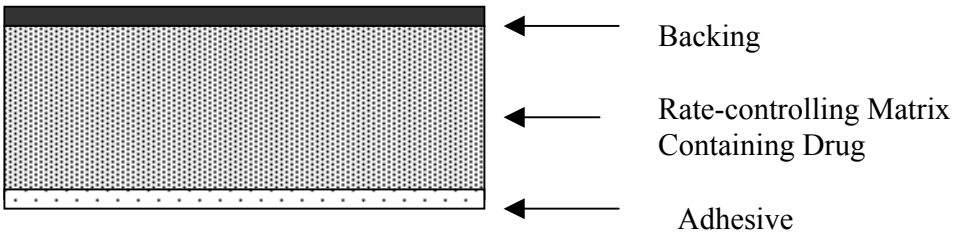

Reservoir Device

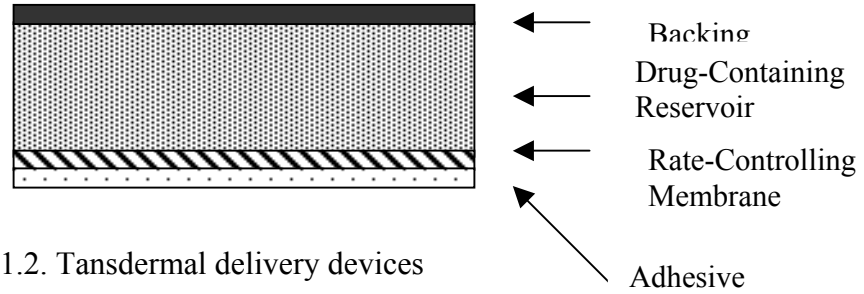

Figure 1.2. Tansdermal delivery devices

1.1 Crystallization of drug in TDS

For effective delivery, the drug is required to be in the amorphous state either dispersed or dissolved in the TDS. The high internal energy and specific volume of the amorphous state can provide enhanced dissolution and bioavailability[24], which are desirable to deliver the active agent through the adhesive/skin interface. However, crystallization of the drug or other components has been reported in many TDS[25,26] system after a certain period of time in storage. The presence of crystals will adversely affect the diffusion of drug and thus the performance of transdermal system mainly by reducing the driving force for diffusion due to the reduced concentration of drug in the solvated state. Also, when the dissolution rate of the drug in the crystals is smaller than the diffusion rate, the diffusion is reduced due to the diminished concentration of the diffusing drug molecules.

Supersaturation of the drug in this system is often required to target the drug delivery rate within the required "therapeutic window" in order to achieve the maximum effect with minimum harmful side effect. However, the supersaturation in the medium often results in crystallization of the drug. As outlined above, it has been reported that bioavailability of the drug decreases due to the formation of crystals dispersed in polyacrylate adhesives, which usually occurs when the TDS is stored over six months at room temperature at moderate relative humidity[27]. A comprehensive study of TDS 1% estradiol carried out using optical microscopy[28] showed that the growth of drug crystals in the polymer TDS matrix occurs only in the middle third of the polymer matrix (Figure 1.3), away from the interface. Using Raman microscopic studies, two types of crystals were identified in the matrix, one due to the drug and the other possibly a polymeric component in the matrix.

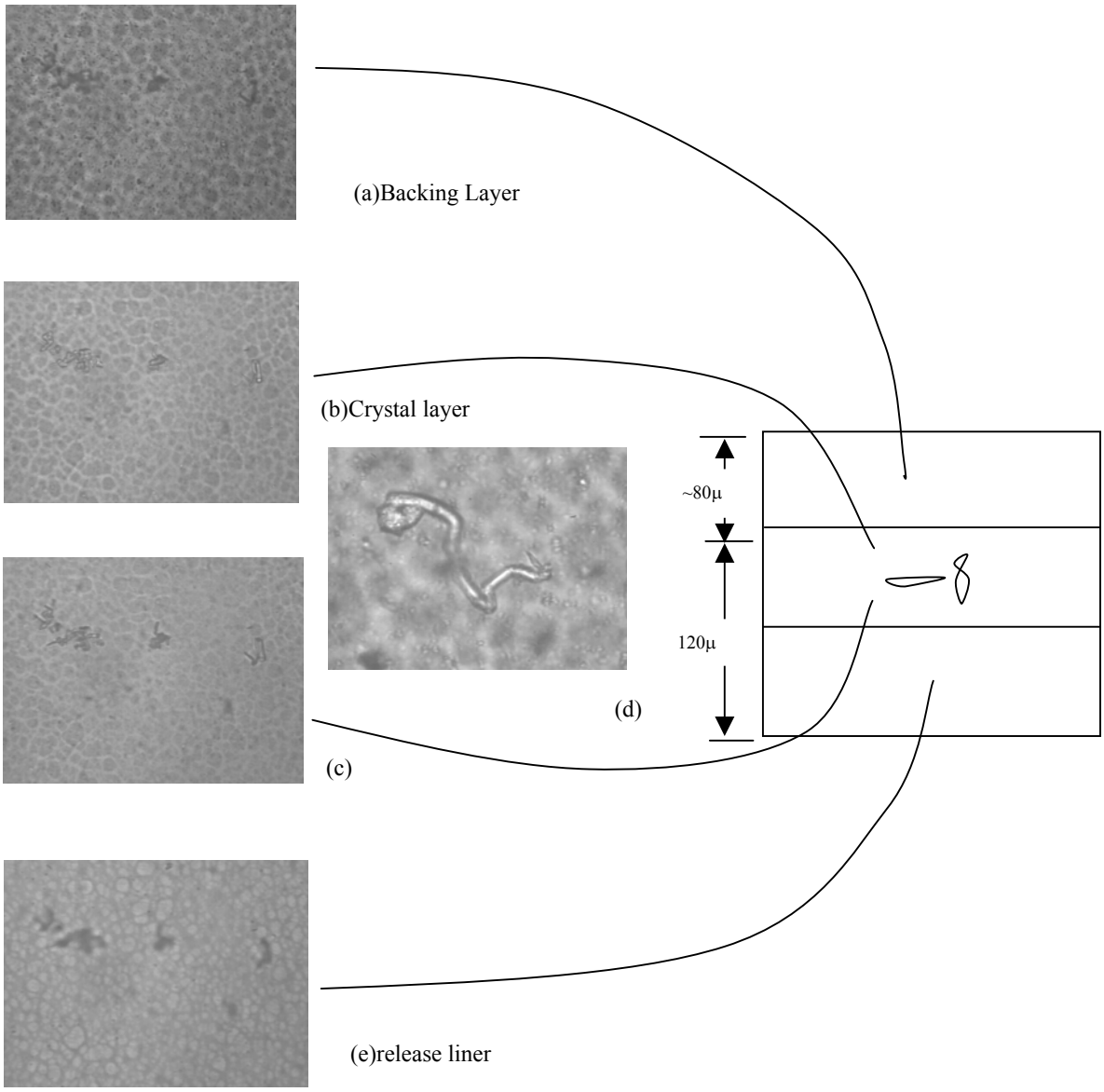

Figure 1.3. Optical micrographic structure through the thickness of the patch. The polarizer and analyzer were crossed in figure (c) to obtain better contrast. A magnification of 16 × was used for (a), (b), (c) and (e). A higher magnification of 40 × was used for (d) to study the morphology.

1.2 Objectives

Previous study showed that there are two types of crystals in this estradiol transdermal system: one is the needle-like crystals and the other is an aggregate in the matrix. Although much work has been done to characterize these two crystal forms, a definite conclusion can not be yet reached on the identity of the needle like crystals. Only by studying the chemical microstructure of the specific crystal form can one reach a definite conclusion, however, the small size of these crystals prevents one from removing them from the patch for such a study. The aggregate crystal has been confirmed by Raman microscopy as the purely estradiol drug, however the needle crystals are yet to be identified[29].

Since the presence of drug crystals could weaken the performance of the TDS, it is important to understand the kinetics of crystallization in the TDS so that crystallization of drug in the polymer can be reduced or prevented if possible. The behavior of a drug in a TDS is determined by the drug properties which can influence the characteristic of the delivery system. Understanding the release profile of the drug from a TDS could play a significant role in designing effective TDS systems with reduced influence of crystals in the system, but also could provide the mechanism of the drug release needed to optimize the release kinetics.

After a certain period of shelf time, the bioavailability of the active agent and its permeability are controlled by the microstructure of drug dispersed in the center of matrix. As mentioned earlier, supersaturation of the drug in the matrix results in drug crystallization. Hence, a thorough investigation of the crystallization mechanisms and the

resulting crystal form in the polymer matrix are very useful to design an effective transdermal delivery system. Thus, one of the objectives of this study is to identify the needle shaped crystal in the estradiol transdermal drug delivery system. Previous studies using Raman microscopy couldn't conclusively identify this type of crystal form. In this investigation a combination of FTIR and fluorescent microscopy are used to study the chemical microstructure of the needle like crystal form. The energy disperse spectroscopy (EDS) is also applied by focusing on the crystal in the polymer patch to collect relevant information to help identify the needle crystal.

The other important objective of the study is to characterize the crystallization kinetics of the TDS. A first approximation of nucleation and crystal growth in TDS is obtained with a modified Potts model of Ostwald ripening. This model was first used to describe the grain growth in liquid phase sintered materials under the stress free condition. The drug release history from TDS is also studied to understand the effect of TDS morphology on the diffusion and transport of a drug during its release. For a better approximation, the bond fluctuation model, which has been used to describe the polymer behavior in dense polymer systems, is implemented to study the drug crystallization phenomenon in a polymer media.

Chapter 2

Crystal Identification

2.1 Fluorescence Microscope

2.1.1 Method

In fluorescence microscopy, the specimen is illuminated by a light of short wavelength and part of this light is absorbed by the specimen, and re-emitted as fluorescence. This re-emitted light has a longer wavelength than the incident beam. In order to observe this relatively weak fluorescence, the excitation light is filtered by a barrier filter appropriately placed before it reaches the eyes.

Fluorescent probes used in fluorescence microscopy are isothiocyanate dextran (FITC-dextran) probes of molecular weights 20, 40, and 70.5 kDa which were purchased from Sigma-Aldrich, the wavelength of absorption maxima (abs) and emission maxima (emis) for the FITC-dextran probes were 492 and 518 nm, respectively. The excitation wavelength was 488 nm, and total emissions were collected for wavelengths from 515 to 670 nm. The concentration of the FITC-dextran probe was 0.4 mg/mL, belonging to the linear region of the fluorescence intensity versus FITC-dextran probe concentration plot.

Experiments using fluorescence microscopy were carried out using a Leica TCS NT laser scanning confocal microscope with a 10 × 0.3NA dry PL Fluotar Objective and an argon ion laser (488 and 514 nm). For the purposes of imaging, the 488 nm line of the Ar-ion laser was used in conjunction with a 40× NA 1.25 oil immersion objective.

The laser scanning confocal microscope (LSCM) scans a xy image of the sample at a specified location on the z-axis. The xy image is referred to as the confocal plane, which means that only light emitted from this plane is detected by the photomultiplier tube (PMT) detector.

2.1.2 Sample preparation

Three types of estradiol samples were used in this study, namely, crystal grown from methanol solution, amorphous estradiol, and estradiol hemihydrate crystals. A controlled crystallization was carried out to obtain an estradiol crystal from methanol solution (EM) in order to obtain samples of sufficient size for fluorescence study. A supersaturated solution of estradiol in methanol solution was prepared in a 10ml vial (solubility of estradiol in methanol is 25.48 mg/ml[30]). Estradiol powder attached to the tip of a fiber is then suspended to the solution as nucleation seeds. The crystallization is allowed to proceed for three days. The grown crystals were then dried by heating to 85°C in an oven for 10 minutes to ensure complete removal of trace methanol on the surface of the crystals. Amorphous estradiol (AE) is prepared as follows: Estradiol was heated on an aluminum pan on a hot plate. Care was taken to allow for liberation of lattice water at 175-180°C. The pan was then cooled to room temperature and immediately used (to minimize crystallization) for spectral analysis. Estradiol hemihydrate (EH), the most common crystalline form of estradiol was obtained by Sigma Co. and used as received. Transdermal patches were obtained from Novartis Pharmaceuticals. They contain a nominal amount of 1 %(w/w) estradiol in the acrylic adhesive. These patches were stored in sealed pouches at ambient conditions for approximately 12 months.

2.1.3 Results and discussion

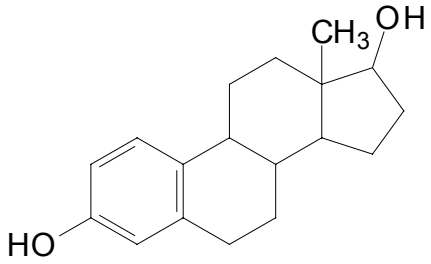

Figure 2.1 Structure of β-estradiol.

A molecule can be excited by absorption of a photon of sufficient energy to produce a transition from the ground state to the excited state. This molecule in an excited singlet state may return to the ground state by emission of the surplus energy as fluorescence.

The fluorescence of a molecule is governed by the structure and the environment in which this molecule is situated. Estradiol has a benzene ring and planar structure (shown in Figure 2.1) and therefore is reported as being a fluorescent material. As described from an earlier work, there are two kinds of crystals in the trandermal patch of estradiol, and one is identified by Raman microscopy as pure estradiol aggregates. The Raman spectrum of the needle crystal did not correspond to that of estradiol. Confocal fluorescence microscopy could be used in identifying the chemical structure of these crystals if they are fluorescent. The images in Figure 2.2 show clearly that there are two different crystals; the needle like crystals are fluorescent material and aggregates are not. The spectrum of this fluorescent material shows that the excitation wavelength is at 500 nm. The absorption spectrum of fluorescence of estradiol water solution shows that the estradiol only absorbs light at a wavelength of 300 nm. Figure 2.3 gives the fluorescence

excitation spectrum of the amorphous form, estradiol hemihydrate and the EM, which all have an excitation wavelength of 300 nm. However each peak profile is different probably due to the different morphologies of estradiol. The different environments surrounding the estradiol also have effect on the excitation peak for estradiol. Figure 2.4 shows the excitation peak of estradiol in different solvents. Compared to the fluorescence image of a placebo patch without drug, it is found that there is no fluorescence material in the placebo using the same excitation wavelength light. It suggested that this fluorescent material is not due to the presence of trace material in the polymer patch (like initiator or monomers). There were some reports that binding to the polymer can alter the fluorescence properties of small molecules[31, 32]. The fluorescent material may form dimer or trimer with a shift in the emission spectrum toward longer wavelengths. The results agree with the conclusion that needle-like crystal may be some kind of combination of polymer and estradiol. Further experiment had to be done to confirm this result and to explain the reason for the large emission shift.

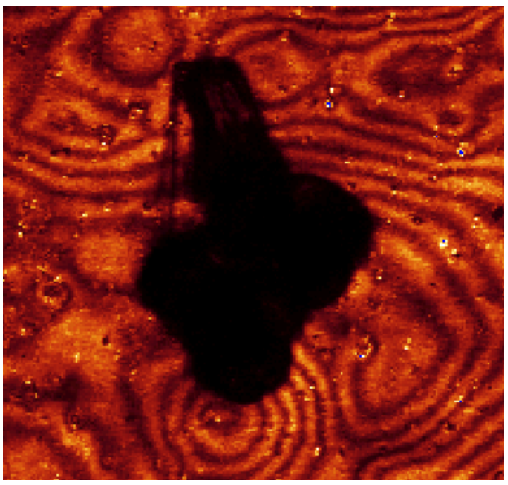

Non-fluorescent crystal

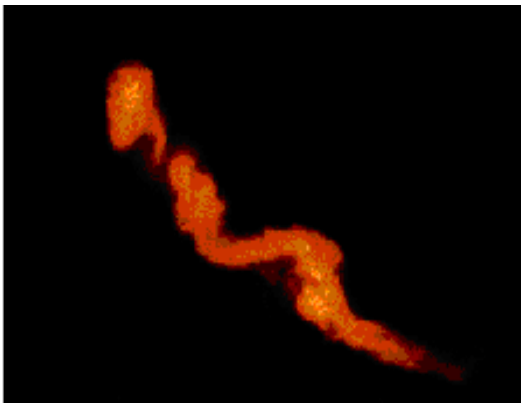

Fluorescent-crystal

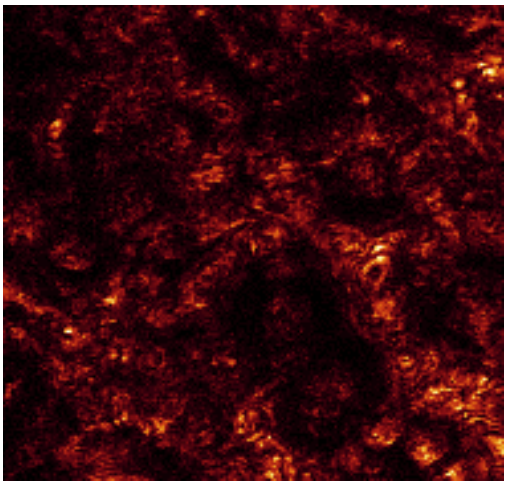

Placebo of only polymers

Figure 2.2. Image of x-y plane from Microscope fluorescence

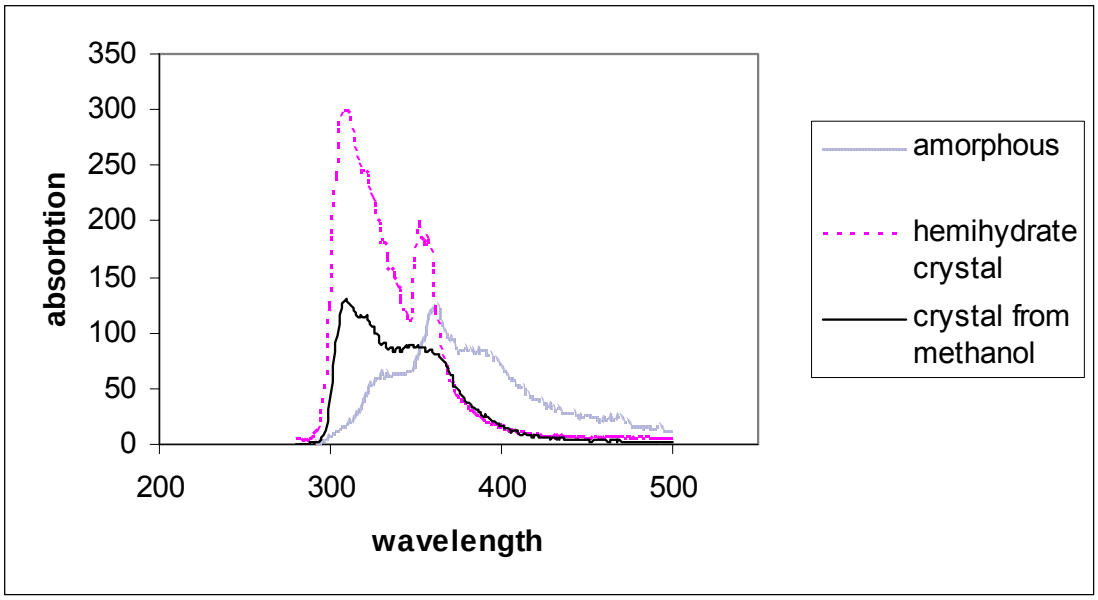

Figure 2.3. Fluorescence excitation spectra in different solid states.

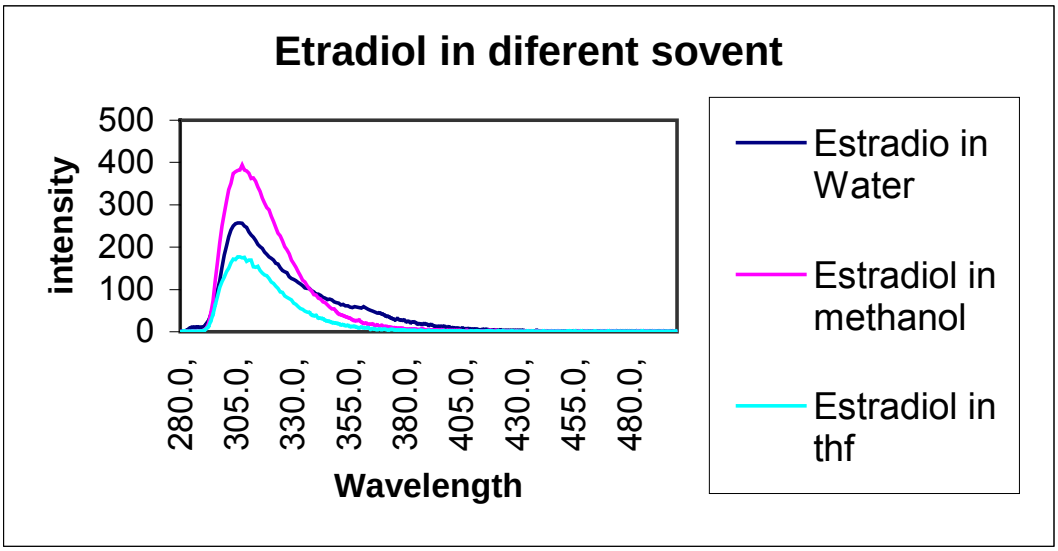

Figure 2.4. Fluorescence excitation spectra in different solvents (water, methanol, tetrahydrofulan).

2.1.4 Conclusions

The fluorescence spectrum of estradiol has an excitation maximum at 300 nm (excitation) and shows small differences in the shoulder region corresponding to different morphologies of the estradiol. Fluorescence microscopy studies found two different types of crystals in TDS: the needle like crystal is fluorescent and the aggregate one is not. The fluorescent one most probably is a combination of estradiol and the polymer matrix. More evidence was obtained from EDS.

2.2 EDS

2.2.1 Method

Chemical analysis (microanalysis) in the scanning electron microscope (SEM) is performed by measuring the energy or wavelength and intensity distribution of the X-ray signal generated by an electron beam focused on the specimen. With the attachment of the energy dispersive spectrometer (EDS), the precise elemental composition of materials can be obtained with high spatial resolution.

Scanning Electron Microscopy with Energy Disperse Spectroscopy was carried out on a LEO 1530 instrument operating at an accelerating voltage of 7.5 kV. The extraction voltage was 3.8 kV and the operating current was 10 μA. All micrographs were obtained at a magnification 300 x at three locations on the patch cross-section. All samples obtained from Novartis Company were cut along the height and cross section and coated with gold in 2 minutes. Three samples were analyzed.

2.2.2 Results and Discussion

A combination of SEM and EDS is a technology which can give not only a focused image but chemical element information of the materials. However, this information is not directly related to the chemical structure, therefore one has to combine other information to obtain meaningful results for the chemical structure. In the present case, the chemical structures of the drug and matrix materials are known and their ratio of C and O elements is different, hence the elemental information at least could tell us if drug or matrix materials are present at the focused area. One difficulty with conventional EDS is that it cannot give information for carbon. Fortunately the LEO 1530 can detect the presence of the C element.

Figure 2.5 shows the image of the needle crystal on the surface of a cross section of the patch. Table 2 gives the C and O ratio of the spot shown in the figure. The ratio of C to O is 81.02:18.98 which is close to the C:O ratio of the polymer matrix 78.46:21.54. This is further evidence that the needle crystal is not the pure estradiol drug, which has a C/O ratio of 87.1:12.9. Figure 2.6 gives the image of an aggregate crystal. The corresponding EDS give the C to O ratio of 87.58:12.42 at three sampling spots. The EDS results show that the needle crystal is probably some combination of the polymer matrix and estradiol drug. Further studies are needed for conclusive identification of the needle like crystals.

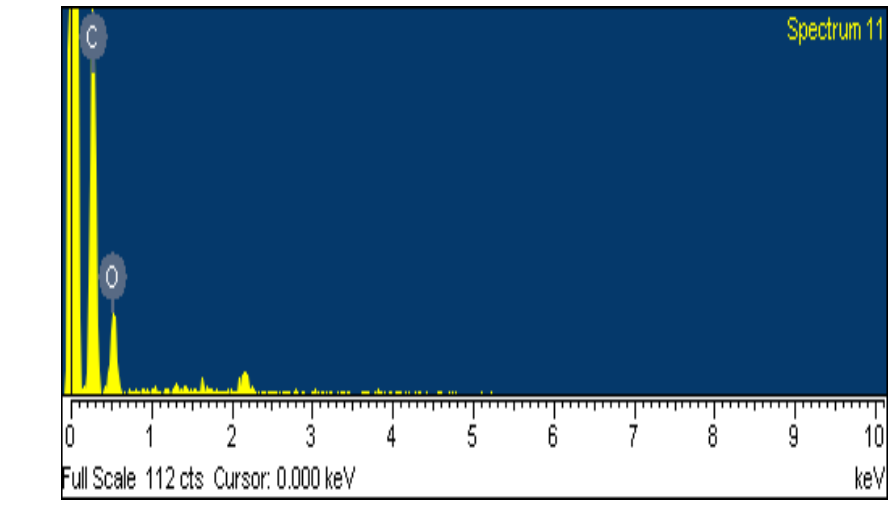

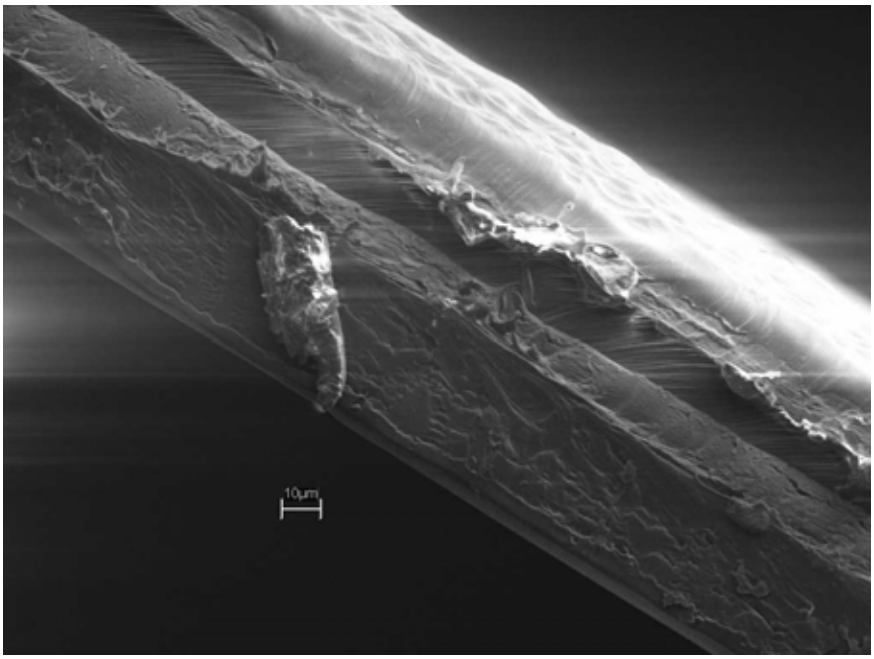

Figure 2.5. SEM image and EDS spectrum for needle crystal

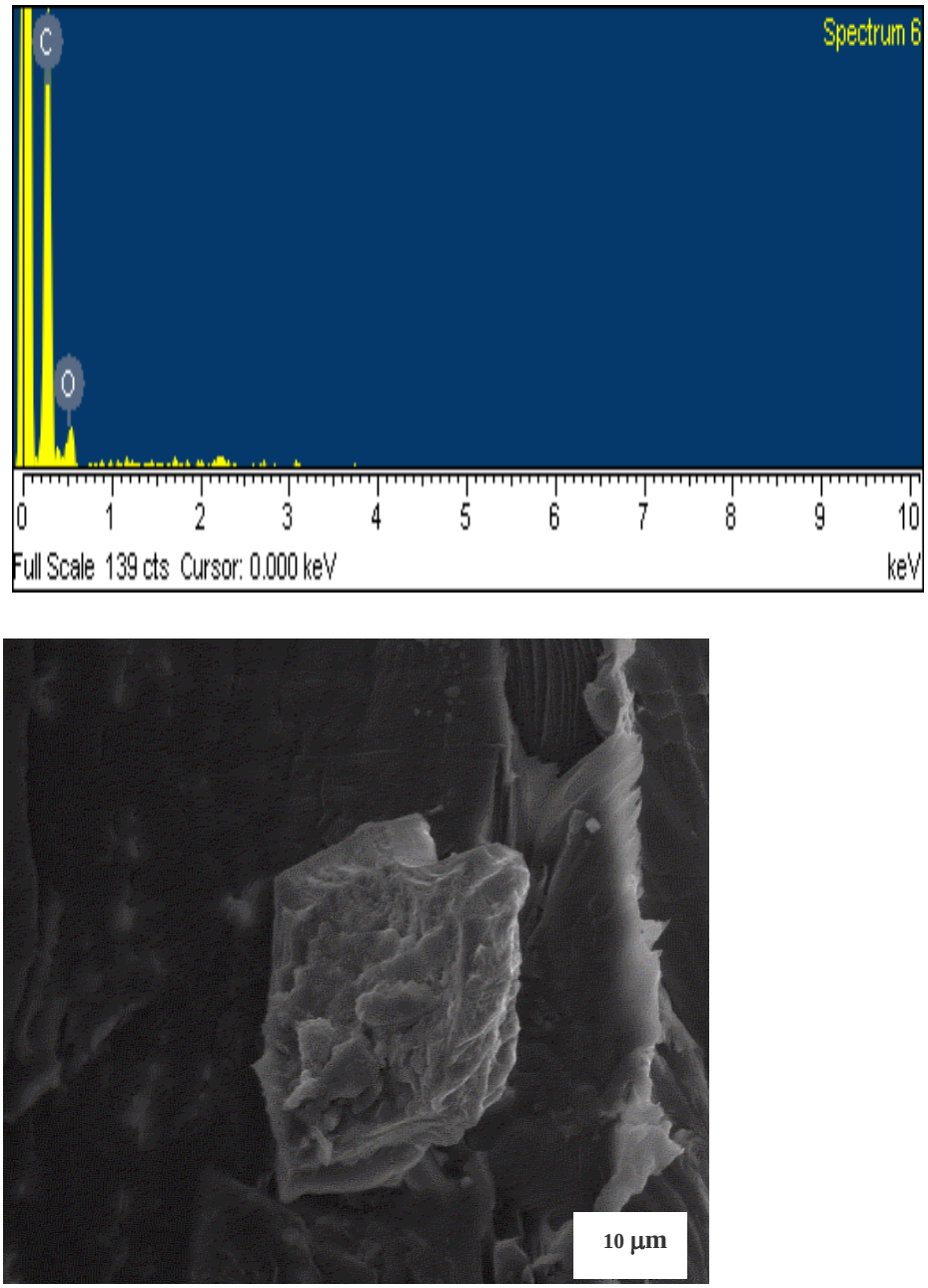

Figure 2.6. SEM image and EDS spectrum for aggregate and matrix

Table 2.1. Processing option: All elements analyzed (Normalized)

Spectrum	C	O	Total
Matrix	78.53	21.47	100.00
Matrix	77.61	22.39	100.00
Matrix	79.33	20.67	100.00
Needle	81.02	18.98	100.00
Needle	80.58	19.42	100.00
Needle	81.44	18.56	100.00
Aggregate	88.44	11.56	100.00
Aggregate	87.44	12.56	100.00
Aggregate	86.87	13.13	100.00

All elements in atomic percentage

2.3. *Raman and IR Study*

2.3.1 Materials and Methods

The transdermal patch was obtained from Novartis Pharmaceuticals Corporation and used as received. Acrylic Solution Duro-Tak 87-2853 was obtained from National Starch which was used as the matrix, β-estradiol from Aldrich was used as provided.

Model reaction preparation:

A solution was prepared by adding 0.6% wt of estradiol to the acrylic solution, then 0.5 grams of solution was put on the micro slide and placed in a 85°C oven for 2 hours to remove the solvent, DSC indicate that there is no residual solvent. The dried film was peeled off the slide and IR microspectroscopy was carried out on the film.

2.3.2 Raman microspectroscopy

Raman microscopy was used to characterize the chemical structure of the various crystal forms in the patch. This technique allows the incident light to be focused on a relatively small area (e.g. a circle of radium 2 μm) to obtain a Raman spectrum. The microscope can be focused to different depths in the sample. Raman spectroscopy was carried out on a Kaiser Holoprobe Raman Microspectrometer with a solid diode laser operating at 758 nm, with backscattering optics. All the spectra were obtained with 5 accumulations, each of 30 seconds duration. The plane of focus was that in which the crystals were present. The depth where crystals are found was approximately 200-250 μm from the upper surface of the backing.

2.3.3 Infrared spectroscopy

The infrared spectroscopy was carried out on a FTIR spectrometer. The accumulation used was 16 scans. The sample films were mounted between sodium chloride disks, and placed in the path of the IR beam.

2.3.4 Results and discussion

Two crystal forms were found in the polymer patches. Raman microscopy can give chemical information about the focused crystal and therefore, in our case can help one to identify the crystals. Figures 2.7 and 2.8 show the Raman spectra of needle crystals and aggregates. From both spectra, the double peak near 1610 cm^{-1} confirms the presence of the aromatic ring of estradiol. Steroids with aromatic rings show their strongest band below 1450 cm^{-1} in both aggregate and needle crystals. The bending of CH_2 group and the degenerate bending of CH_3 show bands of medium intensity in the Raman spectra.

These are often described as internal standards for evidence of the presence of steroid skeleton[33]. It is interesting to note that the presence of a peak in the carbonyl region from needle crystal occurs at spectrum around 1760 cm^{-1} while corresponding peak occurs at around 1725 cm^{-1} for the aggregate crystals. The 1725 cm^{-1} peak corresponds to the absorption of saturated aliphatic ester but the 1760 cm^{-1} peak is characteristic of a phenyl ester absorption. The peak for the carbonyl group connected to the aromatic ring is shifted to the higher wave number due to the electron withdrawing effect of the aromatic ring. The presence of this peak indicates that there could be a chemical reaction between estradiol and acrylic resin during the manufacture and storage to form the corresponding aromatic ester.

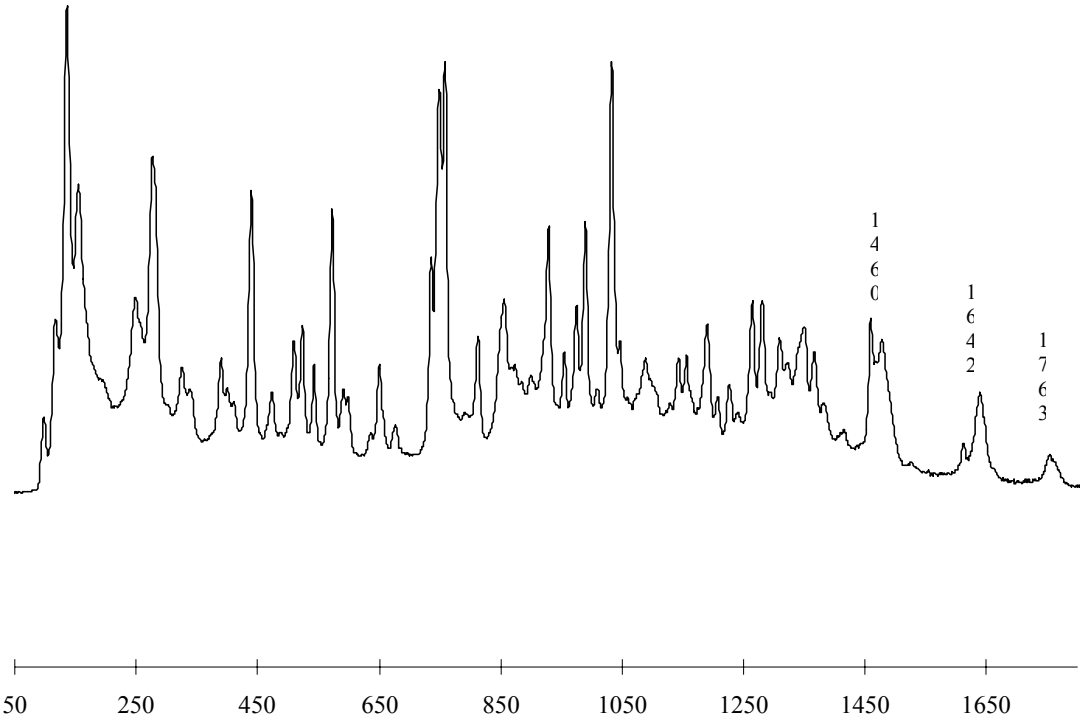

Figure2.7. Raman spectrum of needle crystal in the patch.

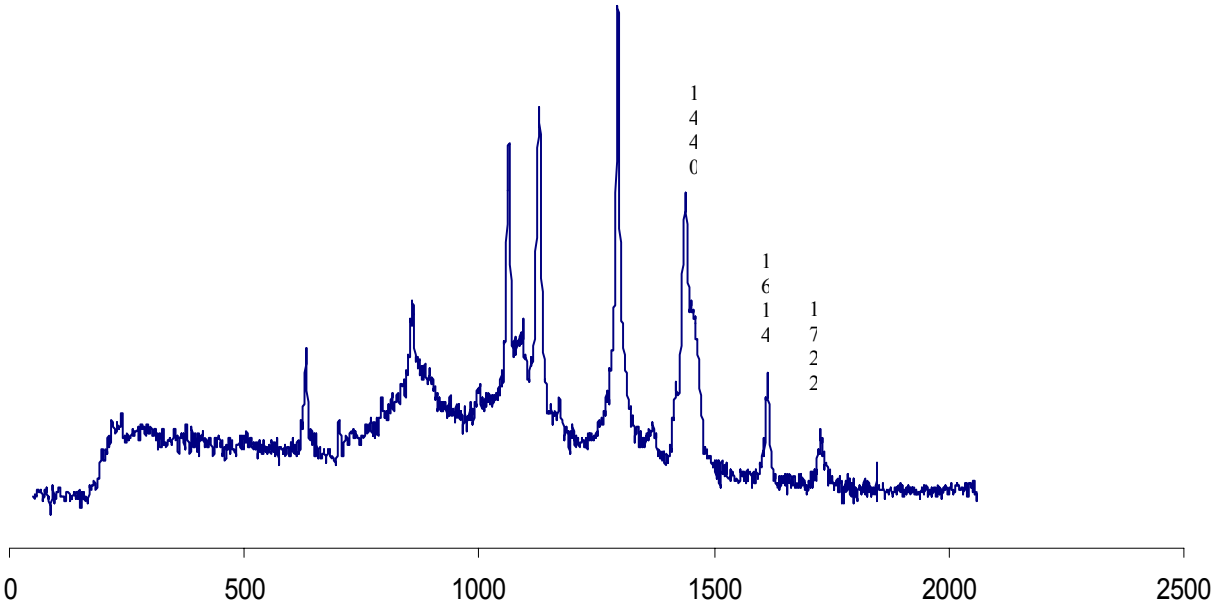

Figure 2.8. Raman Spectrum of aggregate in the patch.

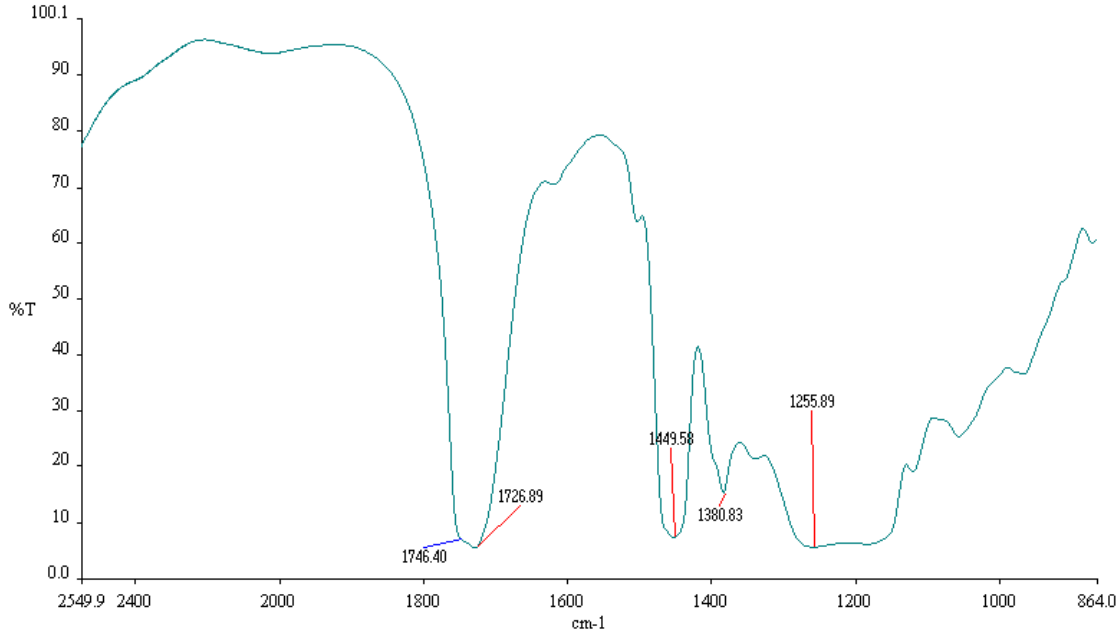

Figure2.9. IR spectrum of model sample.

To confirm the existence of the ester exchange reaction a model sample was prepared by dissolving estradiol in acrylic solution and a film was cast by drying the solution on a micro slide in an oven at 85°C. The IR spectrum is shown in the Figure 2.9. From this figure, it is clear that the peak around 1730cm^{-1} is split into a doublet which contains contributions from a carbonyl connected to an aromatic ring with a longer wavelength and a carbonyl connected to a saturated aliphatic with a shorter wavelength. The reaction would be as follows:

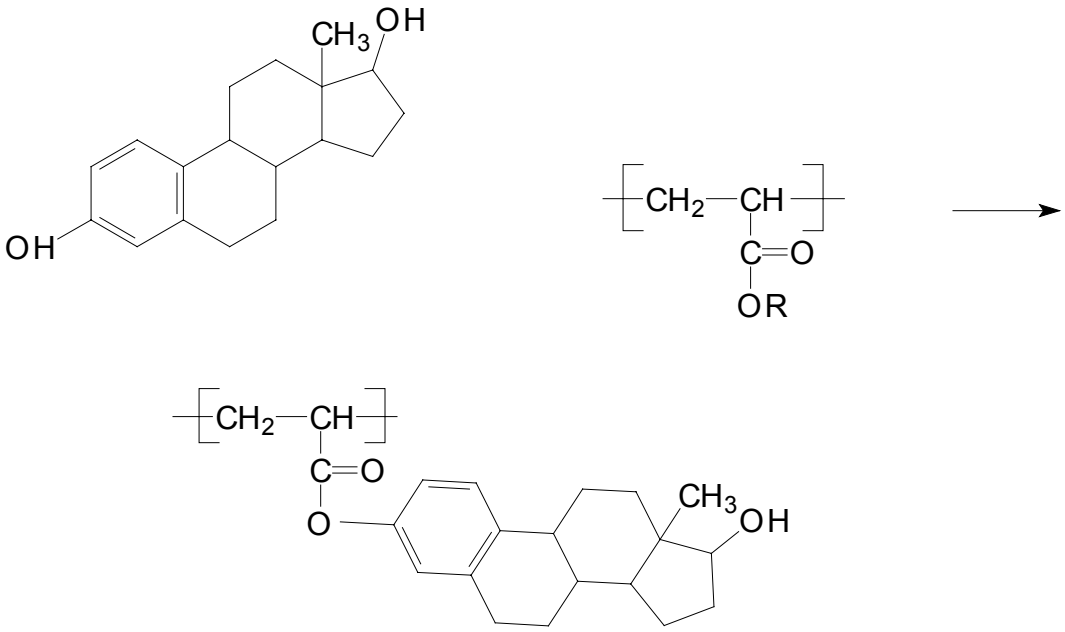

2.3.5 Conclusions

The two crystal forms found earlier was studied by Raman microscopy, SEM, EDS and IR. The Raman spectrum of the aggregate shows the peak characteristic of the aromatic ring and the alkyl carbonyl group and therefore is identified as pure estradiol crystal. The EDS of SEM gives the elemental ratio of C and O similar to the theoretical ratio of C:O in estradiol. The peak in the Raman spectrum of the needle crystal shows that the

carbonyl peak is shifted to higher wave number at 1760 cm^{-1} which is characteristic of a phenyl ester. This probably resulted from the transesterification reaction during the manufacturing process. The IR spectrum of the model reaction sample prepared at 85°C give a carbonyl group absorption as a doublet which is corresponding to aliphatic and aromatic component. This demonstrates evidence for the occurrence of the transesterification reaction. The formation of this estradiol and acrylic resin conjugate will further decrease the availability of drug because it is very difficult for the drug to leave polymer chain when it is chemically attached in the ambient environment during the application of transdermal patch, thus prevention of the transesterification reaction during the manufacturing process is a very important issue to address.

Chapter 3

Crystallization Kinetics

A number of simulation techniques, such as Monte Carlo methods, and their modifications, can be used to simulate crystallization kinetics. A brief overview of these techniques are given in section 3.1. Crystal growth in an unstressed matrix (small molecule or polymer medium) of a dissolved crystallizable drug component was simulated using a kinetic Monte Carlo model and described in section 3.2 and 3.3. The drug release profiles are given in section 3.4.

3.1 Monte Carlo Simulation

Monte Carlo (MC) methods are stochastic techniques--meaning they are based on the use of random numbers and probability statistics. Since it was developed by von Neuman, Ulam and Metropolis more than 50 years ago, Monte Carlo method has became one of the most useful tools to simulate the behavior of condensed systems and polymers.

Instead of evaluating forces to determine incremental atomic motions, Monte Carlo simulation could simply impose relatively large motions on the system and determine whether or not the altered structure is energetically feasible. The system jumps abruptly between different conformations, rather than progressively evolving in time as in the case of molecular mechanics as illustrated in Figure 3.1. It can skip barriers without waiting to overcome them; however the relative energy associated with conformations before and after a jump is taken into account. Because MC simulation samples conformation space without a true ‘time’ variable or a realistic dynamics trajectory, it cannot directly provide

time-dependent quantities. However, it may be better than molecular mechanics or molecular dynamics in estimating average thermodynamic properties for which the sampling of many system configuration is important.

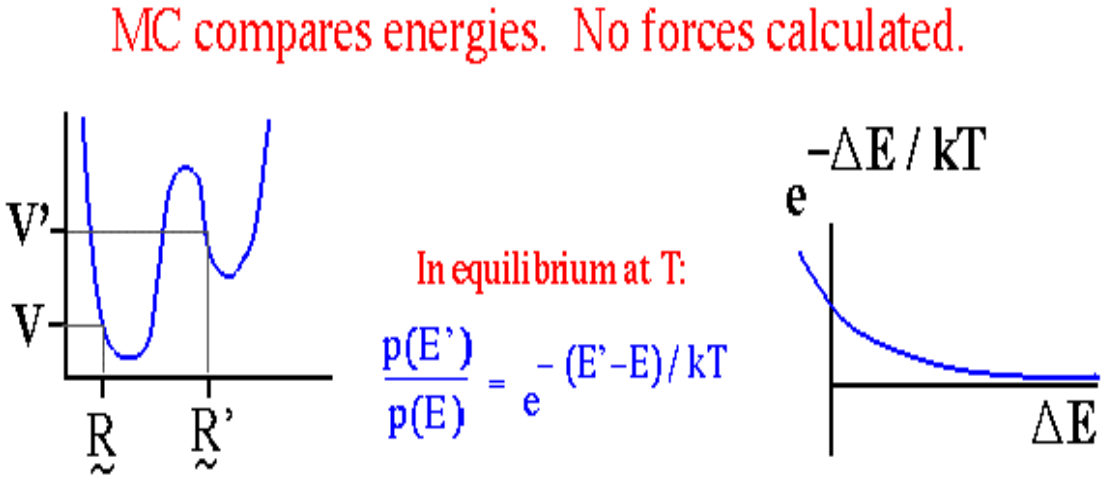

Figure 3.1. Monte Carlo simulation vs Molecule Dynamics. (a) While Monte Carlo technique makes larger changes in configuration thus more effective in sampling the all energy spectrum than minimizing to a local minimum as in molecular mechanics; (b) Molecular mechanics sets to minimizing the energy by progressively altering the configuration in a continuous manner.

From the classical statistical mechanics, the average property of system can be described as following:

$$< Z >_{NVT} = \frac{\int dr\, Z(r) \exp(-H(r)/\kappa_B T)}{\int dr\, \exp(-H(r)/\kappa_B T)} \qquad (3.1)$$

Here Z is the parameter for which the average value is calculated for a chosen domain (could be crystal size or mean square radius gyration for polymer), particle number N, volume V, temperature T for the system are constant in this particular system. However, average could be defined by fixing other thermodynamic variables. Here, r is a point in configuration space, k_B is Boltzmann's constant, and H(r) is the Hamiltonian of the system.

It is well known that the procedure to obtain an analytical solution of the equation (3.1) is a nontrivial problem. By solving this equation with numerical integration, Monte Carlo simulation can give an approximation solution by sampling a finite number of points as the system evolves.

$$< Z >_{NVT} = \frac{\int dr Z(r) \exp(-H(r)/\kappa_B T)}{\int dr \exp(-H(r)/\kappa_B T)} \approx \frac{\sum_{\tau=1}^{\tau=\max} Z(r) \exp(-H(r)/\kappa_B T)}{\sum_{\tau=1}^{\tau=\max} \exp(-H(r)/\kappa_B T)} \qquad (3.2)$$

Important sampling techniques will be targeted at the relevant region of the phase space by altering configuration at random from a distribution. Therefore equation (3.1) reduces to a simple arithmetic average,

$$\overline{Z} = (A - A_0)^{-1} \sum_{\tau = M_0 + 1}^{M} Z(r) \qquad (3.3)$$

Up to this point, the problem is just simplified but not solved. To solve this problem, a Markov chain of states is constructed to explore each state with the appropriate probability. In this process $r_1 \rightarrow r_2 \rightarrow \ldots r_{v-1} \rightarrow r_v \rightarrow \ldots$, each state r_v follows from the previous one with an appropriate transition probability $P(r_{v-1} \rightarrow r_v)$ and this probability has

to satisfy the condition of "microscopic reversibility" with the equilibrium probability Weq(r):

$$Weq(r)P(r_{v-1}\rightarrow r_v) = Weq(r)\, P(r_v\rightarrow r_{v-1}) \quad (3.4)$$

Another condition for a successful construction of this phase space trajectory in the canonical ensemble is that in the absence of H the process can explore any phase state r_v in a finite number of steps to ensure ergodicity.

The first such scheme is designed by Metropolis et al. The probability of exchange between two states is simply decided by equation:

$$P(r_v\rightarrow r_{v-1}) = \exp(-\Delta H/kBT) \quad (3.5)$$

If $\Delta H = H(r_{v-1}) - H(r_v) > 0$,

$P(r_v\rightarrow r_{v-1}) = 1$ else.

If the move lowers energy in energy state ($\Delta H \leq 0$) then the probability of new state is greater than old state thus this move will be accepted. If the move increases the energy (($\Delta H \geq 0$), then the move is accepted with a probability according to the equation (3.5). A random number between 0 to 1 is chosen to decide if the move for this transition is accepted or not, if P greater than this random number, the exchange is accepted and continue exploring phase state. Otherwise, the move is discarded and the new trial move is made.

The length or duration of MC simulation is conveniently measured in 'cycles', N indicating trial moves weather selected sequentially or randomly. The computer time involved in MC cycle is directly related (although obviously not equivalent) to that in MD time step. A dynamic interpretation of this MC simulation data is based on associating a 'time' with the cycle number ν of successive configuration, so that $W(r_v)$

can be interpreted as W(r, t). Under this interpretation, the unit of "time" is still quit arbitrary, and it is not obvious (and generally also not true) that this "time" of Monte Carlo sampling is simply proportional to the physical time. However, if this transition process is also related to the "time", then the Markov chain of phase space points $r_1 \rightarrow r_2 \rightarrow \ldots r_{v-1} \rightarrow r_v \rightarrow \ldots$ can be described:

$$\frac{dW(R,T)}{dt} = -\sum_{\vec{R}'} P(R \rightarrow R')W(R,t) + \sum_{\vec{R}'} P(R' \rightarrow R)W(R',t) \qquad (3.6)$$

The physical meaning of this equation is obvious since the probability of configuration R from phase space is the summation of the process which leads to the state R and away from it to configuration R'. This gain and loss is counteracted by each other and will be balanced to reach dW(R,t)/dt = 0 in thermal equilibrium. Therefore, in Markov process, Weq(R) can be reached in the limit $t \rightarrow \infty$, irrespective of the initial conditions. Thus, Monte Carlo averaging can be rewritten as a "time average" along a stochastic trajectory in phase space:

$$\bar{Z} = (t - t_0)\int_{t_0}^{t} dt' Z(R,t') \qquad (3.7)$$

where t is the total "time" of the Monte Carlo run and t_0 the beginning of the simulation. Equation here is the same as the equation used by molecular dynamics (MD), where one carries out a time-averaging procedure along deterministic trajectory other than a stochastic one in MC. The trajectory in MD is determined by the initial conformation evolved through the Newton's equation of motion, while the Monte Carlo trajectory depends on the path for the "move" $X \rightarrow X'$ on the microscoptical lead to. It is also noted that this move does not conserve the energy therefore it will result in fluctuation around

the constant energy hypersurface sampling phase space. However, this fluctuation is small if the number of degrees of freedom is very large.

3.1.1 Periodic Boundary condition:

The size of any simulated bulk system is generally limited by the power of available computers, and more specifically, by the computational speed in executing the program. Therefore computer simulations are usually done on a small number of molecules between N = 100 and 10000. The time needed to calculate the force or potential energy is proportional to N^2. Although some special technique may reduce this time dependence to (N), for very large system, the force/potential energy double loop over all distinct pairs of atoms almost cannot be avoided. Thus for large systems, the computation would be very expensive. For systems like microcrystals, the cohesive forces between the molecules may be sufficient to hold them together during the simulation, otherwise the molecules have to be confined in a potential representing a container, preventing them from moving away. In such an arrangement, an appreciable fraction of atoms would lie close to the periphery of the system, and significant surface effects would be evident. The standard approach is therefore to introduce so-called periodic boundary conditions, in which the system is considered to be surrounded on all sides by replicas of itself, forming infinite macrolattice. A two dimensional periodic system is showed in the Figure 3.2. In the course of the simulation, as a molecule moves in the center box, its image molecules move in exactly same way in other boxes. When a molecule in the center leaves the box, there will be another molecule move in the center box in the opposite face. There is no wall or restriction at the interface of different boxes, molecules can enter or leave freely.

Therefore, the density of box will be a constant. By introducing this periodic boundary condition, there is no need to store the coordinates of all images. When a molecule crosses the boundary, the coordinates of corresponding image molecules can be tracked.

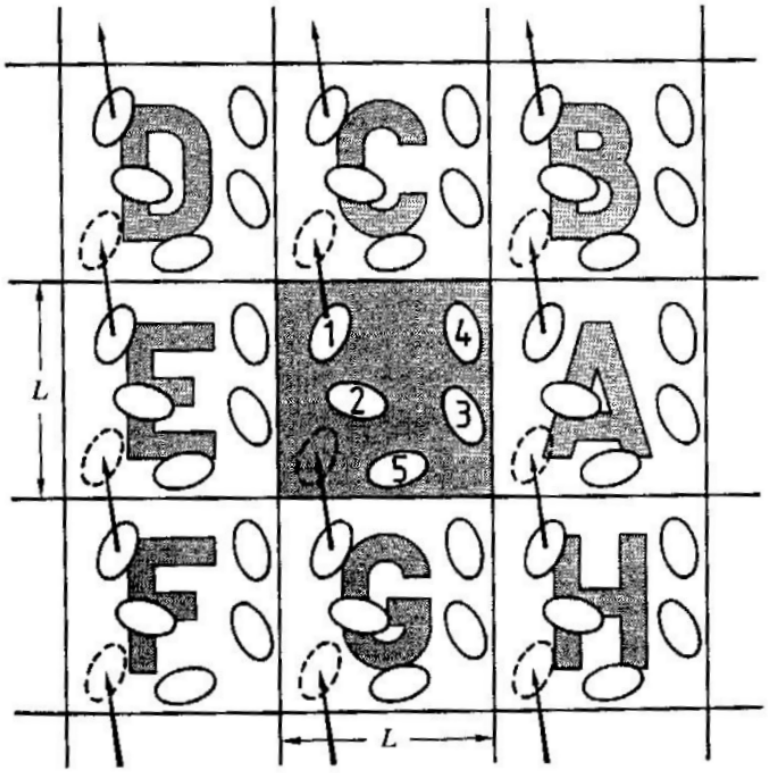

Figure 3.2. The demonstration of periodic boundary condition.

In any periodic system containing polymers, it is clear that atoms from the same molecule may be lying in different cells. Therefore, the convention introduced to polymer modeling by Theodorou and Suter[34] is employed. All polymer chains whose promary backbone atoms lie in the central box, referred to as parent molecules and all others as image molecules.

3.1.2 Monte Carlo for Polymer dynamics

For a polymer chain, the Hamiltonian of the system includes four parts. To be more specific, we consider the popular polyethylene (PE) as an example. For an N bond PE chain, H is the summation of bond length potentials H_l, bond angle potential H_θ, tortional potential H_ϕ, and nonbonded interaction potential H_{LJ} mostly described as Lennard-Jones potential.

$$H = \sum_{i=1}^{N} H_l(l_i) + \sum_{i=1}^{N-1} H_\theta(\theta_i) + \sum_{i=1}^{N-1} H_\phi(\phi_i) + \sum H_{LJ}(\vec{r}_{ij}) \quad (3.8)$$

If the harmonic potential is chosen for bond length and bond angels,

$$H_l(l_i) = \frac{f_l}{2}(l_i - l_0)^2 \quad (3.9)$$

$$H_\theta(\theta_i) = \frac{f_\theta}{2}(\cos\theta_i - \cos\theta_0)^2 \quad (3.10)$$

where f_l, l_0, f_θ, θ_0 are constants. The torsion potential can be chosen for the Flory three minima model:

$$H_\phi(\phi_i) = f_\phi \sum_{n=0}^{5} a_n \cos^n \phi_i \quad (3.11)$$

where f_ϕ, a_1, a_2, a_3, a_4, a_5 as constants.

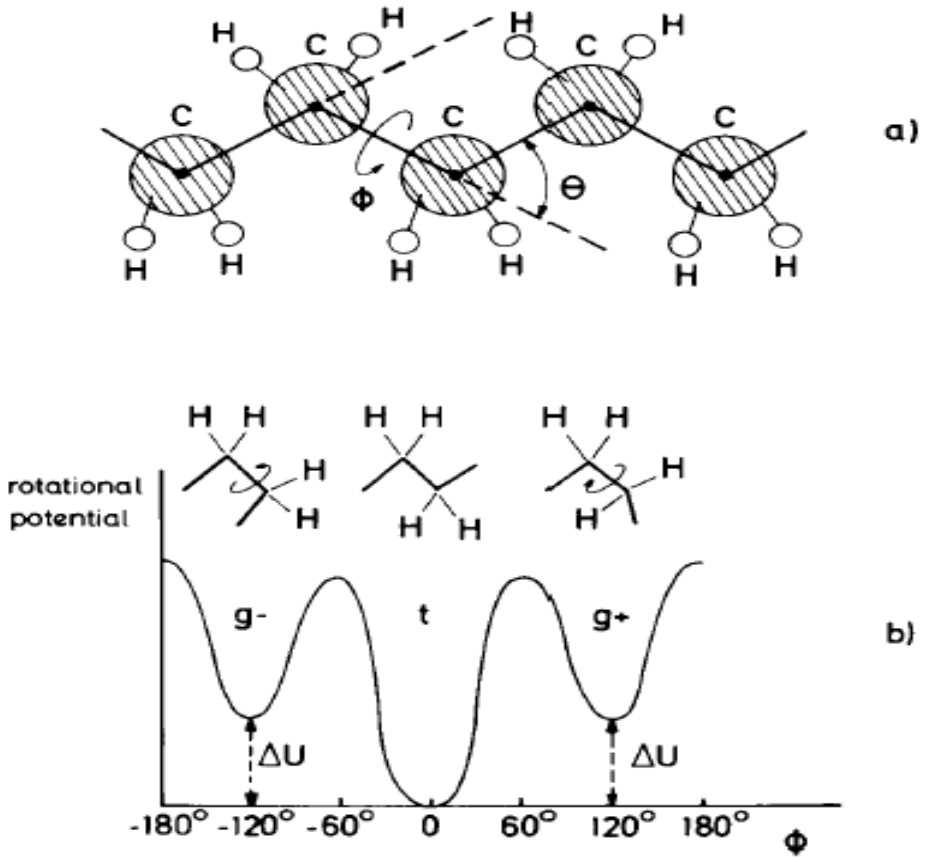

Figure 3.3. (a) Schematic Model of a piece of polyethylene chain. (b) Qualitative sketch of the three energetically preferred state "gauche minus" g-, "trans"(t) and "gauche plus" g+. The minimum of the trans configuration is deeper by a specific amount U. From Kremer and Binder[35].

The nonbonded interaction is described by Lennard-Jones:

$$H_{LJ} = 4\varepsilon\{(\sigma / r_{ij})^{12} - (\sigma / r_{ij})^{6}\} \qquad (3.12)$$

where r_{ij} is the distance between monomers i, j, and ε, σ are constants.

As shown in Figure 3.3, the hydrogen atoms (H) are not treated explicitly in the "united atom" approximation, but rather one introduces effective spherical segments (shaded) representing a whole CH_2 unit. The segments are connected by harmonic bonds (shown as straight lines), with bond lengths l_i. Segments are labeled consecutively by an index i; i = 0 to I = Np - 1. Three successive segments i-1, i, i+1 define bond angel θ_i and four successive segments i-2, i-1, i, i+1 a torsional angel ϕ_i, namely the angel between the plane spanned by the bonds formed from the segments [i-2, i-1, i] and the plane built from i-1, i, i+1. It is noted that the ϕ_i's are all zero in the all-trans configuration drawn here.

3.1.3 Coarse-Grained Models for polymers

The computer simulation of polymers presents a formidable challenge due to the considerable range of length and time scales relevant in the physical system[36]: flexible polymer chains in solution or as melt exhibit nontrivial geometric structure from the scale of the chemical length(~1 Å) to the coil size (~100 Å) and even larger length scales occur for collective phenomena (for example, the correlation length of concentration fluctuations in polymer blends is of the order of 1000 Å[37]), Atomistic simulation with

accurate chemical nature of polymer is extremely expensive, if at all feasible. To make things more complicated, there is a wide distribution of relaxation time for polymers: time for bond length and bond angle vibration is around 10^{-15}-10^{-13}s, while a typical time for a reorientation jump of monomer groups in the torsion potential may be $W^{-1} \approx 10^{-11}$s. The time to change the configuration of a chain containing N monomers is much larger: $\tau_N \approx W^{-1}N^2$, if the Rouse model holds[38,39] (for chain length N less than entanglement chain length N_e). For longer chains ($N > N_e$), an even bigger increase of τ_N with chain length occurs in polymer melts[39,40] $\tau_N \approx W^{-1} (N/N_e) N^2$, which can bring this relaxation time to the order of 10^{-4}s, nine orders of magnitude larger than τ_{vib}. Even larger relaxation time up to a time scale of 10^3s occurs near the glass transition.

For many questions of interests in computer simulations, reliable results must be based on the equilibrated system. In MD which can include all the dynamic processes, the time for system equilibration is huge. Therefore MD simulation relying on better initial configuration closer to the equilibrium is far beyond reach. In addition, the results depend on the proper choice of force fields related to the chemical structure. Even for PE, there are significant differences between the force fields used by different authors[41, 42].

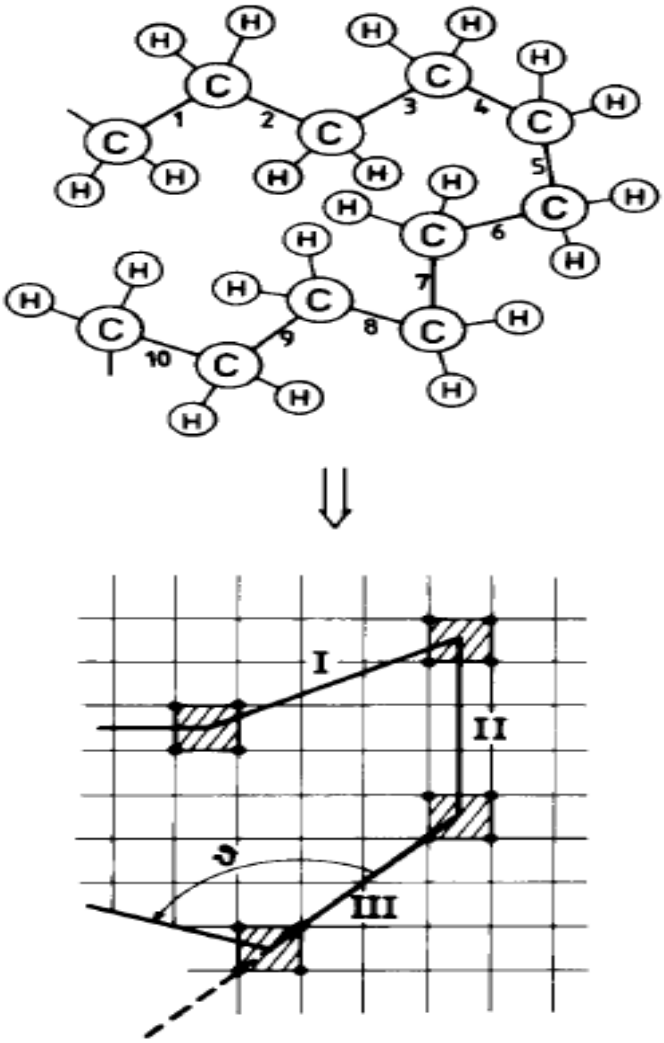

Figure 3.4. Use of the bond fluctuation model for one a lattice (lower part) as a coarse-grained model of a chemically realistic polymer chain (upper part, using PE as an example). In the example shown 3 covalent bonds form one “effective bond” between “effective monomers”: chemical bond 1, 2, 3 correspond to the effective bond I, chemical bonds 4, 5, 6 to the effective bond II, etc. An effective monomer blocks is an elementary cube containing eight lattice site (or square containing four lattice sites in d=2 dimension, respectively) from further occupation. From Baschnagel et al[43].

Based on the discussion above, there is an alternative approach to omit the fastest movement on small scale and focus on the long wavelength properties along the backbone of the chain. This approach is called "coarse grained model" which can reduce the computation tasks tremendously without sacrificing the accuracy of description of long wavelength properties. In this model, several chemical bonds are "integrated' into one "effective bond" as show in Figure 3.4. Therefore, a chain of N_p degree of polymerization is mapped to a chain of N effective bonds under the coarse grained concept, where N = Np/n, usually n represents around 3-6 chemical bond. Computer simulation of self-avoiding walk (SAWs),[35, 44] "bead-spring chain"[39, 45] and recent bond fluctuation model [46, 47]all belong to this class. Obviously, the SAW is extremely simplified, without very complicated chain architecture; this simulation can only give the universal properties of flexible polymer chains as general.

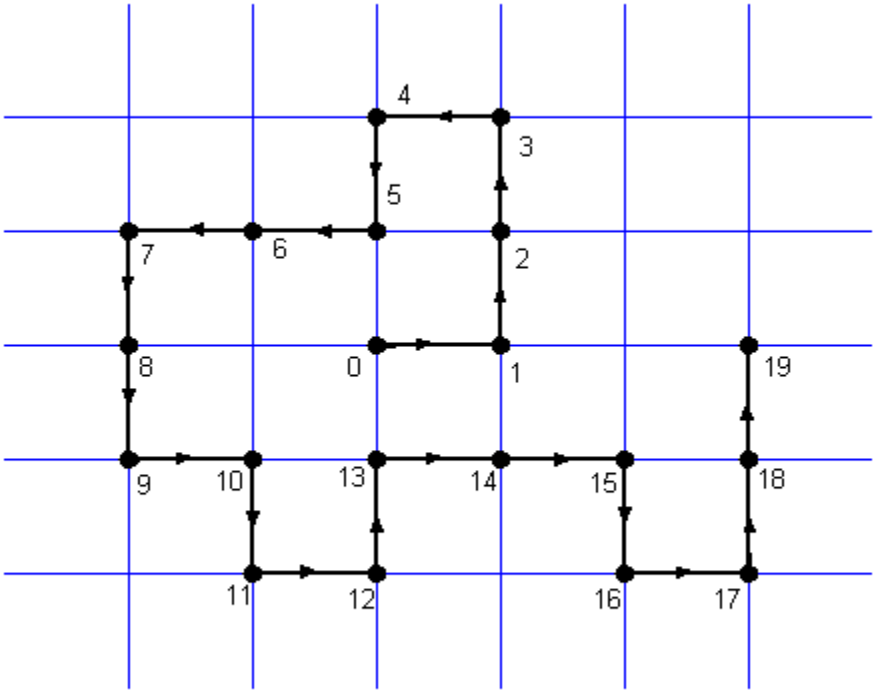

Figure 3.5. Example of self-avoiding walks (SAW's)

On the other hand bond fluctuation model, though still is a in lattice model (polymer chains of specific length are built up randomly on a lattice and can only move on the lattice), can describe many local properties related to some chemical structure in dense polymer systems in a qualitatively reasonable way by introducing effective potentials for the lengths of the effective bonds and angles between them. These effective potentials are generated from more realistic models which depend on the input from quantum-chemical calculations.

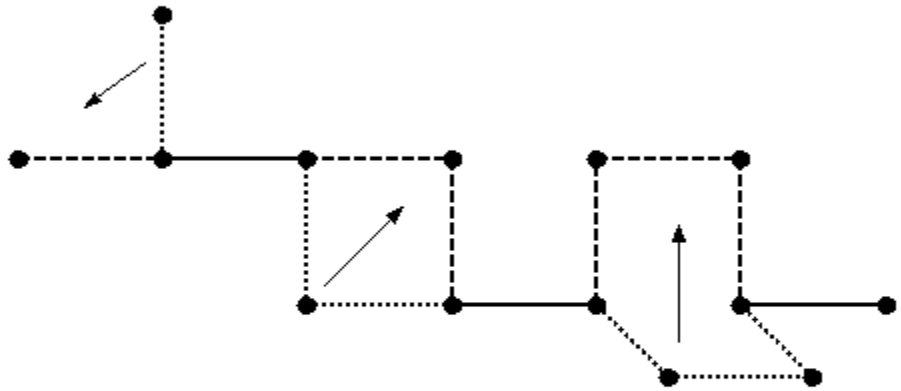

Figure 3.6. Generalized Verdier-Stockmayer algorithm on the simple cubic lattice showing three types of motion: end-bond motion, kink-jump motion, and crankshaft motion.

For the standard SAW, there are varieties of algorithms to deal with the Monte Carlo move. Each model includes the excluded volume interaction feature automatically by allowing each lattice site to be occupied by at most one bead. In the original Verdier-Stockmayer algorithm[48,49], only single bead ("effective monomer") was moved. As illustrated in Figure 3.6, only "end-bond" and "kink-jump" but no "crankshaft" was allowed. If both lattice sites and lattice bonds may be multiply occupied by the beads and links of the chain, the results of these simulations were in agreement with the Rouse model for the long time properties.[50,38] In fact, for the freely jointed polymer chain in the

continuum, some authors proved exactly this equivalence between the kink-jump model and the Rouse model. However, if the excluded effect of the chain is included, the simulation is radically different: Verdier[49] suggests that τ_N is proportion to N^3, which is much larger than it should be $1+2\nu \approx 2.2$ for the SAW in 3 dimentional problems (d=3). This inaccurate prediction has resulted from the fact that the excluded volume of S-shaped configurations (built up by two successive "crankshaft" in a plane) could only be relaxed by kink-jumps if one of the kinks has diffused toward the chain ends. Hoping to get quicker relaxation, Hilhorst and Deutch then introduced crankshaft motions but restricted them on to a plane. Due to the lack of interchanges of nearest-neighbor bond vectors along the chain, it still leads to τ_N proportional to N^3 with a reptaion-like motion[51,52,53]. Therefore, it is crucial to include the out of plane crankshaft rotation to create new bond vectors. Thus in three dimensional off-lattice simulations which generated new vector for out of plane crankshaft configuration, the results are consist with the theory $1+2\nu \approx 2.2$. Note that in the two-dimensional simulation, one cannot apply this out of plane crankshaft algorithm at all.

Another problem related to this algorithm is the lack of ergodicity [54,55,56]. One can always identify configurations of "knot" which cannot relax by the motions allowed in this algorithm. Thus by the kink-jump method and its variants one does not sample all the phase space, but only an "ergodic subclass" of the configuration space from which these "forbidden configurations" are omitted, since these "knots" cannot relax. However, for the chain and lattice for which the "kink-jump"-method can be applied, the system error due to this "knot" configuration seem to be smaller than the statistical error, considering

that the total number of configurations exponentially grown with N, therefore in practice consequences seem irrelevant.

The kink-jump method is most useful when one is interested in time-dependent properties of the chains, since this algorithm rather closely corresponds to the Rouse model, as has been demonstrated by a number of studies[48, 57, 58, 59, 60, 61, 62]. But most valuable outcome is that this algorithm can be applied for the simulation of many chain systems.

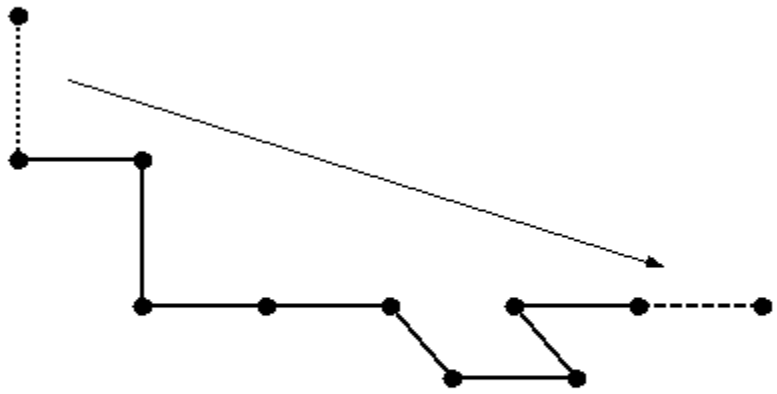

Figure 3.7. “Slithering snake”-(“reptation”-) algorithm

Kron[63,64, 65] and Wall and Mandel[66,67] first introduced the “Slithering Snake” algorithm to generate the SAW configuration (Figure 3.7). In this algorithm, one end of the chain is randomly selected and removed to the unoccupied space next to the other end with random orientation. Since it is still under SAW, this trial move has to satisfy the excluded

volume condition. Obviously, this is a very simple algorithm and does not describe the realistic chain movement, but it can lead to the equilibrium rather quickly, resulting in a smaller relaxation time compared to the Rouse model.

It is also clear that this algorithm is not completely ergodic: if all the nearest-neighbor sites of both ends are occupied, no movement is possible to relax this configuration. Again presence of this lock-in configuration makes this algorithm the "ergodic subclass". There is a general feeling that for the study of athermal SAW's, system errors can be neglected comparing to the statistical errors[68,69]. Probably this non-ergodic problem would become serious if the simulation is dealing with dense configuration such as studies of the collapse transition of a single chain. However, major applications of this algorithm is in the simulation of multiple chain system, thus it is a very effective tool. For multi-chain systems, one is often interested in dynamical properties on long wavelengths such as phase separation of polymer mixtures[70], in which the N-dependence of characteristic times associated with the process is calculated correctly. In addition, this algorithm is much faster than the kink-jump routine.

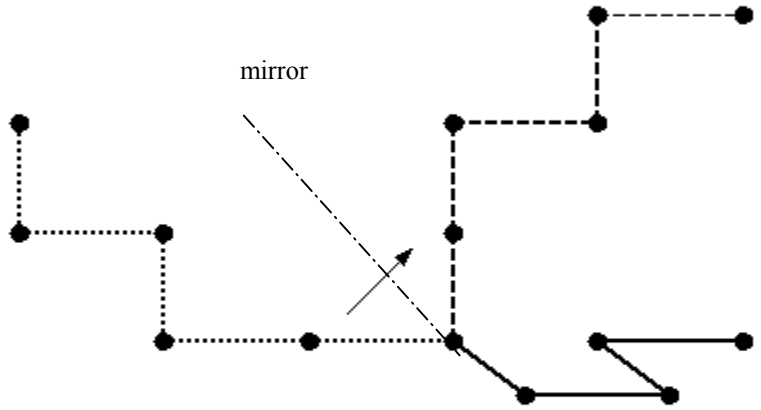

Figure 3.8. “Pivot”-(“wiggle”-) algorithm.

The “wiggle” (“pivot”) algorithm (Figure 3.8) was first introduced in 1967[71] and found little attention[72], but gained more popularity[73, 74, 75] when it was reinvented by Donald, Jan and Hunter. One of the reasons for its popularity is associated with the work of Madras and Sokal, whose analytical studies for ordinary random walks proved that for the SAW it is ergodic. In this algorithm a given configuration of a SAW is divided into two parts randomly and then the mirror image (across the line passing through the bond between the two parts) of the first part is connected with the second part. This new chain will be accepted if the excluded-volume condition is not violated; otherwise the new chain will be discarded and restarted from the old one with a different random division of the chain.

Although this algorithm is extremely efficient (with N such elementary motions one generates an essentially new configuration), one has to be careful in "equilibrating" the system since the large relaxation time needed for this algorithm if started with some arbitrary initial configuration. This problem can be fixed if one uses an equilibrium configuration generated by one of the other methods. One has to note that without further modification this algorithm is useful for studying long isolated chains, but not for generalization to simulate dense polymer chain systems.

For very long chains, these methods are seen to fail in equilibrating melts[76], hence the "broken chain" algorithm is introduced[77,78] (Figure 3.9). This algorithm includes two kinds of motions. In the "bond flip"-type, a pair of parallel bonds is rotated if the bonds belong to neighboring chains. If the two bonds belong to the same chain, this move is not allowed since it would result in "cyclization" (ring formation). This motion does not involve the chain ends of either chain. The second move is the so-called "end attack". A bond is rotated from a site of a chain that is the nearest neighbor to a chain end of another chain, so that the previous chain end is now an inner bead of one of the chains, and the site from which the bond move away becomes a chain end.

Obviously, these reactions by which chains are "broken" and reconnected again in a different fashion do not conserve chain lengths. As a matter of fact, the resulting distribution of chain length turns out to be broad.

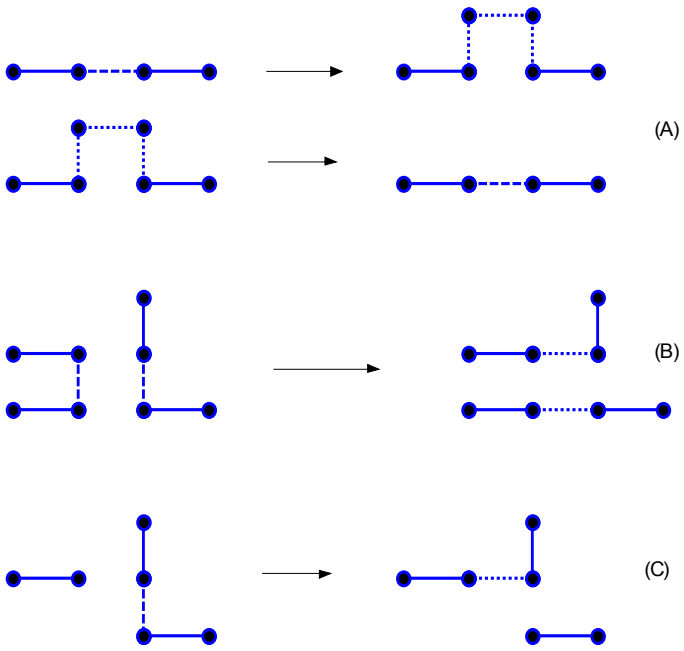

Figure 3.9. “Broken” chain algorithm

In principle, the extension of both the “kink-jump” method and its variants and of the “slithering snake”-algorithm to dense polymer lattice system are fairly straightforward. However, both methods need sufficiently large mount of empty sites or vacancies. For the “slithering snake”-algorithm, it is even necessary to have vacancies adjacent to the end of chain.

A nontrivial step in such studies is the generation of a realistic initial configuration. It is not possible to fill lattice so densely with chains and then apply one of the numerical methods such as “simple sampling” or “biased sampling” methods. So the common practice is to fill the lattice with chains which are completely stretched out linearly with

the required volume fraction of vacancies. Then this configuration`is relaxed carefully until the system is well equilibrated before starting the calculations for any desired properties.

3.2 Free Growth by Potts model

As described in the previous section, crystallization of a drug in the TDS system results mainly from the supersaturation of the drug, in order to maintain the required drug delivery rate so that the desired drug level is kept in blood. However, the bioavailability of the drug decreases due to the formation of crystals dispersed in polyacrylate adhesive of TDS after they were stored over six months at room temperature with moderate relative humidity[4]. Optical microscopy studies of 1% estradiol TDS showed that the growth of drug crystals in the polymer matrix of TDS occurs generally in the middle third of the polymer matrix (Figure 1.3), away from the interface.

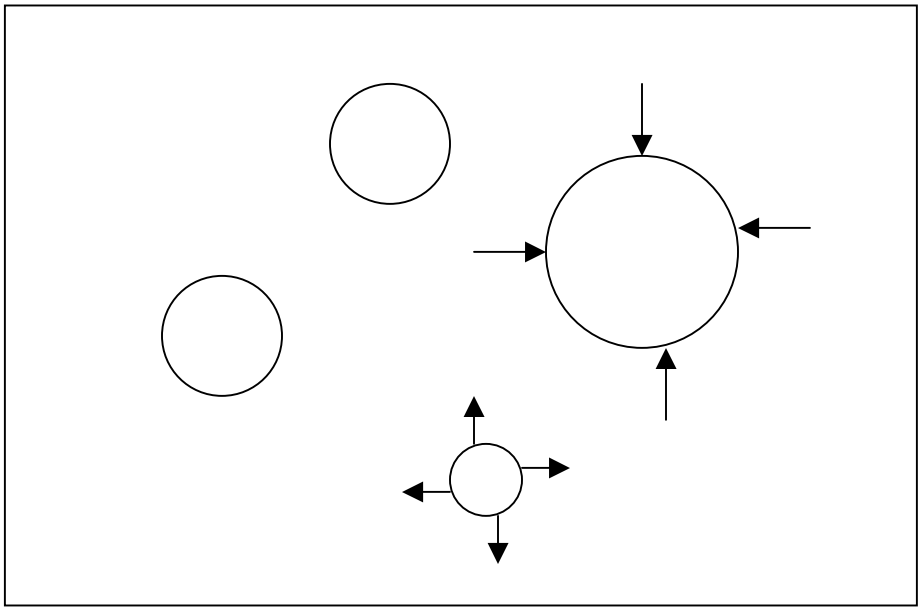

Figure 3.10. Demonstration of Ostwald Ripening process.

Since the presence of drug crystals will weaken therapeutic performance of the TDS, it is important to understand the kinetics of crystallization in the TDS so that appropriate steps could be taken to reduce crystallization of drug in the polymer. As the amount of drug in the matrix is unaffected during the storage, crystallization in TDS is occurring with a fixed quantity of available crystallizable component dissolved in the matrix. The crystal growth mechanism treated here is similar to that investigated by Tikare and Cawley[79,80], who studied the grain growth in liquid phase sintered materials described by Ostwald ripening (Figure 3.10), which incorporated the thermodynamic condition of a two-component two-phase system and their corresponding interfacial energy to simulate evolution of solution, precipitation and diffusion. A first approximation of nucleation and crystal growth in TDS could be studied by modifying this model to the conditions of TDS. However, an assumption implicit in this method is that the matrix does not offer

any resistance to grain growth as a result of the internal stresses developed due to this growth. We use the kinetic Monte Carlo model to simulate the nucleation and growth of the solid phase in a stress free matrix by the diffusion of the crystallizable components through the matrix. The model has the ability to incorporate the concentration gradient of the solute in the matrix and to simulate grain growth at low concentrations. We assume full wetting of the drug crystals by the matrix. The details of the chemical structure of the drug and the matrix are not considered as this is not an atomistic model; rather the drug and matrix are approximated by sites of equal size. The Monte Carlo model uses the classical Metropolis algorithm to simulate time dependent evolution of crystals in the TDS. The patch is treated as an infinite strip by using periodic boundary conditions in the length direction. However, across the thickness of the strip periodic conditions are not used so that edge effect in the thin TDS strip can be incorporated. The details of the modeling procedure are described in the following section.

3.2.1 Numerical Simulation procedure

As in reference 79, the microstructure was represented digitally on a square lattice with different q states representing either the matrix or solute and solute clusters of different orientation. The drug is represented by the q-states 1 to Q = 100 and the matrix by just one q-state. Periodic boundary conditions are applied on the plane of the TDS, but not normal to the plane of the TDS patch. Grain growth of *A*-component (i.e., drug) was driven by the reduction of interfacial energy. The Hamiltonian H for this two-phase system was determined by the summation of the interfacial energy between each site i and each of its first and second nearest neighbors j as:

$$H = \frac{1}{2}\sum_{i=1}^{N}\sum_{j=1}^{8} E(q_i q_j); \tag{3.13}$$

where $E(q_i,q_j)$ is the interaction energy for neighbor sites i and j. If these sites contain different components, i.e., an idealized drug site and a matrix site, there is a possibility of exchanging these components between the sites i and j. If these sites contain identical components, either drug or matrix, the possibility of exchange has no significance. The exchange probability is given by W(*A*->*B*), which was calculated using the Boltzmann statistics as[81]:

$$W(A\text{->}B) = \exp(-\Delta H/k_bT);$$

$$\text{If } \Delta H > 0 ; \tag{3.14}$$

$$W(A\text{->}B) = 1 \text{ else} \tag{3.15}$$

where k_b is the Boltzmann constant and T is absolute temperature and has units of bond energy divided by the Boltzmann constant. In this work, a temperature parameter k_bT is used for the conventional Monte Carlo simulation with units of energy rather than just temperature. The Metropolis algorithm is used to determine whether or not an exchange occurs in proportion to the probability calculated by (3.14) and (3.15). The number of iterations is given in Monte Carlo steps, MCS. At 1 MCS, the number of attempted transitions is equal to the total number of sites in the simulation. It has been shown [82] that MCS is linearly related to the time by the factor ι. Two artifacts of simulation, coalescence and direct-exchange, was prevented explicitly in this grain growth process. The thickness (i.e., the X-direction) is divided into three layers. The initial concentration of the drug could be set differently in each layer. The interfacial energies between identical Q-states are assumed to be zero indicating that no interface exists between

identical sites. The interfacial energies between different components are assumed to have non-zero values. The energy values could be calculated from molecular modeling or by experiments for the particular systems of interest. However, in our preliminary work we used the values from another work as we are only interested in the general pattern of crystal growth rather than the exact crystallization kinetics of a particular drug/matrix system. All grain growth simulation was run in the fully wetting condition with interaction energies, E(drug-matrix) = 1.0, E(drug-drug of different orientations, q) = 2.5, E(drug-drug of same orientation, q) = 0, and E(matrix-matrix) = 0. The total number of orientation states of the drug Q is taken to be 100. The composition was varied by changing the concentration of drug X_D from 0.05 to 0.1 (given in volume fraction), and the temperature parameter ranges from k_bT = 0.3, 0.6, and 0.9. The digitized simulation matrix has 100×100 sites. Although this small size was suitable for gaining insight into the crystallization process in TDS with reasonable computing requirements, larger sites (eg. 300x300 or 500x500) must be used for more accurate simulation results. Since no periodic boundary conditions exist along the thickness, particles near the outer boundaries have "reflective" boundary conditions, i.e; a particle on a boundary is only allowed to move towards the center layer of the patch.

3.2.2 Results and discussion

The mechanisms necessary to simulate precipitation from a supersaturated solution and growth of the precipitates are dissolution, diffusion and precipitation. The model simulates these in the following manner. Detachment of individual drug sites from a grain is dissolution. The successive movement of a single drug sites in the matrix by

exchanges is diffusion. Finally, precipitation is simulated when a drug site attaches to a drug grain. In clusters growth three stages have to be distinguished[83]: fluctuations in size of subcritical clusters (for radius R < critical radius R_C), diffusion limited growth in the near critical region (R = Rc) and a deterministic growth when the cluster is larger than the critical size (R > Rc). All three stages can be simulated by this model as will be shown in this section.

Simulations were carried out for three different simulation temperatures (k_bT = 0.9, 0.6, and 0.3) with (1) an uniform composition of 10% drug (as volume fraction, X_D=0.1) for the whole region and (2) with a concentration distribution of 5 % for the outer third of the thickness and 10 % for the inner third. While the drug concentration in a typical TDS is 1%, we used higher in order to reduce the time requirement for the simulations. This is not expected to change the simulation results as the physics and geometry of the problem were not fundamentally altered at the slightly higher concentrations. Figure 3.11 shows the evolution of the size and distribution of the grains at simulation temperature k_bT= 0.9 and uniform drug concentration of 0.1. The dark continuous region is the matrix and the gray areas are grains of different orientation. Initially, the drug was distributed randomly primarily as single sites and a few small clusters. In this simulation a grain is defined as two or more contiguous drug sites of the same state q. As the simulation progressed small grains are formed, some grains become larger due to precipitation from a supersaturated solution and by growing at the expense of others. As the simulation progressed further, one large grain formed in the middle third. Figures 3.12 and 3.13 show the evolution of clusters from uniformly distributed drug at simulation temperatures of k_bT = 0.6 and k_bT = 0.3, respectively. At temperature k_bT = 0.6 many smaller grains

are formed distributed throughout the strip. As simulation progressed one or two large grains are formed close to the middle of the strip, although not exclusively in the middle third of the thickness. At temperature $k_bT = 0.3$ grains grew slowly and are distributed throughout the thickness of the TDS patch. Many small grains are found both in the middle third and the outer layers of the strip (Figure 3.13).

The arithmetic mean of the grain radii is plotted against simulation time in Figure 3.14a and the corresponding drug concentrations is plotted in Figure 3.14b for simulations shown in Figures 3.11 to 3.13. In both Figure 3.14a and 3.14b, three distinct regions can be observed for each temperature. At the beginning, subcritical fluctuation of grains occurs with negligible change in the drug concentration in the solution. At the end of this stage a few nuclei of critical size form. In the second stage, these nuclei grow rapidly accompanied by a drastic reduction in the solution concentration of the drug. In the last stage, Ostwald ripening of the grains occurs. However, at the lowest simulation temperature $k_bT= 0.3$, there is not sufficient diffusion to give significant growth. At the highest temperature $k_bT= 0.9$, there are too few grains in the simulation to get smooth grain growth curves, but an examination of the microstructures shows grain growth by Ostwald ripening until only a single grain is left as seen in Figure 3.11d. The second moment average of the grain radius follows similar pattern as the average grain size, indicating that the increase in the average grain size occurs mainly from the growth the largest grains.

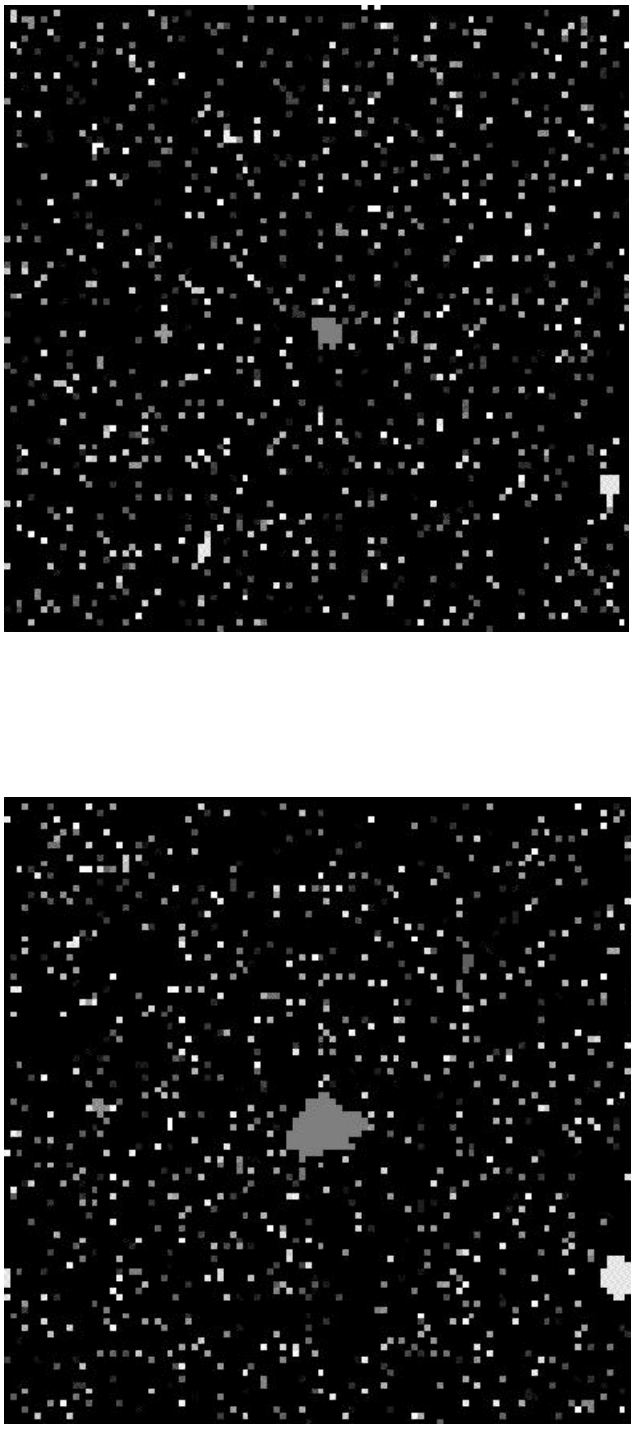

Figure 3.11. (a and b)

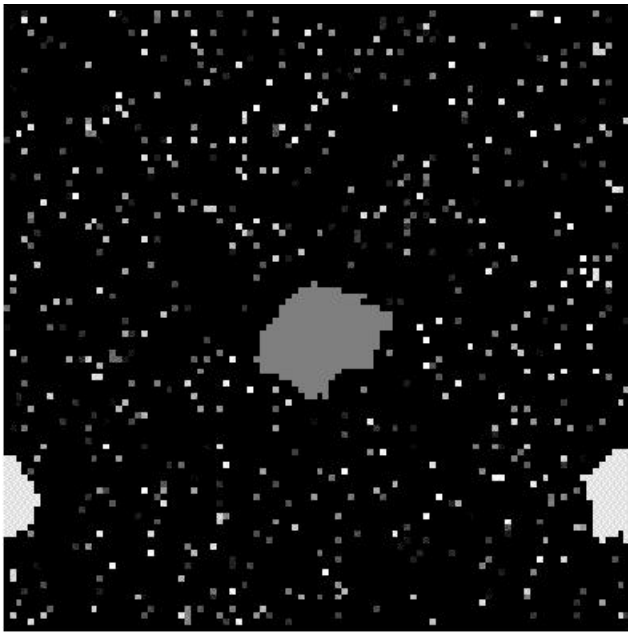

(c)

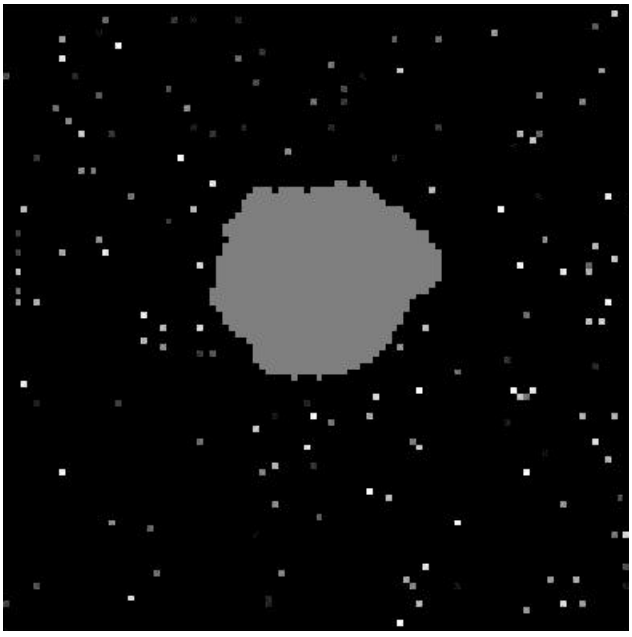

(d)

Figure 3.11. Microstructure at different stage of the grain growth simulation for $K_bT=0.9$ Concentration of A component 0.1: (a) MCS=2086 (b) MCS=9072 (c) MCS=20000 (d) MCS=16000000. The dark continuous feature is the liquid matrix and the different gray features are grains with different orientation.

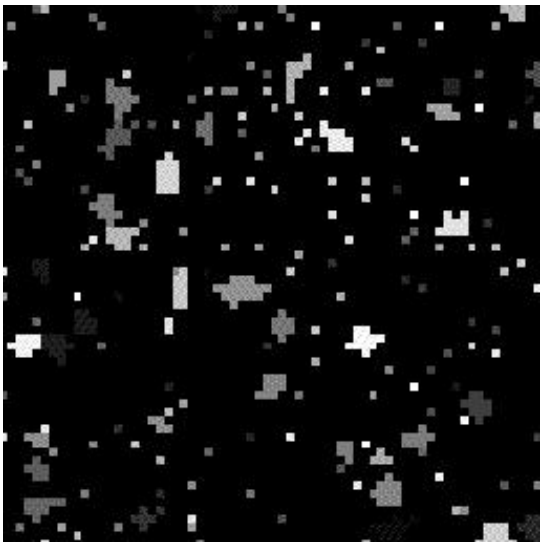

(a)

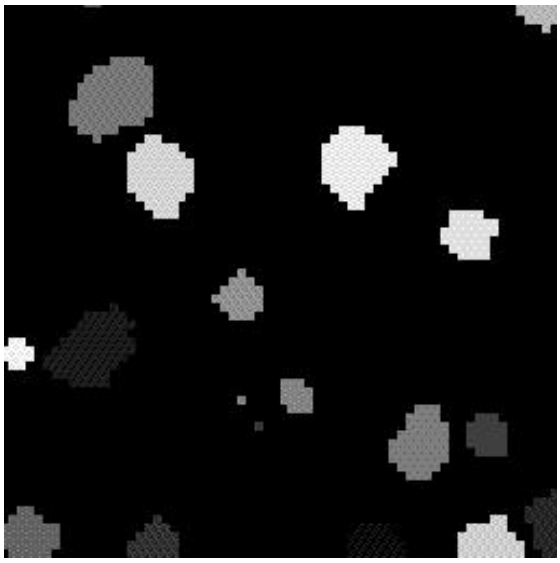

(b)

Figure 3.12 (a and b)

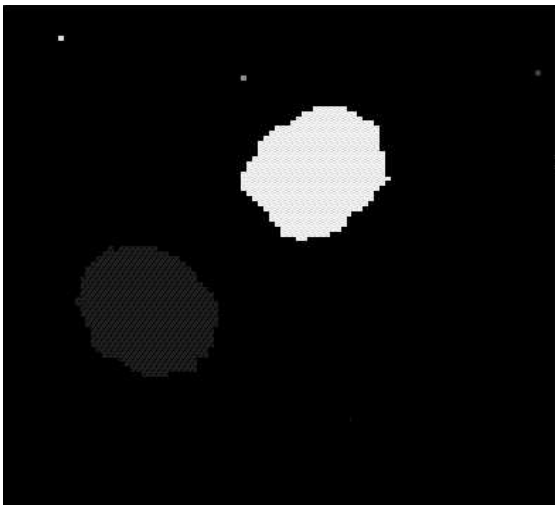

(c)

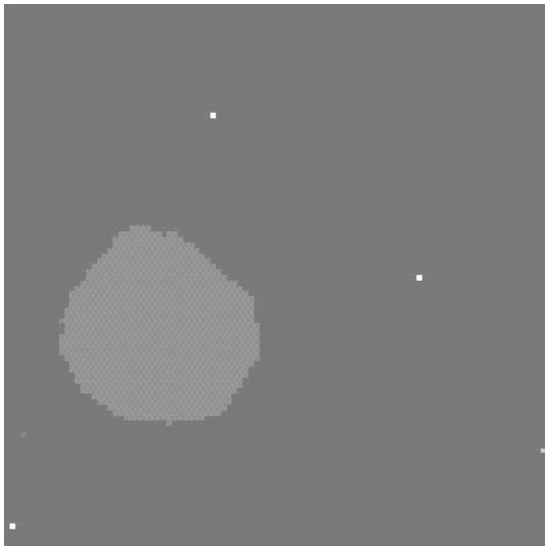

(d)

Figure 3.12. Microstructure at various stages of the grain growth simulation at the k_bT=0.6 and the concentration of A component 0.1 for Monte Carlo Steps (a) 2086, (b) 656348, (c) 3.2×10^7 and (d) 4.1×10^7 respectively.

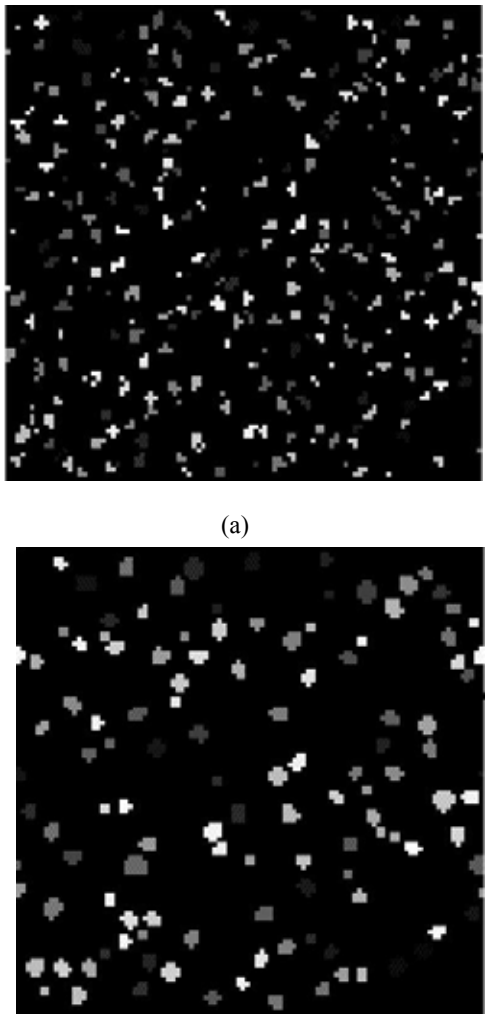

(a)

(b)

Figure 3.13. Microstructure at various stages of the grain growth simulation at the k_bT=0.3 and the concentration of A component 0.1 for Monte Carlo Steps (a) 1045, (b) 32000000 respectively.

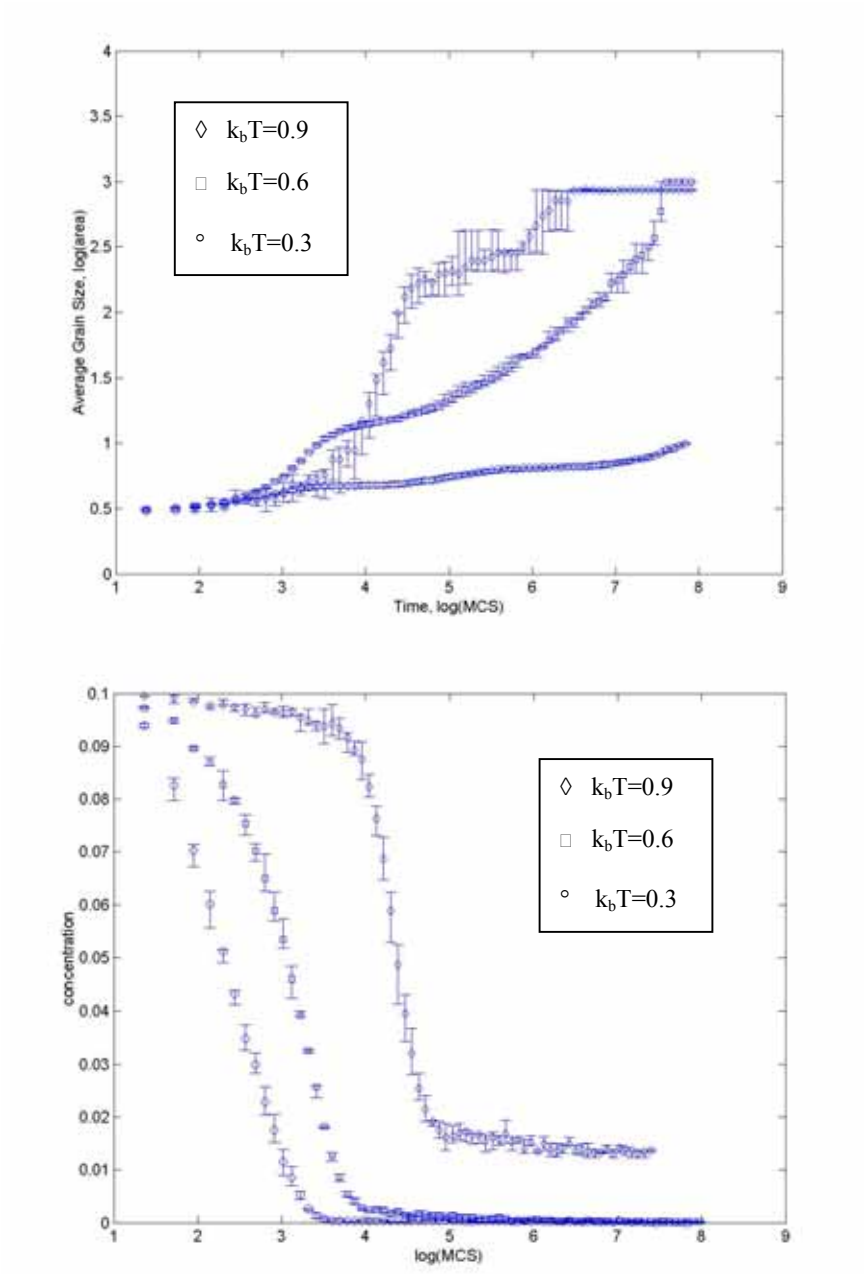

Figure 3.14. (a) Grain growth curves for the simulation run with drug concentration of 10% at temperature k_bT = 0.9, 0.6 and 0.3 (b) The variation of solute concentration in the matrix due to clustering.

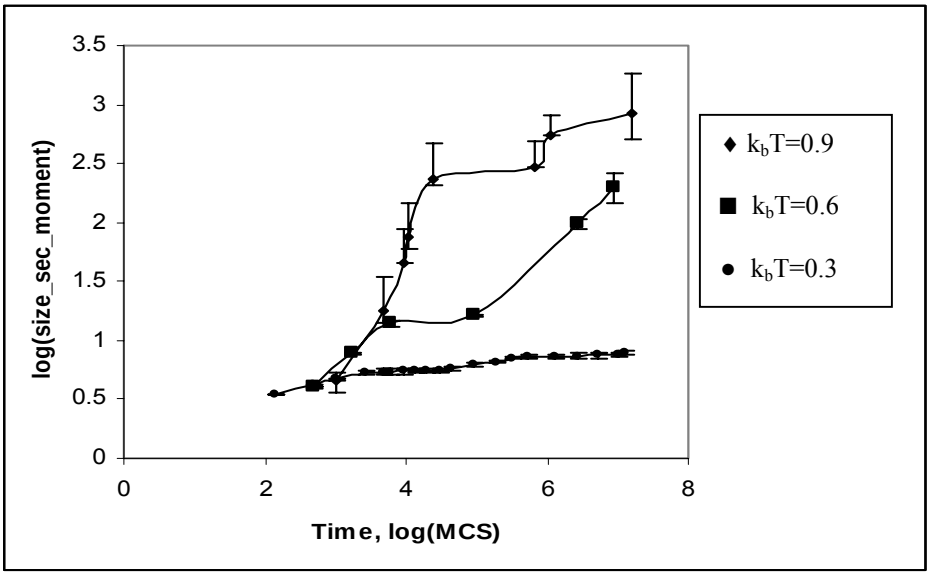

Figure 3.15 . Second moment of grain size vs MC steps for three different values of k_bT.

The second moment averages of the grain radius for the three temperature parameters is shown in Figure 3.15. Also, the average radius of the five largest grains (or all the largest grains if they are smaller than five) is shown in Figure 3.16. For $k_bT = 0.9$, the second moment average grain size follows a similar pattern as the average grain size, i.e., sudden increase from log(MCS) = 3.7 to 4.38, then remain relatively constant, followed by a small sudden jump at log(MCS) = 6.1 then by a gradual steady increase. This indicates that the increase in average grain size results mainly from the growth of the largest grains in the system. Figure 3.16 indicates that the average size of the largest five (or fewer if five large grains are not available) grains increases even after log(MCS) = 4.5, and no sudden increase is noted at log (MCS) = 6.1. This indicates that the sudden decay and growth of grains did not affect the average radius of the largest grains. It can be seen from Figure 3.11 c and d that the growth of one large grain at the expense of other grains,

indicative of Ostwald ripening process, occurs only at the very last stage, i.e., when log(MCS) is more than 4.96, which is further supported by the data shown in Fig. 3.16.

For grain growth at a temperature $k_bT = 0.6$, the average grain size does not show any particular stage with a significantly rapid grain growth. The average radius of the grains does not show any sudden transitions, it grows gradually after log(MCS) = 3.6, although close to log(MCS) = 4.4 the average grain size increases more rapidly. From Figure 3.13b, the depletion of solution concentration of A reduces slightly, then decreases rapidly from log(MCS) = 2.3 to 3.87 to reach a plateau close to zero concentration. However, the fastest growth of average grain size occurs only after the solution concentration of A reached a minimum. Thus, at intermediate temperature ranges the last stage of the grain growth, i.e., coarsening, occurs only due to Ostwald Ripening by the growth of larger grains accompanied by decay of smaller grains. This conclusion is further supported by the data from Figures 3.15 and 3.16. It can be seen that the second moment average of the grain size and the average of largest five (or fewer) grains increases steadily after the solution concentration of *A* has reached a minimum.

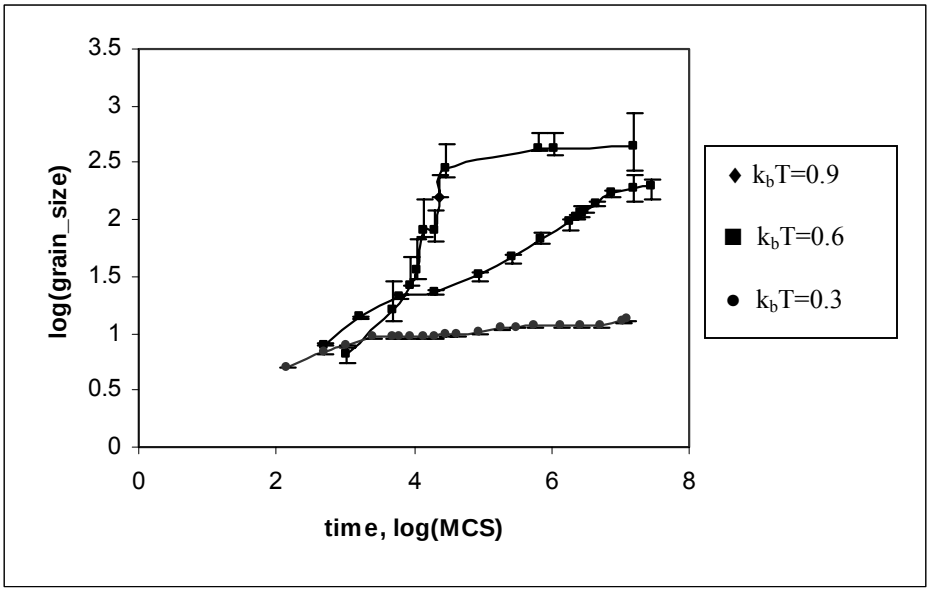

Figure 3.16. Largest grains grow with the MC steps for three different values of k_bT. (Grain_size is average size of largest five or less grains)

Grain growth at temperature $k_bT = 0.3$ shows a different pattern. The solution concentration of *A* component was reduced to close to zero (at log(MCT) = 3.5) much earlier than that for higher temperatures. However, no significant increase in the average grain size occurs during the entire simulation, indicating that the reduction of solution concentration produces a large number of smaller nuclei. There is a small but steady increase in the second moment average of grain size as well as the average of the five (or fewer) largest grains, indicating that the largest crystals are growing slowly but in a steady pace without affecting the average grain size in the system. Thus, one could infer that there is only a partial decay of grains during this stage. Large grains are not completely decayed in this process.

Figures 3.17, 3.18, and 3.20 show the positions of grains along the TDS thickness and size of the grains as the simulations progress for $k_bT = 0.9$, 0.6, and 0.3, respectively. At all three simulation temperatures, initially small grains are found randomly distributed across the TDS thickness. At simulation temperatures, $k_bT = 0.9$ and 0.6, Figures 3.17 and 3.18 show few large grains grow at the expense of smaller ones until there are only two grains remaining for $k_bT = 0.6$ and only one grain remaining for $k_bT = 0.9$ at MCS = $3.2x10^7$. In both cases, the grains are in the center portion of the TDS strip. At $k_bT = 0.3$, many small grains remain randomly distributed for the entire simulation. This is because diffusion coefficient of the drug in the matrix is too low to give any significant Ostwald ripening.

In TDS, it is possible that gradients in the drug concentration can occur across the thickness of the patch. In order to understand the effect of such concentration gradients, simulations were carried out by dividing the matrix into three regions with different solution concentration. To prevent the system from averaging out this concentration gradient at the very early stages of simulation, the motion of crystallizable monomers between different layers was prevented before nucleation. Figure 3.19 shows that the crystal aggregate to the middle more quickly for a system with monomer concentration of 10 % at the middle third of matrix, and 5 % in the remaining regions (i.e., 5/10/5) than a 10 % homogeneous system at the same temperature in Figure 3.18. The simulation results

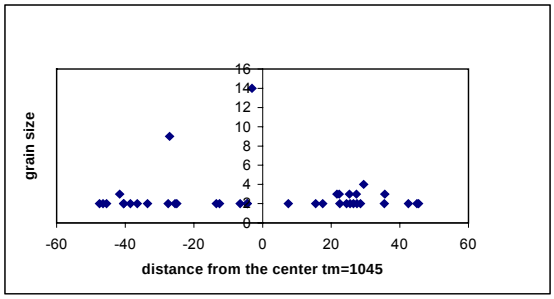

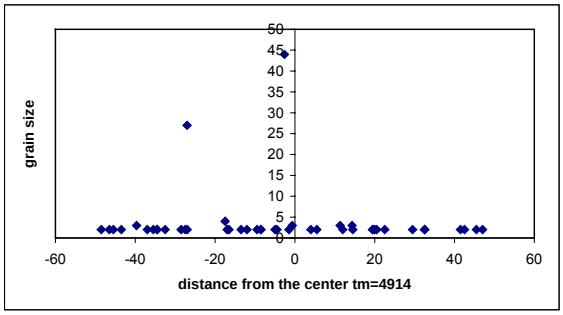

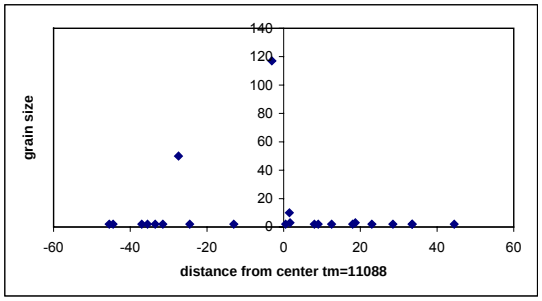

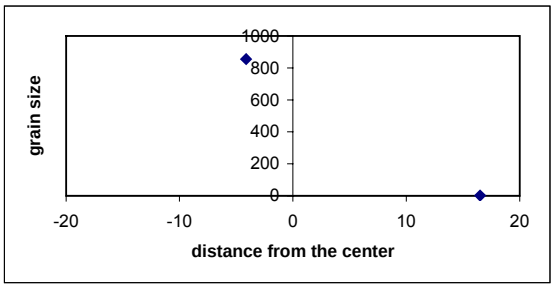

Figure 3.17. Grain size distribution along x direction at different simulation stage for X_A=0.1, k_bT=0.9

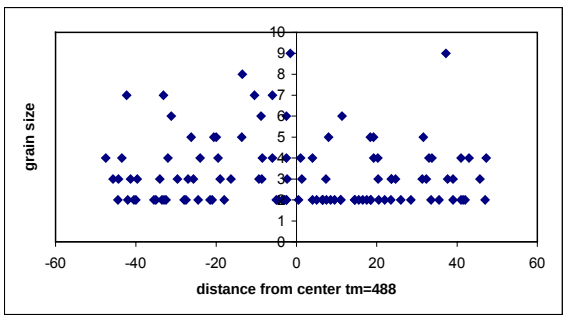

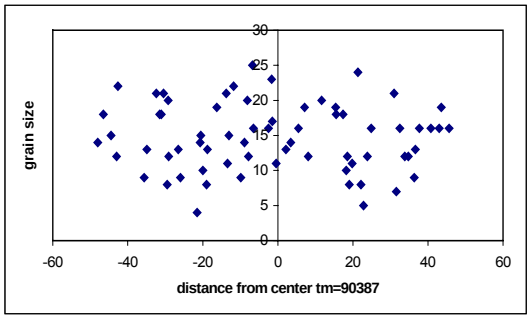

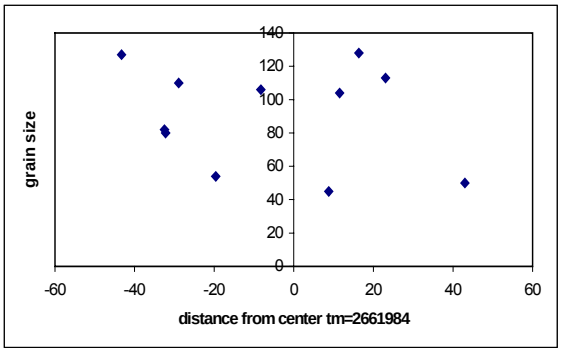

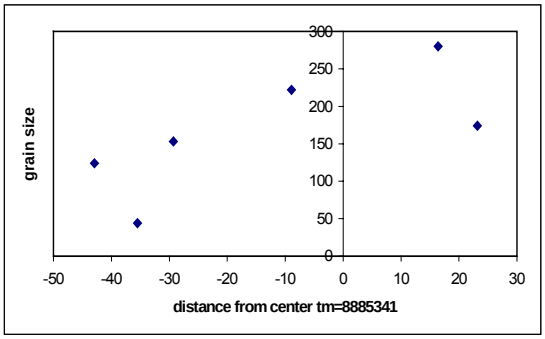

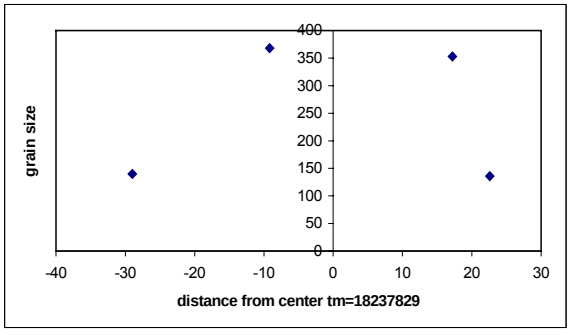

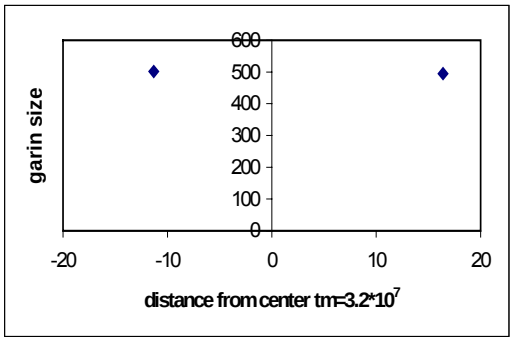

Figure 3.18. Grain size distribution along x direction at different simulation stage for X_A=0.1, k_bT=0.6

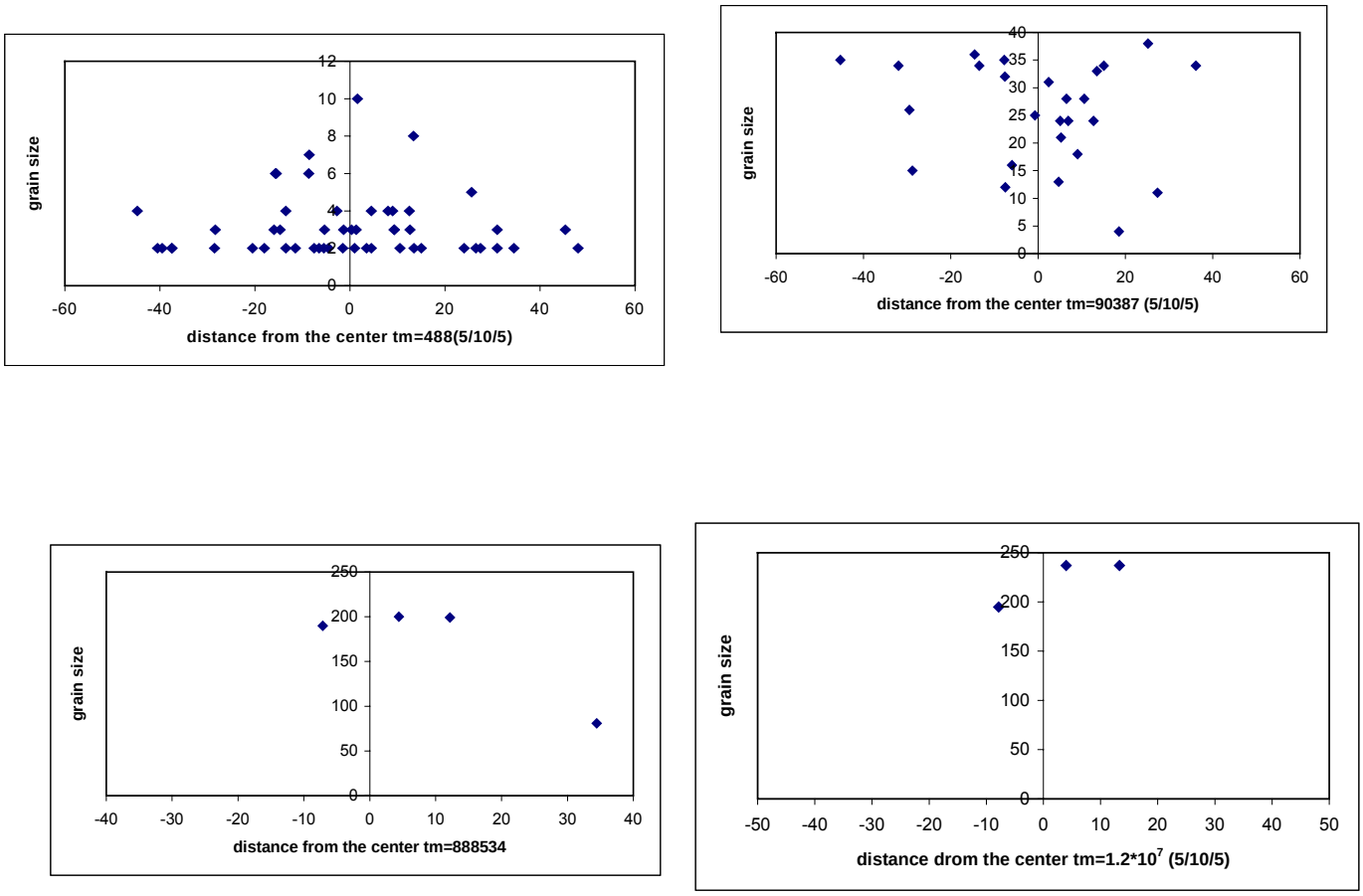

Figure 3.19. Grain size distribution along x direction at different simulation stage for three layers case (X_A is 0.05, 0.1 and 0.5 respectively), k_bT=0.6.

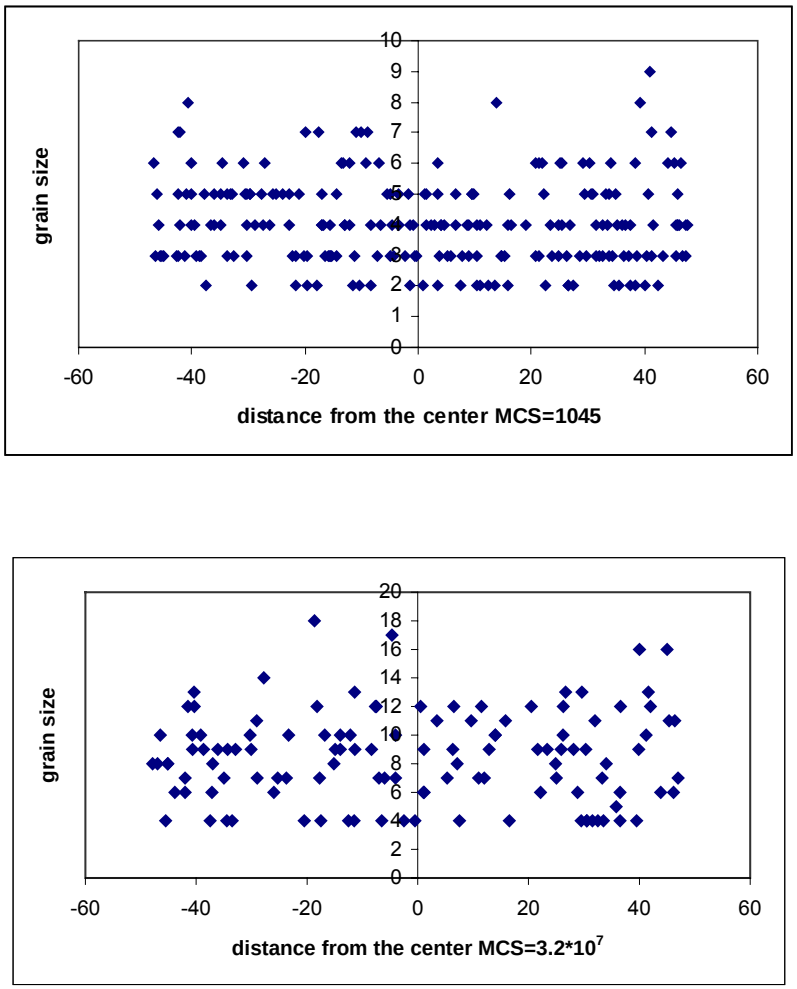

Figure 3.20. Grain size distribution along x direction at different simulation stage for X_A=0.1, k_bT=0.3

show that it took MCS= 3278452 to get all the crystals in the center layer, much less time compared to MCS= $2.0*10^7$ of the 10% homogeneous system at the same temperature. This is because the time to nucleation is shorter at higher solution concentrations. Once nuclei form in the middle, they grow faster due to precipitation from the region surrounding them. Subsequently, these larger grains continue to ripen faster as they have many small grains surrounding them, unlike the grains on the edge. Because of the boundary restriction, this fluctuation in concentration will always favor the center layer of matrix, consequently, increases the probability of crystals appearing in the middle layer of the system.

3.2.3 Conclusions

A qualitative evolution of grain growth in a TDS is investigated using a kinetic Monte Carlo technique. We have demonstrated that this model can simulate precipitation and growth of the drug crystals from a supersaturated solution in a TDS patch. Furthermore, once the solution approaches its equilibrium solution concentration, Ostwald ripening of the drug grains can also be simulated. As expected, simulation temperature significantly influenced the development of microstructures. At higher temperature fewer larger crystals are developed in the middle layer of the TDS, while for intermediate temperatures more number of relatively larger grains is observed close to the middle layer. At low simulation temperature, the grains are evenly distributed throughout the thickness of the TDS patch. From this idealized simulation, it is seen that a large number of small crystals are formed when the TDS is kept at low temperature. Presence of such small crystals will have conflicting effect on the functioning of TDS.

The selection of a storage temperature is very important in determining the effectiveness of TDS. When stored at higher temperature, although larger crystals are formed near the middle layer, the solution concentration of the drug is also higher in the matrix. On the other hand, at lower temperatures, small crystals are distributed throughout thickness, but the solution concentration is much lower. Thus the effectiveness of TDS depends on the dissolution process of the crystal. Further studies are necessary to address the dissolution and diffusion of drug during its usage.

3.3 Bond Fluctuation approach

Grain growth by precipitation and Ostwald ripening in an unstressed matrix of a dissolved crystallizable component was simulated using a kinetic Monte Carlo method of the Potts model[84]. This model was shown to correctly simulate solution, diffusion and precipitation for the low crystallizable regime of interest to the transdermal drug delivery system (TDS) community. The simulation results provide a first approximation for the crystallization occurring in (TDS), as it does not account for the specific structure of polymer molecules. In addition, the polymer chains constrain the crystal growth to some extent. Therefore, computer simulations of crystal growth in polymer matrix will give us insight closer to the real system if one can explicitly specify the architecture of chains in the calculations. In the Potts model, an assumption is made that the size of polymer chains are compatible to that of drug molecules. Thus the size effects cannot be captured by the classical Potts model[85], clearly an over simplification of the problem. In order to account for size effects and to develop a refined approach, the polymer chains must be

treated as longer chains in comparison with the polymer molecules. There are several different ways of dealing with the segregation of drug in a polymer medium. One can use Rouse model to describe the motion of a polymer chain by applying the Brownian dynamics to the monomers of a polymer chain. However, all the dynamic Monte Carlo algorithms with fixed bond length in lattice have some problems associated with them[86]. First, they are not being able to simulate in two dimensions (as described later), second they do not allow simulation of branched polymer chains. The third difficulty is that these lattice models with fixed bond lengths are all non-ergodic system[87,88,89], which is not a serious drawback for an isolated chain but could be a major problem in dense systems. Recently, the bond fluctuation model is developed to overcome all of above problems, while incorporating the size effects of polymer chains. In addition, this coarse-grained model can overcome the time scale demands in the MD simulation and give the long wavelength properties as well as intermediate wavelength properties and even go down to the scale of an effective bond [90, 91, 92], therefore it is suitable for diffusion and precipitation of drug molecules in the polymer matrix. It should be noted, however, that the stress build-up in the matrix due to grain growth is still not accounted in this bond fluctuation model.

3.3.1 Description of bond fluctuation method

The usual dynamic Monte Carlo simulation is very slow for polymer system, because a self-avoiding walk (SAW) or a nonreversal random walk (NRRW) can only make moves at the end of chains. In addition, the center part of the chain gets less chance to move for longer chains in the simulation system. The bond fluctuation model uses variable bond

lengths between monomers, thus can keep the simplicity of lattice model to carry out dynamic simulations for dense system. In coarse-grained model, one "effective bond" always means collection of several bonds. Originally, a square lattice (four lattices sites) representing one monomer with a lattice constant of one unit (length of one side of this square lattice) is implemented. The bond length, which represents an "effective bond", can vary and is smaller than $18^{1/2}$. This representation can prevent different bonds from crossing over, weather they are from the same chain or from the different chains, as a condition of self-avoiding random walk (SAW). In this study, in addition to polymer molecules the drug molecules as crystallizable component are also incorporated. In order to allow neighboring drugs to crystallize, one monomer of the polymer chain is represented as one lattice site. Lattice points unoccupied by drug or polymer units represent for vacancies in the system, are responsible for the free volume.

In this system, the maximum bond length in the polymer backbone is less than $8^{1/2}$ units, hence the possible lengths are 1, $2^{1/2}$, 2, $5^{1/2}$ units (showed in Figure 3.21). While constructing the initial structure, special care must be taken to avoid chain cross-over. Typical moves for monomer units are showed in Figure 3.21, and these movements can obviously avoid the deadlock configurations which are caused by the traditional algorithm[93] and cannot be resolved in two dimensions with fixed bond length by themselves. Therefore the modified bond fluctuation model in our study is ergodic.

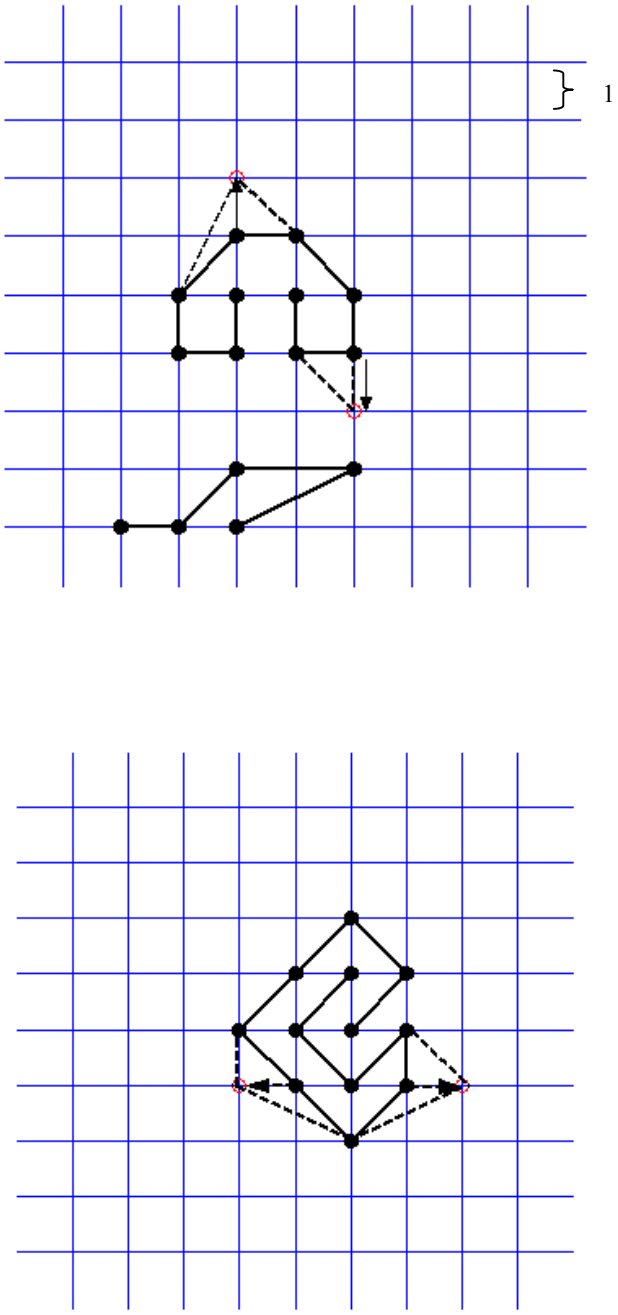

Figure 3.21. Dead lock conformations of fixed bond length model can be solved by bond fluctuation model and possible bond lengths for bond fluctuation model.

The three component system consists of polymer and drug molecules and void space. During the simulation, sites can accept any exchanges between these three components as long as such a move can be made from the neighboring sites. The movement of a component is achieved through exchanging the neighboring sites of different components, including crytallizable components with different orientations.

A step-by-step simulation procedure is described as follows:

1. The two-dimensional, square lattice must be populated using the components with the desired composition. The initial conformation was achieved by assembling the polymer chain first; void second and then the drug molecules. Without applying any energy restriction to the polymer assembly and drug molecules, the random moves of monomer and drug molecules must satisfy the bond length constraint and should prevent any chain session.

2. Using the initial conformation generated by the first step, a lattice site was chosen at random with its four nearest-neighbors. Exchange is possible between components on this randomly chosen site and a neighboring site. If one of the neighboring sites is a void and one is occupied by drug molecule, step 3 is followed. If one is occupied by monomer of polymer chain, one by drug molecule, step 4 is followed. If one has a polymer chain member, and the other one void, then step 5 is followed.

3. A new orientation for grain was selected at random from Q (100) possible orientations. After new position of crystalizable component satisfy the SAW, then the energy difference between new and old configuration was calculated using the Hamiltonian, and

the classical Metropolis algorithm was used to determine if this possible step should be accepted or rejected.

4. A new orientation for crystallizable component was selected at random from Q (100) possible orientations. After checking weather new position of crystallizable component satisfy the SAW, and if the new chain position does not cross other polymer bonds, then the classical Metropolis algorithm was used to determine whether to accept or reject this move.

5. A move can be made to this position while not breaking the chain or crossing over another chain and satisfying the MC Metropolis condition after calculate the energy difference.

6. The number of iterations is increased by 1/N (if 1 was treated as Monte Carlo step) where N is the total number of sites and the program is returned to the step 2.

In order to decide the energy change of a polymer chain, the spring-bead model is used with corresponding stretching " potential", $h(l) = -1/2K(l-l_0)^2$, where $l_0 = 1.68$ and $K = 5$ in the present case. The interaction energy between chain members is fixed at 0.02. One can use L-J potential, but in the lattice model the distance between two objects is fixed and only the energy difference is of importance, therefore fixed interaction energy is provided for a reasonably good approximation.

3.3.2 Results and Discussion

In the free crystal growth process of small molecules, the only driving force is the reduction of surface energy for the crystal/polymer interface. However, when polymer chain and free volume included in the system, the crystal growth is also influenced by the interaction between polymer chain segments. After nucleation, for drug crystals larger than the critical size, further growth is determined by the diffusion fluxes of the drug molecules from relatively distant regions in the system. The diffusion of particles in a polymer matrix is more difficult than matrix consist of small molecules, therefore the crystal growth occurs slowly.

The initial conformation of system is generated by using 400 straight polymer chains with 20 monomer units (N = 20) of bond length 1 and 1000 drug molecules in the 100×100 lattice sites. After the 5×10^7 Monte Carlo Steps (MCS) of simulation in athermal condition, the relaxed polymer chain conformation is taken as the initial conformation and is given in Figure 3.13. The density of system is 80%. The empty space could represent the either drug molecules or voids.

The properties of the polymer resulting from the behavior of polymer chain, such as diffusion properties and glass transition temperature play an important role in the crystallization process. Before investigating the crystallization process, the segmental diffusion in athermal condition is studied to observe the Rouse-type dynamics and reptation in a polymer melt. The segment diffusion can be described as $g_1(t)$ of monomers:

$$g_1(t) = \frac{1}{5}\sum_{i=N/2-2}^{N/2+2} < (\vec{r_i}(t) - \vec{r_i}(0))^2 > \qquad (3.16)$$

$\vec{r_i}(t)$ being the position of monomer i at time t. The brackets <> means an average over all chains in the system. Only the five members in the middle are used in the calculations to avoid the chain end effects. The simulation is carried out for a system containing only polymer chains (N = 20 and N = 80) with the periodic boundary condition. For short chains in a melts $g_1(t)$ should obey the following power laws according to the Rouse model[94, 95]

$$g_1(t) \propto \begin{cases} t^1, t < \tau_0 \\ t^{1/2}, \tau_0 \le t < \tau_N \\ t^1, t \ge \tau_N \end{cases} \qquad (3.17)$$

For time shorter than τ_0, the monomer diffuses freely and $\tau_n \sim N^2$ is the largest relaxation time the chain has (the Rouse relaxation time). However for large chains the reptation behavior[96, 97] can be observed. For the chains larger than a critical entanglement length N_e, $g_1(t)$ should be described by following power-law:

$$g_1(t) \begin{cases} t^1, t < \tau_0 \\ t^{1/2}, \tau_0 \le t < \tau_e \sim N_e^2 \\ t^{1/4}, \tau_e \le t < \tau_N \sim N^2 \\ t^{1/2}, \tau_N \le t < \tau_d \sim N^3 / N_e \\ t^1, \tau_d \le t \end{cases} \qquad (3.18)$$

In the new time range $\tau_e \leq t < \tau_d$, the chain should exhibit a Rouse diffusion along it is a coarse-grained random walk structure. The chain is confined in a so-called tube built by the surrounding chains. Walking out of this tube by performing wormlike displacement is “reptation” of polymer chain.

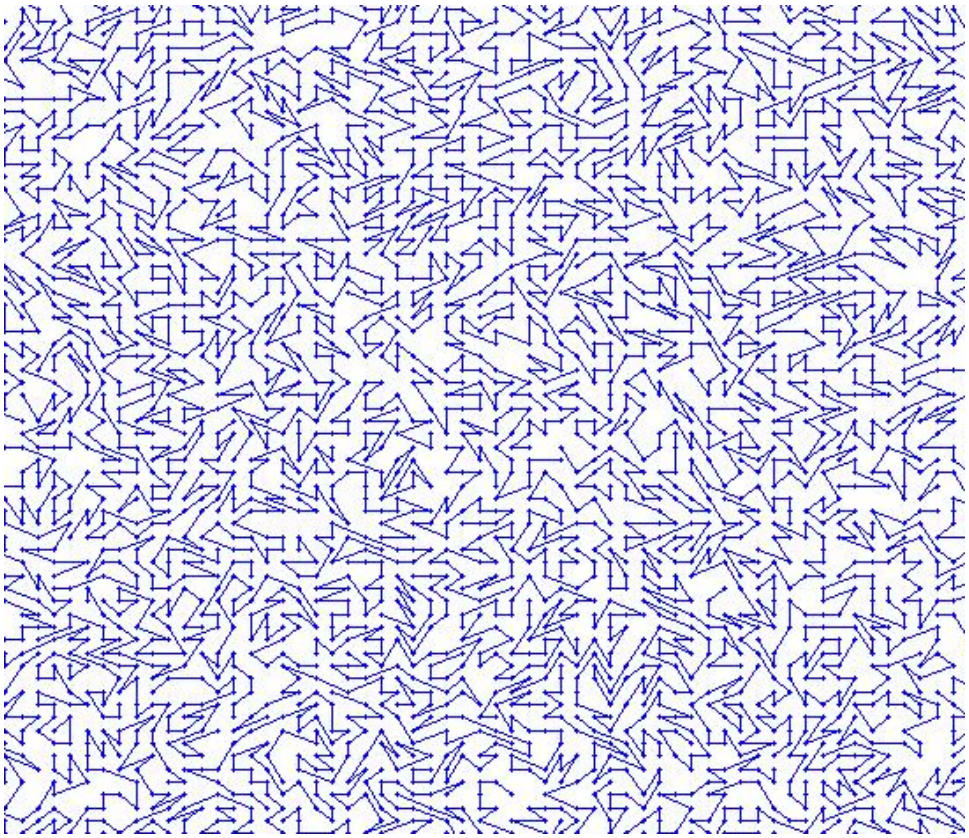

Figure 3.22. Initial conformation for polymer chains (400 polymer chains of 20 monomer units, 1000 voids and 1000 drug molecules in 100×100 lattices)

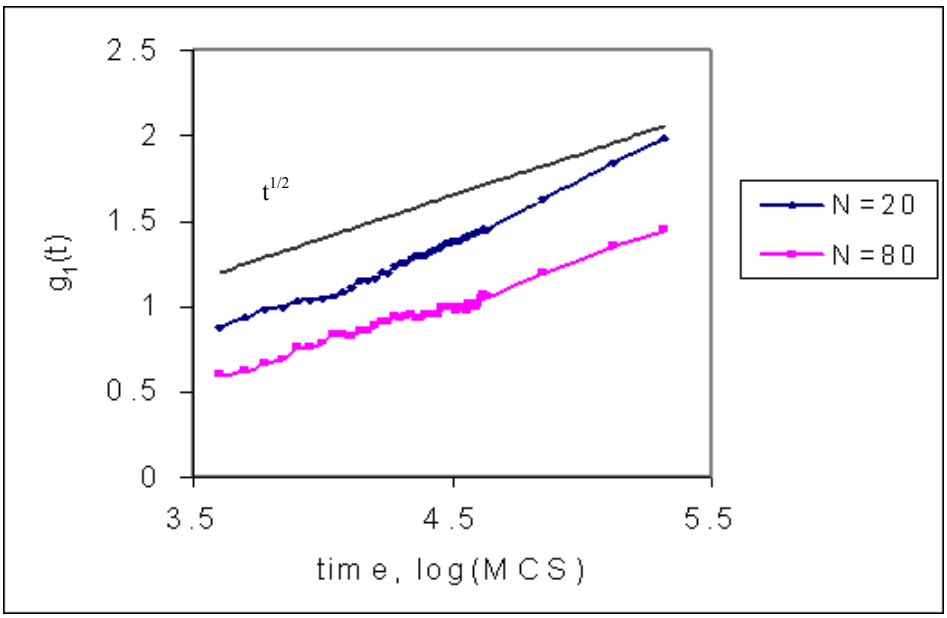

(a) segment diffusion $g_1(t)$ in the intermediate time regime.

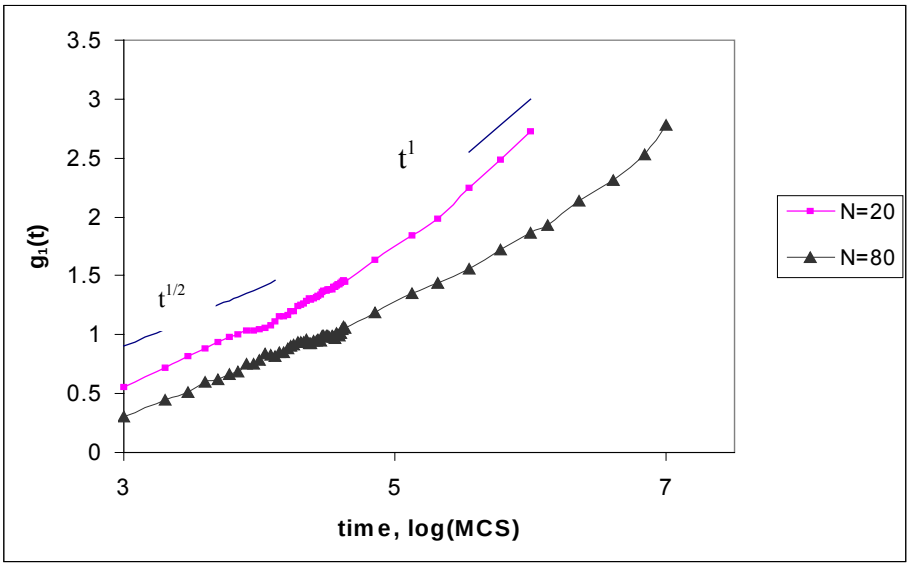

Figure 3.23. (b)Segment diffusion $g_1(t)$ for chain length N = 20 and 80 and polymer density 0.8.

Figure 3.23 gives the $g_1(t)$ of chain length 20 and 80 and polymer density 0.8 in an athermal condition. Since the free move in the initial period (~t) behavior is hard to observe, the data in this time range is omitted. For chain length of 80, diffusion occurs with a time exponent less than 1/2 for intermediate times. In Figure 3.23 (a), it is shown clearly that for chain length 20 the slowdown is around log (MCS) 4 and 4.5 for chain length 80. After a very long time, greater than 10^5 MCS for N = 20 and 10^6 MCS for N = 80, the polymer chain can move freely. These diffusion results confirm that the initial system is liquid like and show some ‘reptation‘ behavior for the longer chain. Overall, the time to generate initial conformation is far longer than that of free moves, therefore the initial conformation is random.

The glass transition is an important property for polymers, both as a theoretical and experimental point of view. Below Tg the polymer chain does not have enough mobility thus the diffusion of the polymer chain or drug molecules is very difficult if not impossible. This behavior can be modeled in the framework of the bond fluctuation model when the polymer melt is cooled down sufficiently by proper technique. A high polymer density is required because the topological constraint in this dense system leads to the slow movement as the temperature drops below glass transition temperature in the polymer. Then some parameter change results from this slow movement can be detected. In order to extract the Tg from the simulation, one has to find some distinguishing property that changes directly with the temperature. Fortunately, the free volume and chain end to end distance can provide this change for this system from the cooling or heating process.

In the Monte Carlo simulation, since only monomers in the nearest neighbor influence the movement of a monomer unit, free volume is only considered as a local quantity. In this study, only monomer jumps satisfying self void movement, new bond length restriction and the jump allowed by the Metropolis procedure are accounted as completed jumps to calculate the free volume. Under these conditions, the free volume V_f is defined as[98]:

$$V_f(T) = \frac{1}{2d}\sum_{v=1}^{2d} v \bullet p(v,T) = \frac{1}{2d}\frac{1}{N}\sum_{n=1}^{N} < v_{npc} >_{pc}$$

Where the free volume is normalized to $0 \leq V_f \leq 1$ by the factor (1/2d). Here d is dimension. Simulations are carried out for systems with polymer density 0.8 and chain length N = 20 and 80 respectively. The cooling temperature is 2.5×10^{-7} ($1°/MCS^{-1}$). The chain length is 80 and 20 respectively. The V_f vs MCS is plotted in the Figure 3.24, from which the Tg is determined to be $k_bT = 1/2.1$ for both N = 80 and N = 20.

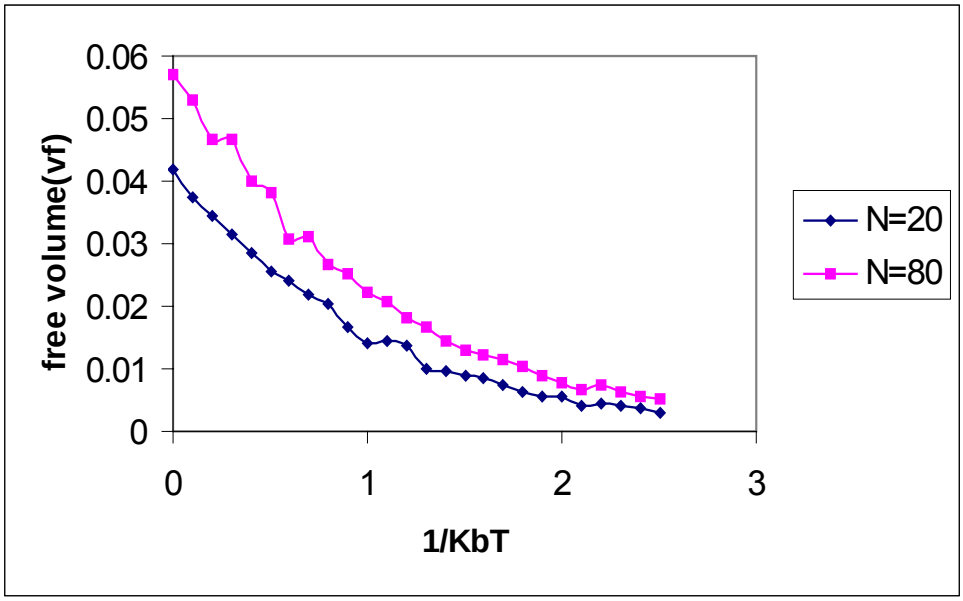

Figure 3.24. Glass transition from free volume for polymer chain length 20 and 80. Polymer density is 0.8 and cooling rate is 2.5×10^{-7} ($1°/MCS^{-1}$).

The Monte Carlo simulation, in contrast to molecular dynamics procedure, is governed by a stochastic hopping process. For this polymer and small molecule system as a lattice model, single monomer of a polymer chain or drug molecule could carry out a stochastic jump. The measure of efficiency of this Monte Carlo simulation is the rate of acceptance of these trial jumps. For the system of 80% polymer and 10% drug molecules, the rate of acceptance can be calculated from the Figure 3.25. For $k_bT = 0.9$, rate of acceptance is around 0.031(jumps/MCS), 0.011(jumps/MCS)) for $k_bT = 0.6$ and 0.0054(jumps/MCS) for $k_bT = 0.3$. The data shows good acceptance for all the simulation process and it drops as temperature decreases.

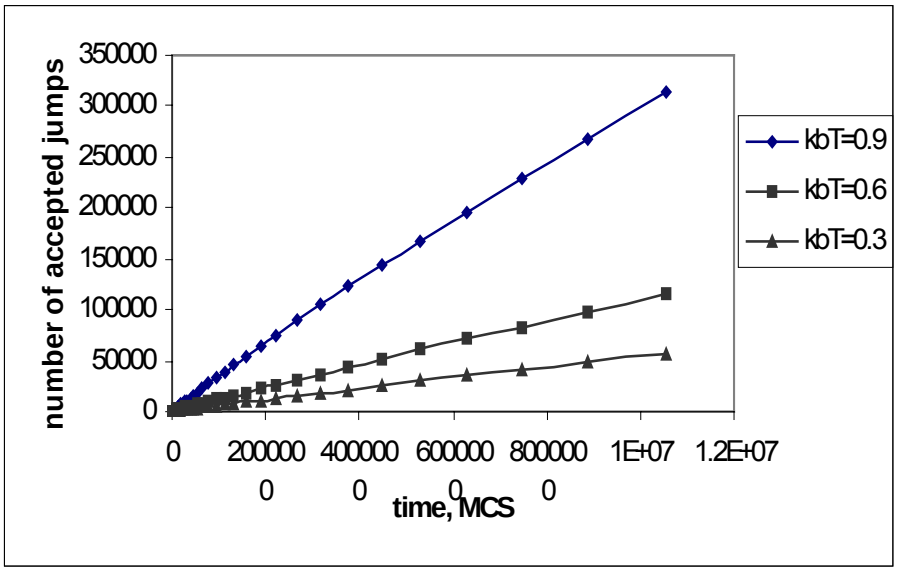

Figure 3.25. Rate of acceptance for N = 20 polymer density 0.8, drug concentration 0.1.

The snapshots of crystal growth process in the different temperature are given in the Figure 3.26.The lines represent bonds in polymer chain, the empty circles are voids and the empty spaces are crystals. The same Ostwald ripening process is observed in these pictures comparing the simulation of the small molecule system. For the lower temperature ($k_bT = 0.6$), small crystals evenly distributed in the matrix, and the crystal size slowly grows. But for the higher temperature ($k_bT = 0.9$), one bigger crystal is

formed in the matrix.

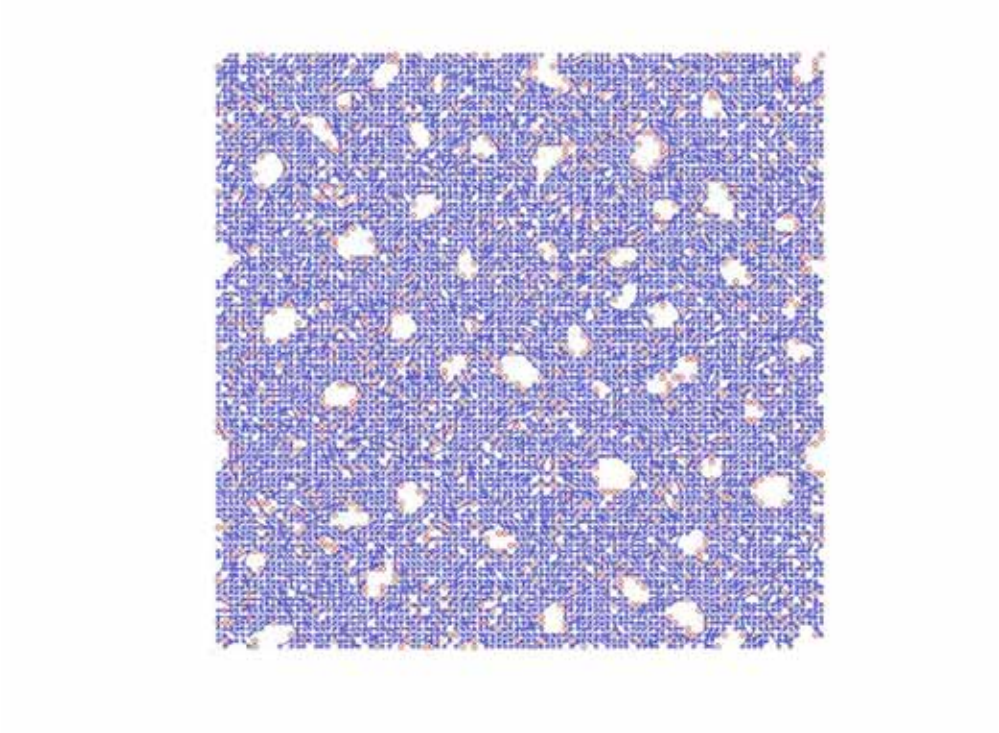

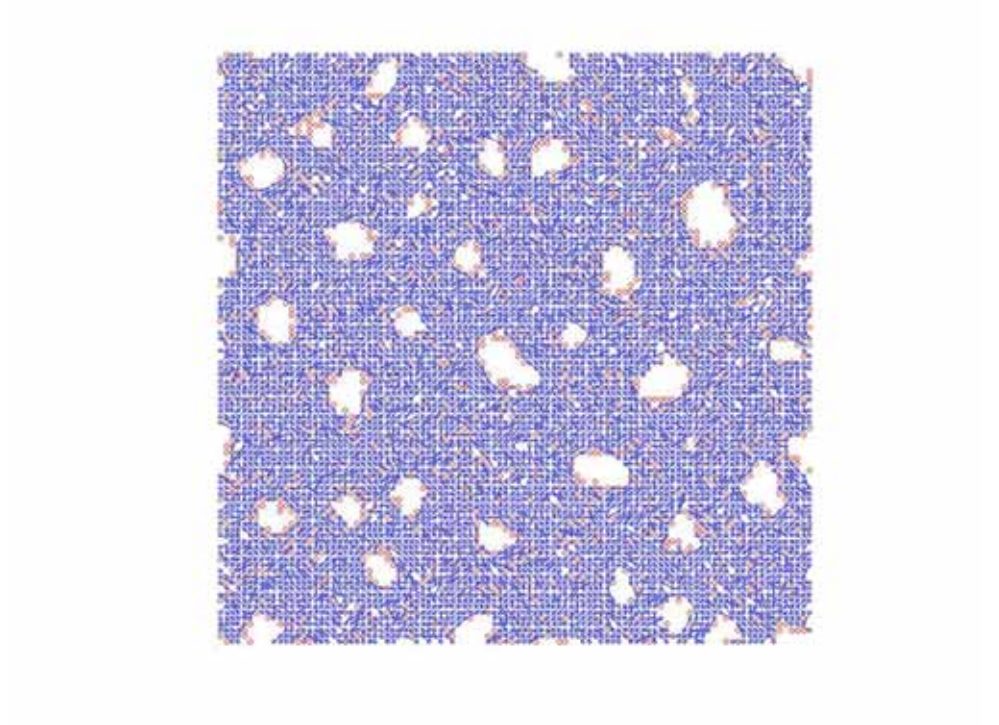

Figure 3.26 (a) and (b)

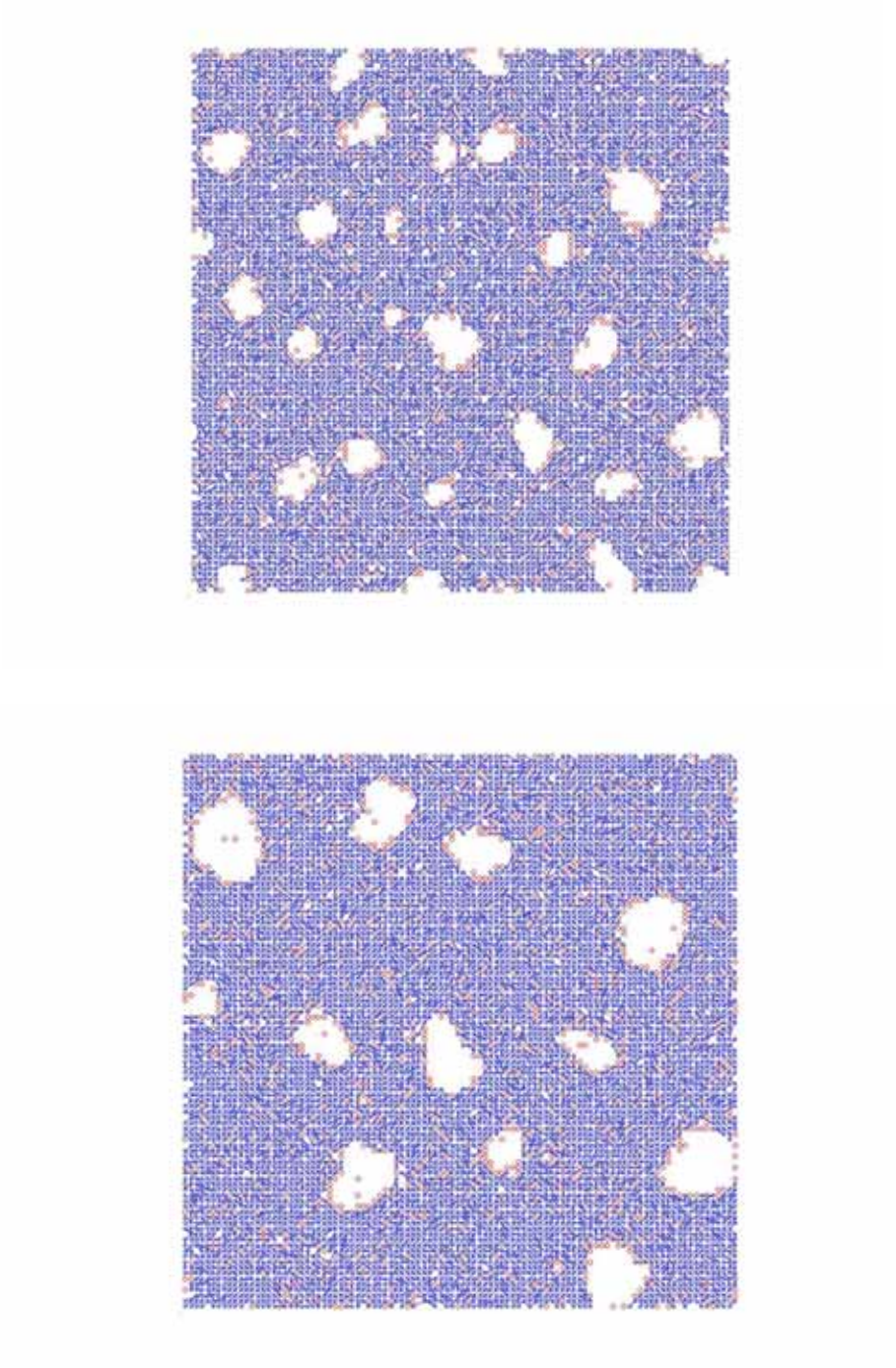

Figure 3.26. Microstructure evolution of crystal growth in k_bT=0.6. (a) MCS=269217 (b) MCS=2661984 (c) MCS=10541884 (d) MCS=90979056. N = 20, polymer density 0.8, drug concentration 0.1. Lines represent polymer chains, empty circle is void, empty space are drug crystals.

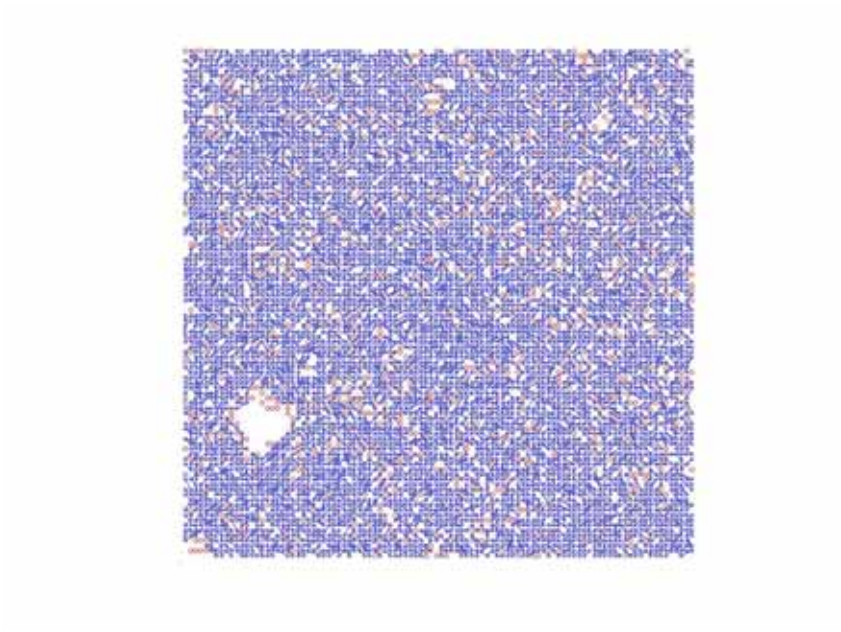

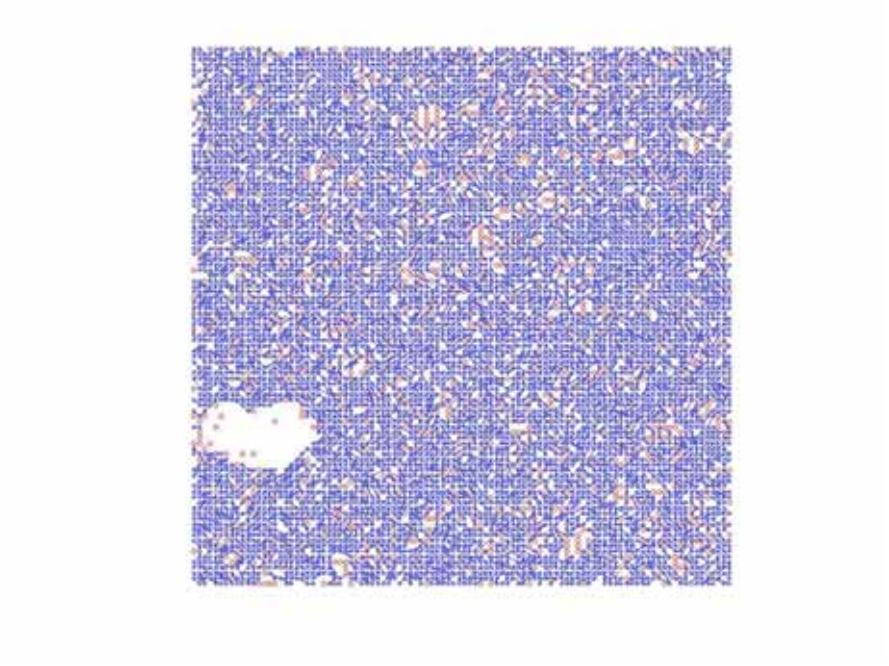

Figure 3.27 (a) and (b)

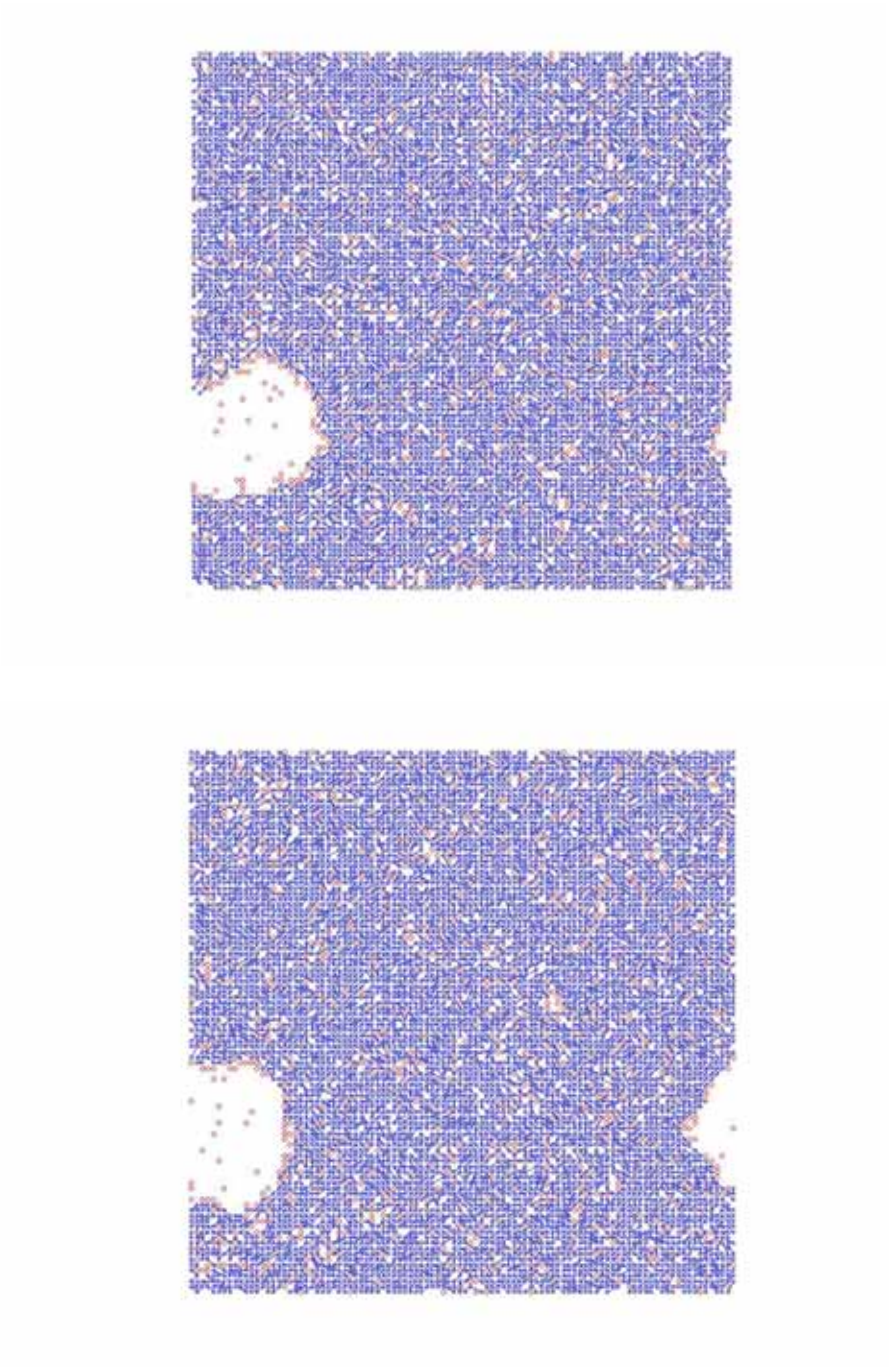

Figure 3.27. Microstructure evolution of crystal growth in k_bT=0.9 (a) MCS=1113242 (b) MCS=1579662 (c) MCS=4471005 (d) MCS=80437176. N = 20, polymer density 0.8, drug concentration 10%. Lines represent polymer chains, empty circle is void, empty space are drug crystals.

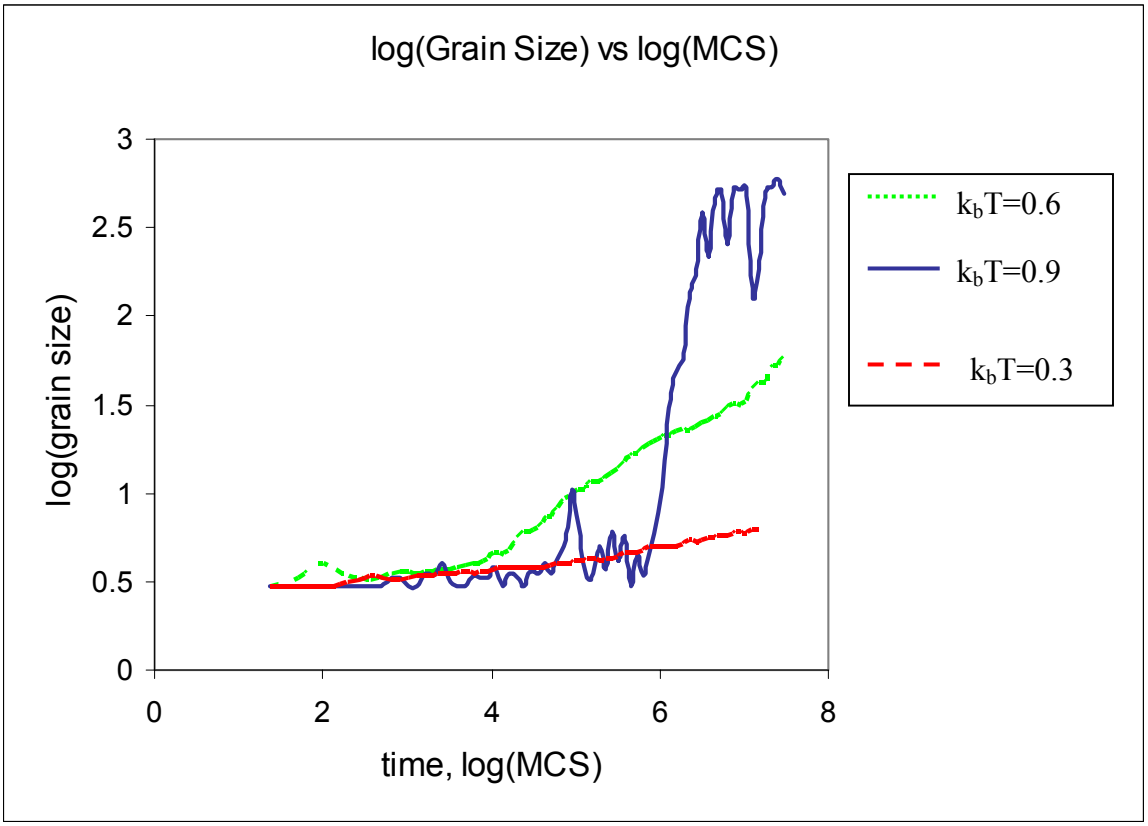

Figure 3.28. Crystal growths in different temperature. N = 20, polymer density 0.8, drug concentration 0.1.

Figure 3.28 shows that the crystal growth process is similar in pattern with the simulation results using the Potts model . However, the nucleation time is much longer compared with the same process at the same temperature due to the slow movement of drug molecule in viscous media. For higher temperature simulation, crystal growth rate is not affected by the size effect of polymer chains. A slowdown of the crystal growth is observed for lower temperature $K_bT = 0.6$ compared to results from the Potts model. The higher the temperature, the longer the nucleation time and faster crystal growth are

observed compared to the Polt model. For $k_bT = 0.9$, when there is only one big crystal in the matrix, the fluctuations are observed for the volume of average crystal size due to the formation of small nuclei. These small nuclei can make the average size drop. However the average size goes back when these small nuclei dissolve. For the $k_bT = 0.3$, the temperature is lower than the Tg, the polymer chain is frozen and diffusion of drug molecules is very slow thus characterization of crystallization is difficult. In this system with a low concentration of drug, a higher diffusion is necessary before several molecules can cluster together. Figure 3.29 shows the concentration changes of drug molecules during the crystallization process. For temperature $k_bT = 0.9$ case, concentration can stay up to 10^6 MCS with little change, and drug crystal grow rapidly after the nucleation accompanied by a dramatic drop in the concentration of dissolved drug in the matrix. For temperature $k_bT = 0.6$ case, small crystals can form at very early stage and concentration drop gradually. For $k_bT = 0.3$, due to the difficulty of diffusion, only small crystals can form and it takes a long time to reach the saturation concentration.

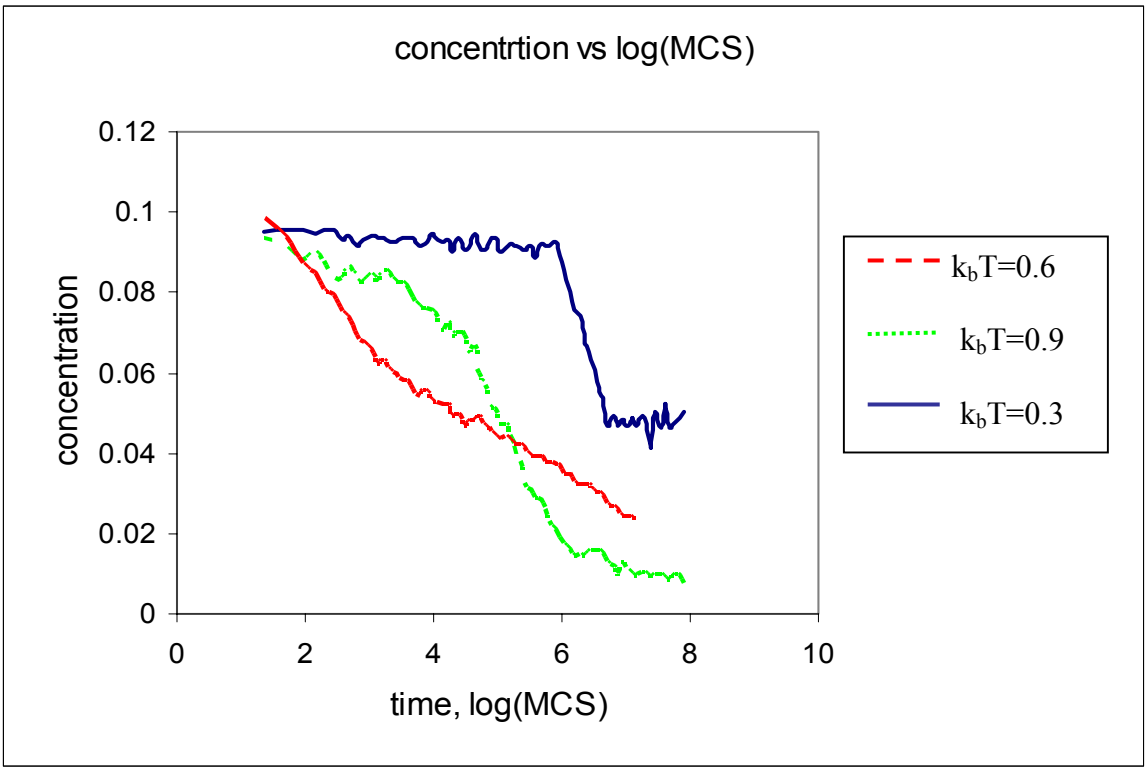

Figure 3.29. Concentration vs log (MCS) for k_bT = 0.9, 0.6 and 0.3. N = 20, polymer density 0.8, drug concentration 0.1.

Figure 3.30 shows enlarged microstructure of this process in two temperatures k_bT = 0.9, and 0.6. The ordered and stretched regions of polymer chains along the interface of the crystal are observed with the growth of the crystal. It is also noted that a larger fraction of voids are located at the interface region between polymer chains and crystals, this is the result of favorable entropy of polymer chains lying along the crystal surface.

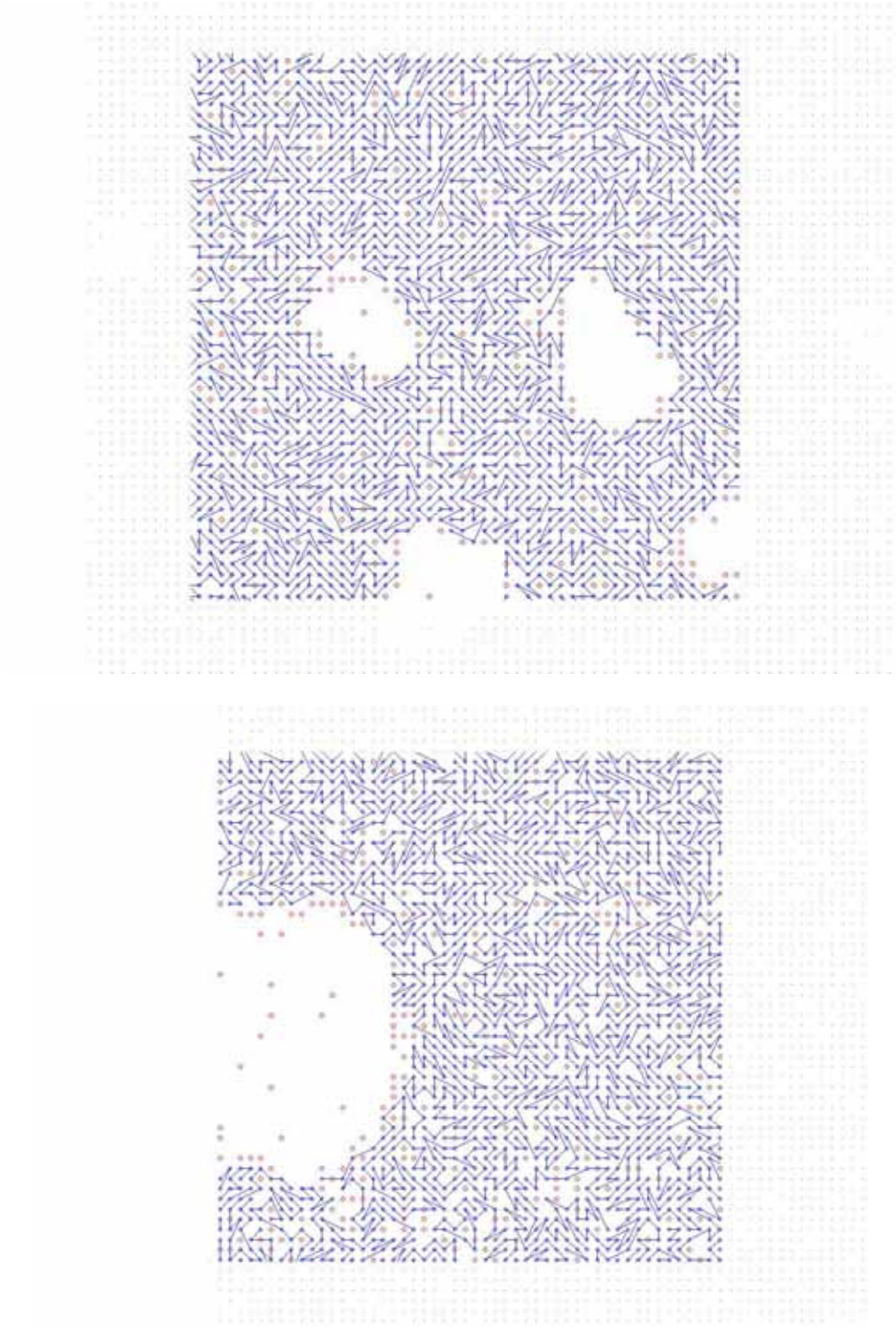

Figure 3.30. Enlarged microstructure of this process in two temperature k_bT = 0.9, and 0.6 for chain length N=20. Polymer density 0.8, drug concentration 0.1. Lines represent polymer chains, empty circle is void, empty space is drug crystal.

3.3.3 Conclusions

The bond fluctuation model was successfully implemented in the three components system. It was found that the algorithm is very efficient. The glass transition temperature for this system is around $k_bT = 1/2$ for N = 80 and for N = 20. The crystal growth process is slower because the diffusion of drug in the polymer media is more difficult in the polymer matrix where the actual size effect of polymer is considered, compared to using the Potts model, especially when the temperature is less than the glass transition in bond fluctuation model. There is no Tg for the system in the Potts model. The stretched and ordered regions of polymer chain along the crystals are found.

3.4 Depletion of Drug in TDS

The mass transportation in TDS is completely driven by the diffusion[99, 100]. Diffusion in TDS takes place as the drug molecules in the matrix move to the skin, which is treated as a perfect sink. Therefore our former model to describe the crystal growth using Potts model for Ostwald ripening mechanism can be modified to simulate both solution diffusion and precipitation.

In this work, the model developed in reference [84] has been modified to allow the diffusion of drug molecules and isotropic grain growth of a fully wetted crystalizable component at the same time. The dispersed or dissolved drug is allowed to be absorbed to the sink due to the concentration gradient realized as random movement of molecules. The details of the chemical structure of the drug and the matrix are not considered in this modeling since this is not an atomistic model, rather the drug and matrix are

approximated by sites of equal size. The Monte Carlo model uses the classical Metropolis algorithm to simulate time dependent diffusion of the TDS. The patch is treated as an infinite strip by using periodic boundary conditions on the plane of TDS. However, across the thickness of the strip periodic conditions are not used. One edge restricts solute from moving out from region, the other one allows complete absorption (Figure 3.31). The details of the modeling procedure are described in the following section.

3.4.1 Simulation Method

A statistical model is used to represent grain migration and its growth. As in reference [84], a square lattice with by different states (q) is used to represent either the matrix or solvent of different orientation. The drug is represented by the q-states 1 to Q = 100 and the matrix by just one q-state.

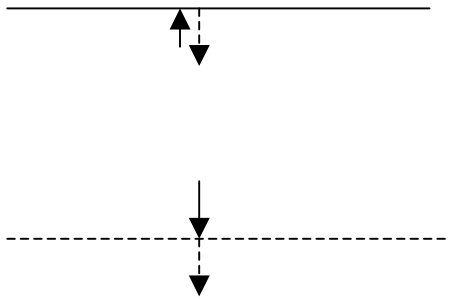

Figure 3.31. Layout of simulation system for drug diffusion.

Dissolution and diffusion of *A*-component (i.e., drug) was driven by concentration gradient caused by the perfect sink. The Hamiltonian H for this two-phase system was

determined by equation (3.13) described in 3.2. The monomers occupying the sites can randomly walk if these sites contain different components, i.e., an idealized drug site and a matrix site. If these sites contain identical components, either drug or matrix, the possibility of exchange has no significance. The exchange probability is given by Boltzmann statistics also described in section 3.2.1

All grain diffusion simulation was run in the fully wetted condition with interaction energies, E(drug-matrix) = 1.0, E(drug-drug of different orientations, q) = 2.5, E(drug-drug of same orientation, q) = 0, and E(matrix-matrix) = 0. The total number of orientation states of the drug Q is taken to be 100. The composition was varied by changing the concentration of drug X_D from 0.05 to 0.1 (given in volume fraction), and the temperature parameter ranges of k_bT = 0.6, and 0.9. The results of former study are used as input to study the drug release pattern in the presence of different kinds of crystals in the matrix. The digitized simulation matrix has 100×100 sites. Although this small size was suitable for gaining insight into the crystallization process in TDS with reasonable computing requirements, larger sites (eg. 300x300 or 500x500) must be used for more accurate simulation results. Since no periodic boundary conditions exist along the thickness, particles near one end have "reflective" boundary conditions, i.e, a particle on a boundary is only allowed to move towards the center layer of the patch where it reaches this boundary, and on the other boundary the drug is absorbed.

3.4.2 Results and discussion

Diffusion is naturally a probabilistic process described by the random walk of molecules. Figure 3.32 shows the diffusion process of initially randomly distributed system of

uniform drug concentration of 0.1 at simulation temperature $k_bT = 0.9$. The dark continuous region is the matrix and the gray areas are grains of different orientation. On the molecular level the system is in a highly dynamic state, thus leads to the drug molecules to flow or diffuse in the system nonselectively and randomly. The "absorption" property of bottom edge in the matrix results in the net mass"movement" caused by the concentration gradient of drug molecules. This concentration gradient ultimately expands through the whole matrix. This concentration gradient towards the "perfect sink" provides the driving force for the drug to move out of the matrix. Simulations are carried out with (1) patch where the drug is uniformly distributed (case 1) and (2) patch after storage which contain crystallized drugs. The second set of simulations can provide insight both on dissolution drug crystals as well as diffusion of drug molecules. Figures 3.33-3.35 show this drug release process in TDS with crystals produced at storage in the $k_bT = 0.9$ (case 3), $k_bT = 0.6$ (case 2) and $k_bT = 0.3$ (case 4) respectively described in section 3.2.3. In these cases, with the crystals presence in the system, the dissolution of the drug molecules is described by the detachment of individual drug particles from grains followed an increase in drug concentration in the matrix which increases the driving force for diffusion into the perfect sink. However, it should be noted that the dissolution mechanism is also governed by the existing concentration of drug in the matrix, which is also controlled by the diffusion process.

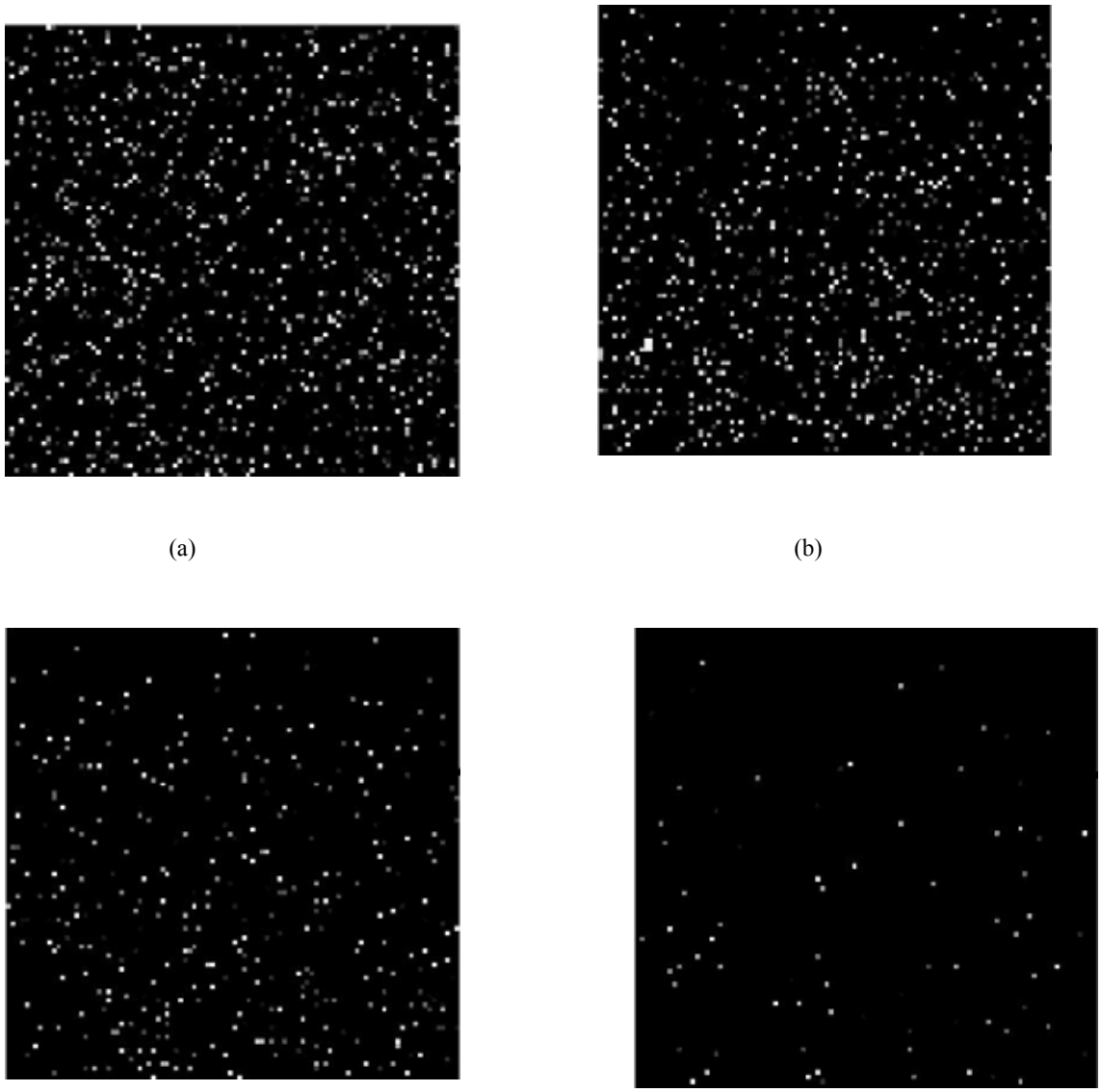

(a) (b)

(c) (d)

Figure 3.32. Snapshot at different Monte Carlo Time Steps (MCS) of the drug release for $K_bT = 0.9$ with random initial conformation (case 1). Concentration of *A* component 0.1: (a) MCS = 0 (b) MCS = 1045 (c) MCS = 6042 (d) MCS = 16464. The dark continuous feature is the liquid matrix and the different gray features are grains with different orientation.

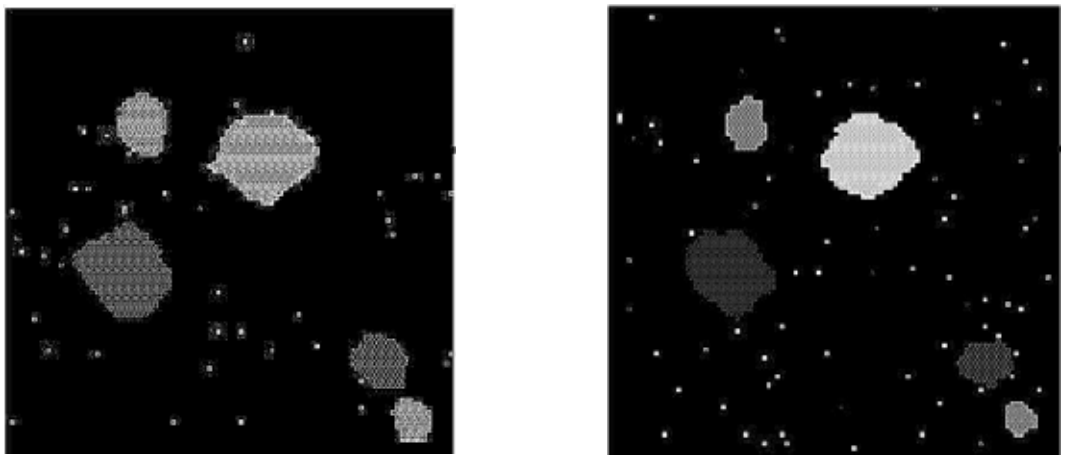

(a) (b)

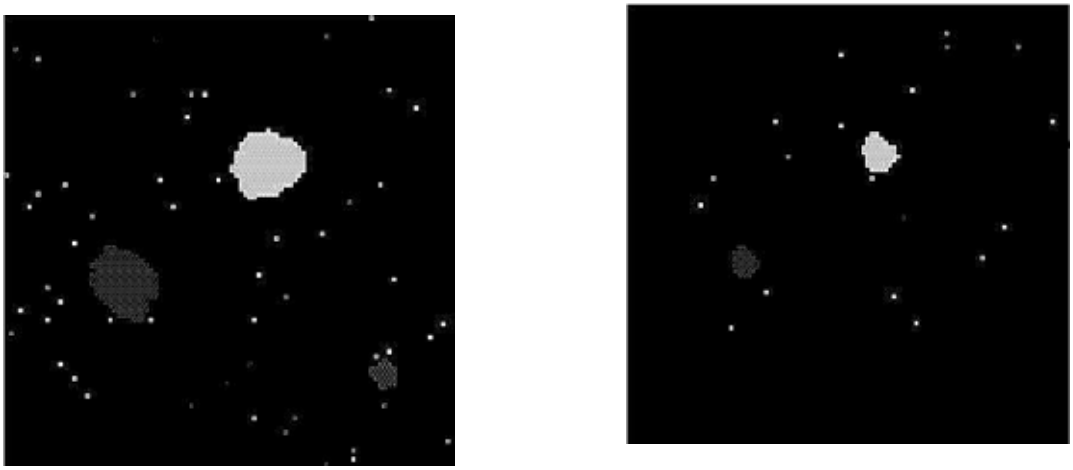

(c) (d)

Figure 3.33. Snapshot at different Monte Carlo Time Steps (MCS) of the drug release for K_bT=0.9 with several crystals in matrix (case 2). Concentration of *A* component 0.1: (a) MCS = 3216 (b) MCS = 20000 (c) MCS = 62403 (d) MCS = 130445. The dark continuous feature is the liquid matrix and the different gray features are grains with different orientation.

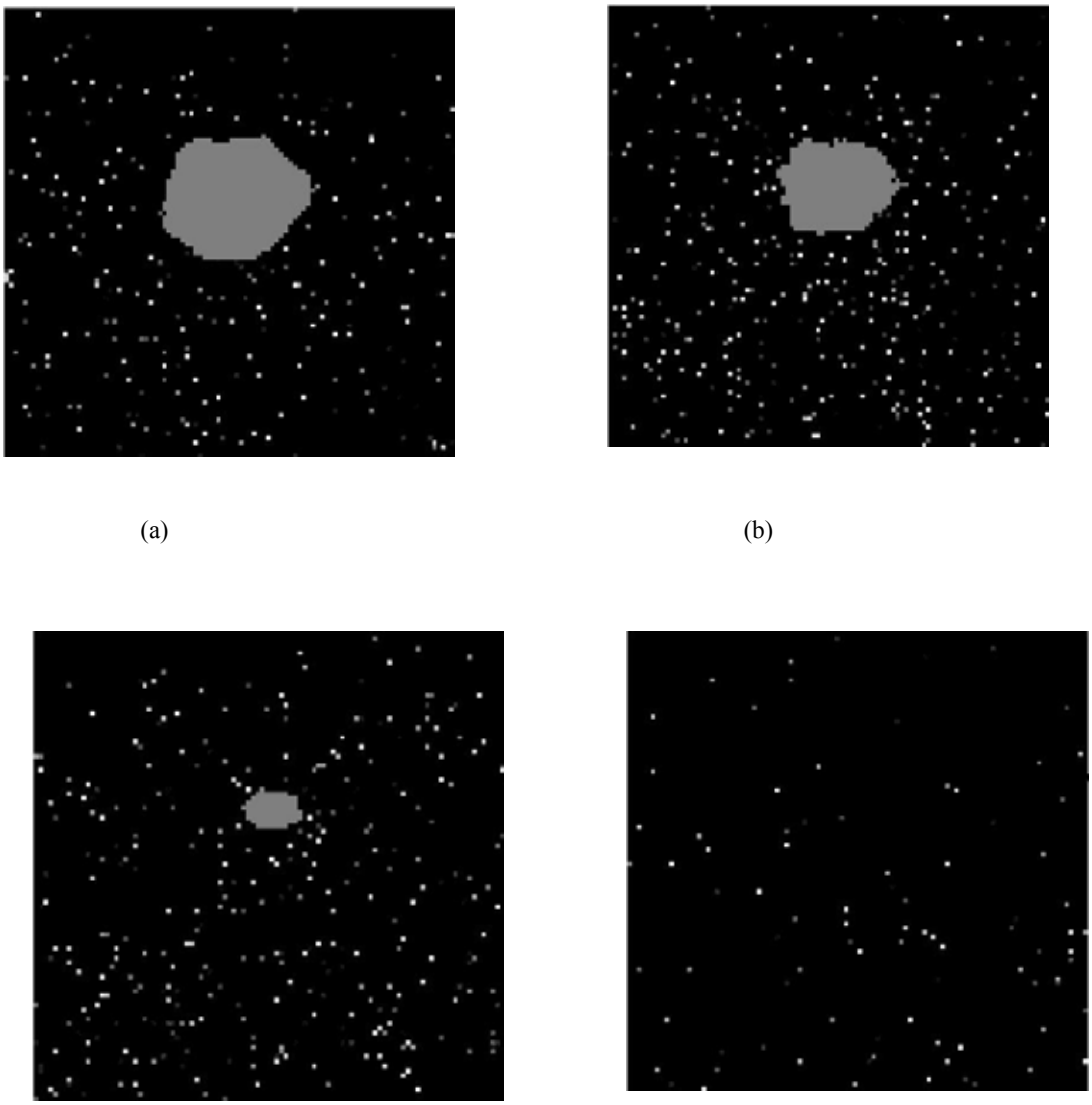

Figure 3.34. Snapshot at different Monte Carlo Time Steps (MCS) of the drug release for K_bT=0.9 with one big crystal in matrix (case 3). Concentration of *A* component 0.1: (a) MCS = 1320 (b) MCS = 51780 (c) MCS = 224846 (d) MCS = 322120. The dark continuous feature is the liquid matrix and the different gray features are grains with different orientation.

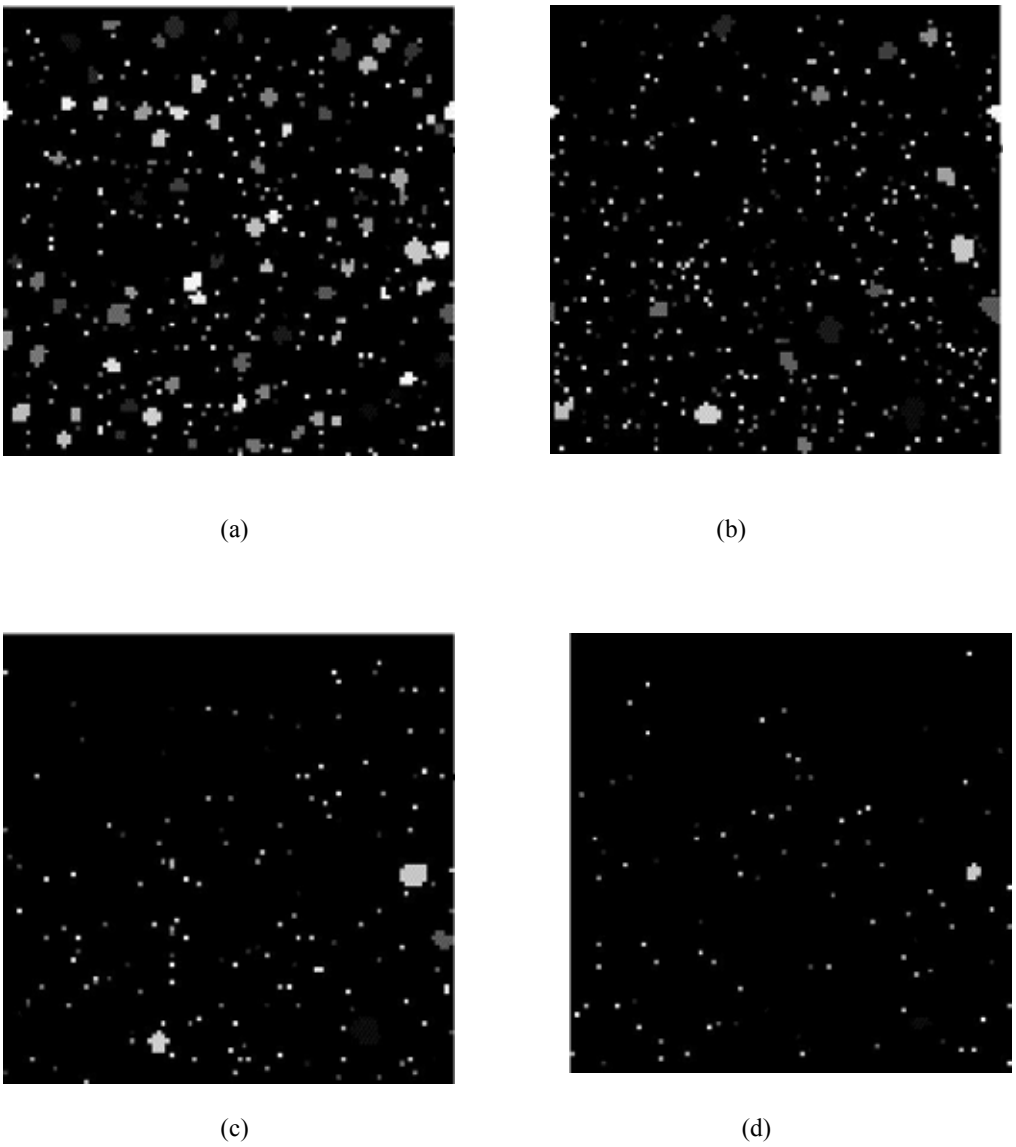

Figure 3.35. Snapshot at different Monte Carlo Time Steps (MCS) of the drug release for $K_bT = 0.9$ with many small crystals in matrix (case 4). Concentration of *A* component 0.1: (a) MCS = 824 (b) MCS = 4914 (c) MCS = 16464 (d) MCS = 24258. The dark continuous feature is the liquid matrix and the different gray features are grains with different orientation.

The release profile of the dissolved or uniformly dispersed drug system can generally be described by the Fick's law and the predicted cumulative mass release M_t is proportional to the square root of time[101]. The Figure 3.36 shows the release profile of random initial conformation which represent the device with dissolved or dispersed drug. As shown in Figure 3.36b that mass release rate drops with time. At the first stage, the drug molecules near the release interface only need to travel small mount of distance to reach the perfect sink. The release of these molecules created the concentration gradient, which favor the drug molecule transportation to this release boundary. As drug molecules from the other side have to travel a longer distance, the release rate decreases with time. For the first 60% of drug release the mass release is linearly proportion to the square root of time. For the lower temperature ($k_bT = 0.6$), the two linear stages are observed (Figure 3.37). This observation results from two competing process, as the diffusion of drug process from the TDS and the crystallization of drug within the TDS. Initially, the drug is uniformly distributed within the matrix. The supersaturation of drug in the matrix causes drug molecules to diffuse out, at the same time minimization of interfacial energy results in the growth of the drug crystals. The initial linear region represents the time period determined by diffusion and during the second linear region diffusion is reduced by the crystallization process. From Figure 3.37a, one can observe the crystal size growth. The presence of the crystal will cause the extra barrier to dissolve it first and then diffuse to the release interface, therefore decrease the release rate further[102, 103].

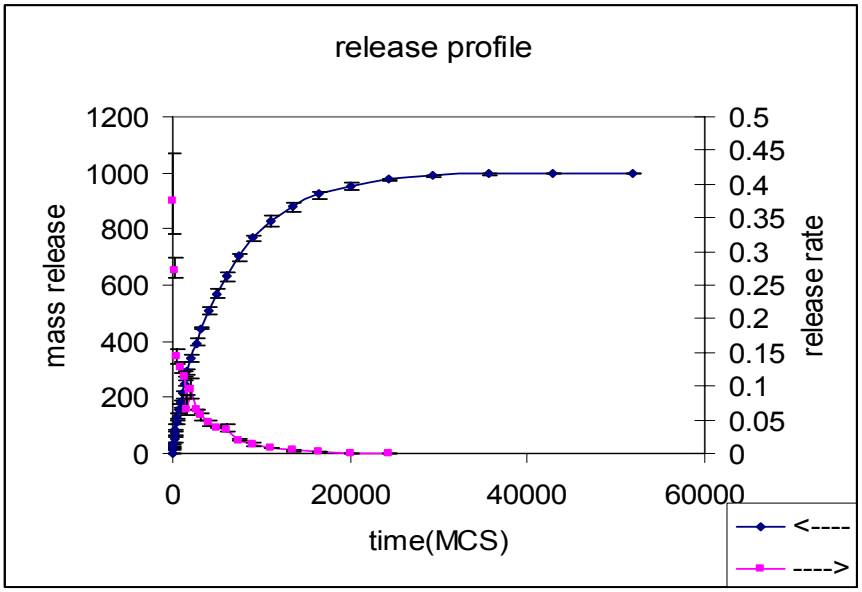

Figure 3.36. Drug mass release vs (a) time and (b) square root of time at $K_bT = 0.9$ for case 1: no crystals in the system initially and the drug concentration is 10%.

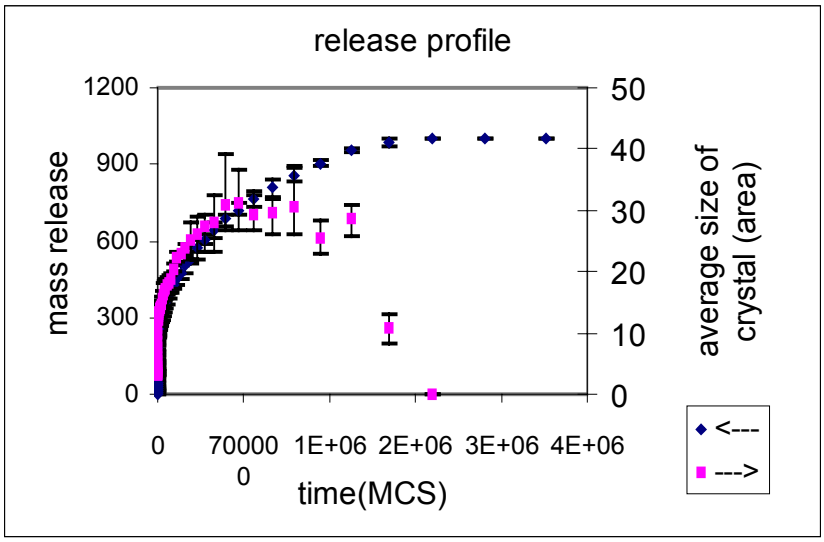

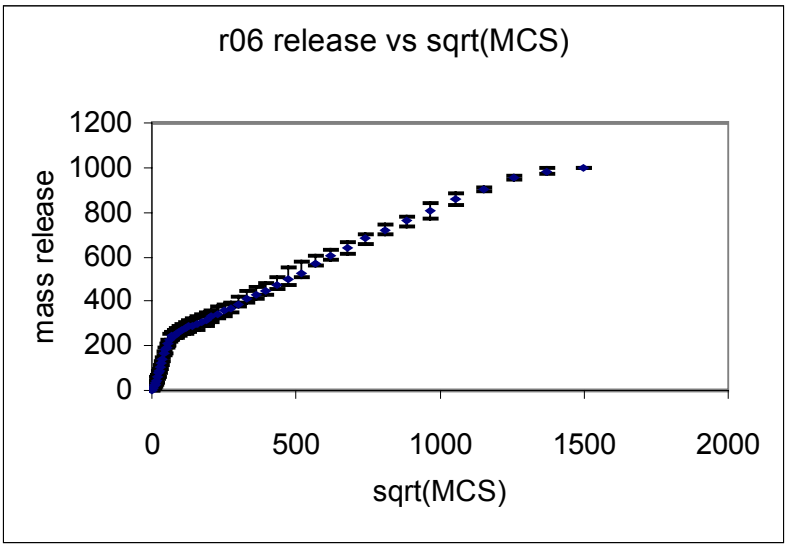

Figure 3.37. Drug mass release vs (a) time (b) square root of time at $k_bT = 0.6$ for case 1: no crystals in the system initially and the drug concentration is 10%.

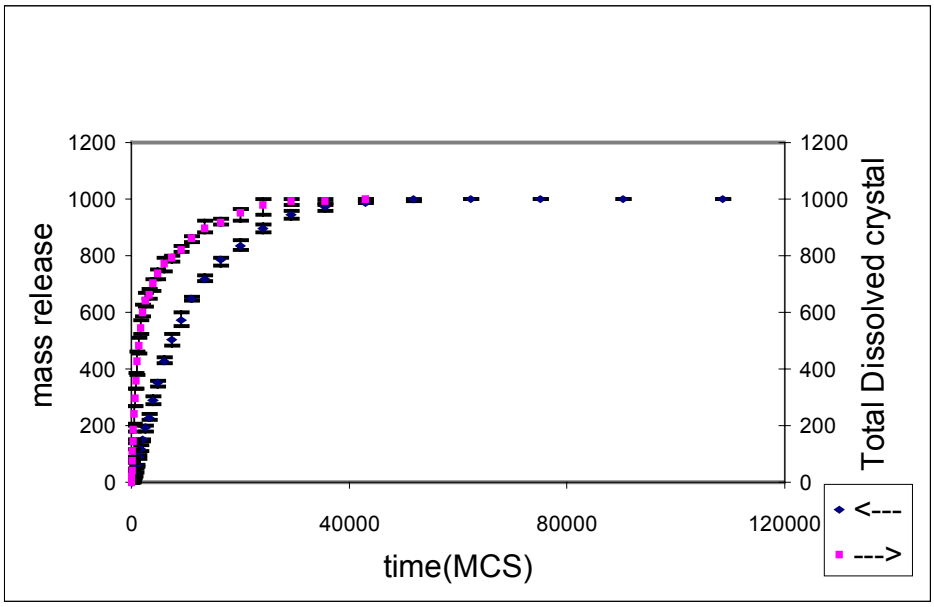

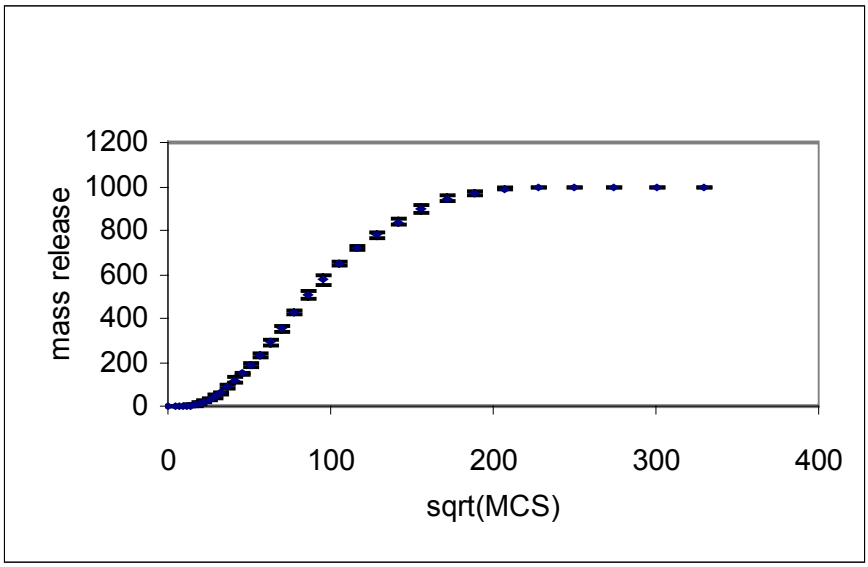

Figure 3.38. Drug mass release vs (a) time (b) square root of time at $k_bT = 0.9$ for case 4: small crystals evenly distributed in the system initially and the drug concentration is 10%

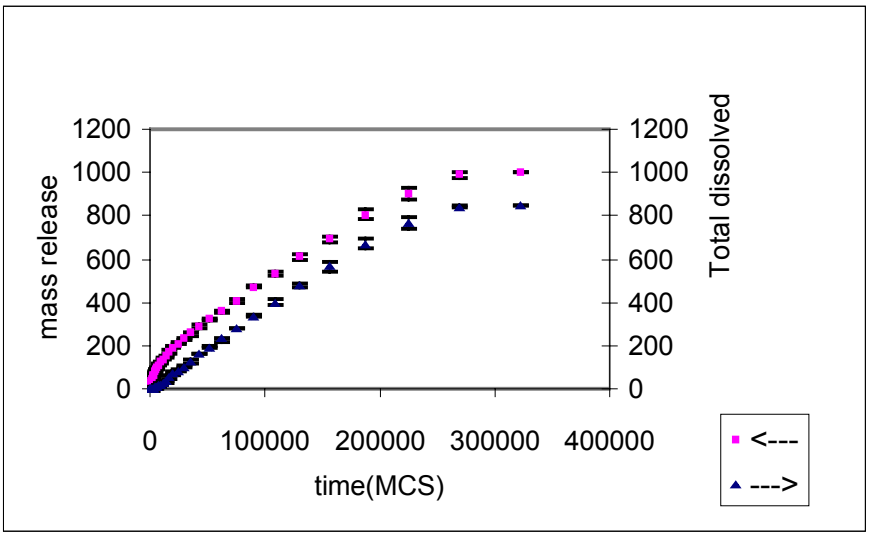

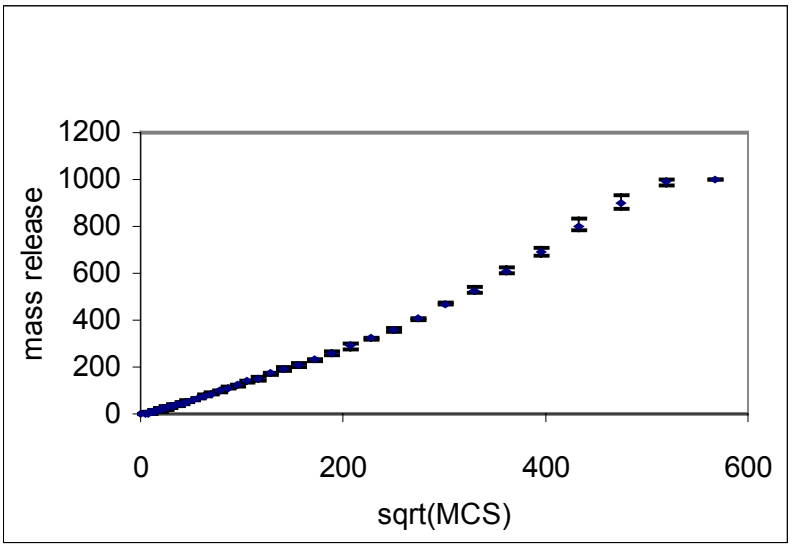

Figure 3.39. Drug mass release vs(a)time (b) square root of time at $k_bT = 0.9$ for case 3: one big crystal in the system initially and the drug concentration is 10%.

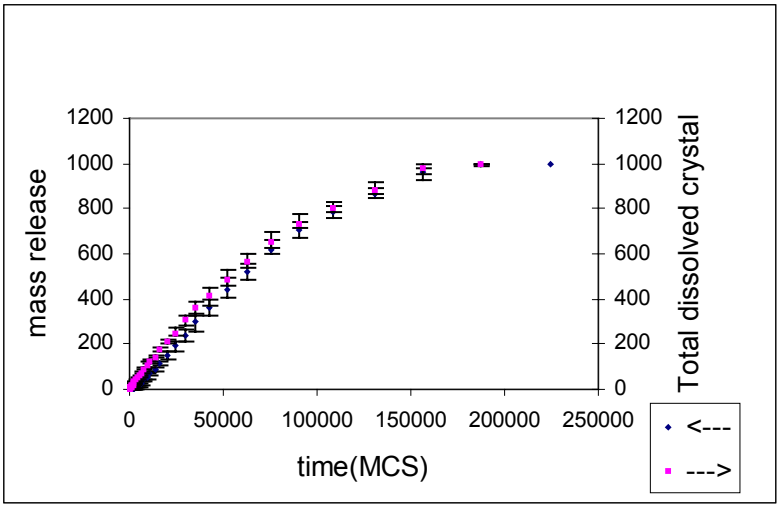

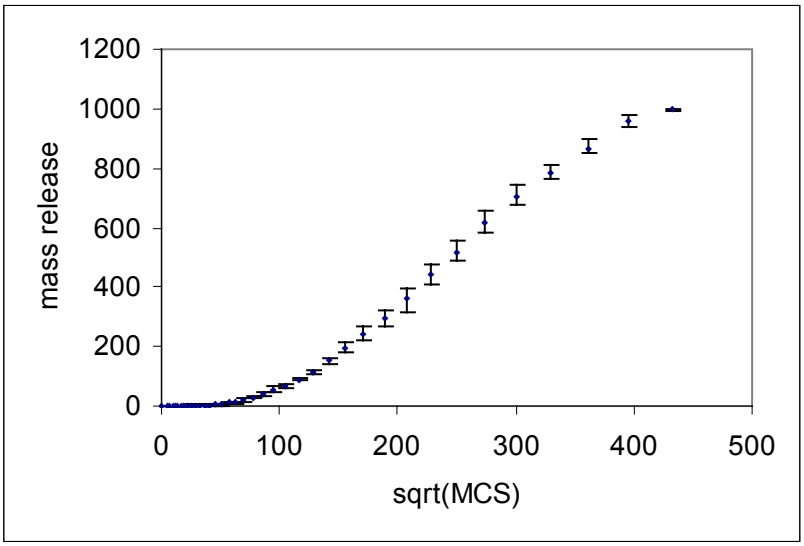

Figure 3.40. Drug release profile at $k_bT = 0.9$ for case 2: several crystals in the system initially and the drug concentration is 10%

The release profiles of drug from a matrix which already contains crystallized drug as opposed to dispersed drug was also investigated with this model. Figure 3.38 shows the results of the release profile for the small crystals generated in temperature $k_bT = 0.3$ with 3.2×10^7 MCS steps. It is observed that the release rate decreases slightly but the mass release profile has a similar behavior and cumulative mass release vs square root time give a similar linear pattern after early stage. In the same figure, it is also observed that dissolution of crystals is faster than mass release because the crystal size is very small, which means that small crystal has little effect on drug release. This behavior describes the system with dispersed drug in the matrix. For the system with one big crystal in the middle produced by simulation in a previous work, the release profile changes significantly (Figure 3.39). The release rate drops quickly after 10000 MCS. The profile shows that fast release is observed only at the very early stage which results from the high saturation concentration in the system at this high temperature. There are still some dissolved molecules in the system except the big crystal, which can diffuse easier than the molecules in the crystal. Drug molecules in the crystal have to dissolve into the matrix first and then migrate to the boundary driven by the concentration gradient. This drug release process is predominantly controlled by the dissolution of crystals. For the case where several crystals are in the middle layer (crystallized in the $k_bT=0.6$), release rate shows a sharper drop earlier in the diffusion process (Figure 3.40) since the saturation concentration is lower at the temperature the $k_bT=0.6$ and hence fewer free drug molecules are available even at the very beginning of this process. Figure 3.40 of mass release vs square root time shows delay of drug release. For this case the mass release and crystal dissolution process of different cases are compared in Figure 3.41. It is

clear that the presence of crystals delays the mass release process. The bigger the crystal, the slower the dissolution and drug release rate.

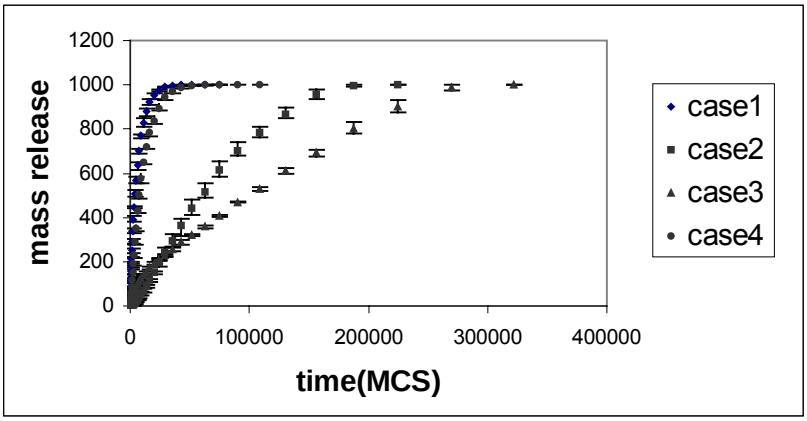

(a) Mass release in different case. All simulation at temperature $k_bT = 0.9$.

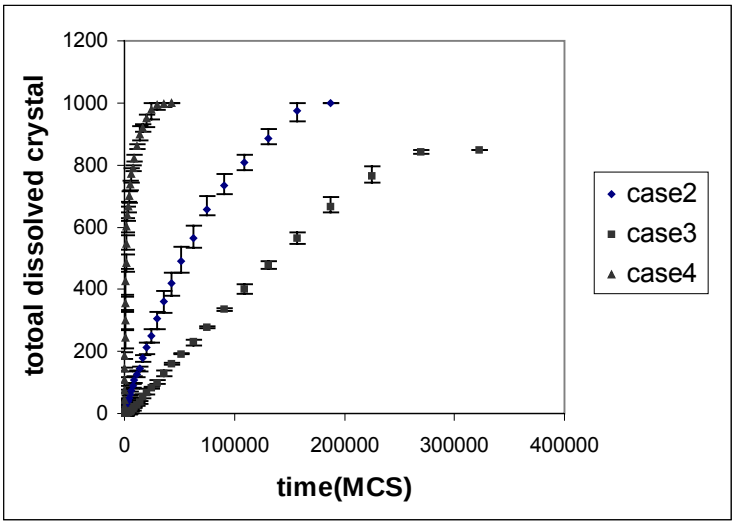

(b) Dissolution of crystal in different case. All simulation at temperature $k_bT = 0.9$.

Figure 3.41. Comparing the mass release and crystal dissolution process in different case. Case 1: no crystal in the system initially, Case 2: Several crystals in the system initially. Case 3: One big crystal in the system initially, Case 4: Small crystals evenly distributed in the system, the drug concentration is 10% for all the cases.

3.4.3 Conclusions

The present study shows that release profile of the drug dissolved or uniformly dispersed in the matrix can be described by the Fick's Law. For example, the release of dispersed dexamethasone from an EVAc matrix follows cumulative mass released proportional to the square root of time[104]. However, for the system having crystals in the middle layer of matrix, the release profile does not have same behavior because the crystal dissolution is a slower process comparing to the molecule transportation rate.

It is clear that the selection of a storage temperature is very important in determining the effectiveness of TDS. When stored at higher temperature, although larger crystals are formed near the middle layer, the solution concentration of the drug is also higher in the matrix. On the other hand, at lower temperature, small crystals are distributed throughout the thickness, but the solution concentration is much lower. Thus the release rate and profile of TDS depend on the dissolution process of the crystal. At low storage temperature, the grains are evenly distributed throughout the thickness of the TDS patch, thus the release rate and profile is similar to the randomly initiated system.

Chapter 4

Conclusions and Recommendations

4.1 Conclusions

1. The two crystal forms are studied by Raman microscopy, SEM, EDS and IR. The Raman spectrum of needle crystal show the peak of aromatic ring and phenyl carbonyl group therefore is identify as a combination of estradiol and acrylic polymer. The IR spectrum of the model reaction sample prepared at 85°C give a carbonyl group absorption as a doublet which is corresponding to aliphatic and aromatic component. This demonstrates evidence for the occurrence of the transesterification reaction.

2. Monte Carlo simulation shows that the crystal growth without stress only gives big crystals in the middle layer by Ostwald Ripening at relatively high temperatures.

3. Bond fluctuation model shows that due to the polymer chain characteristics the crystal growth is slowed down.

4. Depletion study shows that presence of crystal will decrease the transport rate of drug in the matrix.

4.2 Recommendation

1. Diffusion of drug in the polymer media

In order to develop a more efficient controlled delivery system, modeling the release profile plays a significant role because it establishes the mechanisms of the drug release

and provides general guidelines to optimize the release kinetics. Including the mechanistic aspects of the transport processes and structural characteristics of polymer in the drug delivery system, computational modeling can provide a more accurate description of drug release profile. Better analysis of diffusion vs dissolution process also need to be provided.

2. Crystal growth under the shear stress and normal stress.

The crystal morphology could be different if its growth occurs under the applied stress. There is a possibility of the existence of residual stresses when the TDS is prepared and there are shear stresses in the system when TDS is applied to the patient. The shear stress can be introduced by postulating an asymmetry jump rate for the component movement in the direction of flow and in the opposite direction[105]. This work has been done for the pure polymer system under the framework of the bond fluctuation model. The deformation behavior of the glassy polymer system was also studied by T. Holz etc.[106]. Under the same lattice bond fluctuation model, the whole deformation process was divided into separate steps, each initiated by the discreet shift of the minimum of the spring potential on the left and right side of the sample into diametrically opposite direction along the deformation.

3. The process described in section 3.3 can be used for polymer without any drugs, to characterize polymer crystallization, particularly for stress induced crystallization. Such analysis is very useful to characterize crystallization during fiber spinning and drawing.

4. Further characterization of needle crystal

The difficulty of complete characterization of needle crystal is partly due to the lack of knowledge on the formulation of the product. If the needle crystal is the co-crystal of different materials, polymer and small molecule, it is possible that small molecules induce the crystallization of polymer, although matrix polymer acrylic resin is difficult to crystallize by itself as a single component. According to simulation, if there is no stronger associate force between these two or more species, polymer chain will be along the interface of crystals of small molecules. To address this problem, the resolution of microscopy technology has to be far less than the size of the crystal. IR microscopy may be a good route to do this job but the attenuated total reflectance (ATR) is required since our crystal is embedded in the viscous matrix.

References

1. V. V. Ranande, M. A. Hollinger, Drug Delivery Systems, CRC press Inc., Florida, 1996

2. J. R. Robinson, V. H. L. Lee, Drug and the Pharmaceutical Sciences Volume 29: Controlled Drug Delivery: Fundamentals and Applications, Marcel Dekker, New York, 1987

[3] K. Park, Controlled Drug Delivery: Challenges and Strategies, ACS, 1997

[4] J.E. Shaw, M.P. Cramer, and R. Gale, Transdermal Delivery of Drugs, Vol. I (A.F. Kydonieus and B. Berner, Eds.), CRC Press, Boca Raton, Fla., p. 5 (1987)

[5] J.E. Shaw, M.P. Cramer, and R. Gale, Transdermal Delivery of Drugs, Vol. I (A.F. Kydonieus and B. Berner, Eds.), CRC Press, Boca Raton, Fla., p. 106 (1987)

[6] W. R. Good, *Drug Dev. Ind. Pharm.*, 9 (1983) 647.

[7] W.R. Good, M. S. Powers, P.Cambell, and L. Schenkel, *J. Controlled Rel.*, 2(1989)89.

[8] T.R. MacGregor, M. M. Kandace, J.J. Keiras, R. G. A. van Wayjen, A. van den Ende, and R.G.L. van Tol, *Clin. Parmacol. Ther.,* 38(1985)158.

[9] P. Muller, P.R. Imhof, D. Mauli, and D. Milovanonic, *Meth. Find. Exp. Clin. Pharmacol.,* 11(1989)197.

[10] J. P. Dubois, A. Sioufi, P. Muller, D. Mauli, and P.R. Imhof, *Meth. Find. Exp. Clin. Pharmacol.,* 11(1989)187.

[11] J. E. Rose, J.E. Herskovic, Y. Trilling, and M.E. Jarvik, *Clin. Pharmacol, Ther.,* 38(1985)450.

[12] J.R. Varvel, S. L. Shafer, S.S. Hwang, P.A. Coen, and D.R. Stanski, *Anethesiol,* 70(1989) 928.

[13] G.K. Gourlay, S.R. Kowalski, J.L. Plummer, M.J.Cousins, and P.J. Armstrong, *Anesth. Analg.,* 67(1988)329.

[14] P.M. Plezia, T.H. Kramer, J.Linford, and S.R. Hameroft, *Pharmacotherapeutics*, 9(1989) 2.

[15] R. P. Oertel, *Biopolymers*, 16(1977)232.

[16] L.J. DeNoble, K. Knutson, and T. Kurihara-Bergstron, *Pharmaceut. Res. (Suppl.),* 4(1987) S59.

[17] E.R. Cooper and B. Berner, *Transdermal Delivery of Drug, Vol. II* (A.F. Kydonieus and B. Berner Eds.), CRC Press, Boca Raton, Fla., 57(1987).

[18] D.C. Patel and Y. Chan, U.S. Patent 4, 863, 970(1989).

[19] B. Berner, J.H. Otte, G. C. Mazzenga, R.J. Steffens, and C.D. Elbert, *J. Pharm. Sci.,* 78(1989) 314.

[20] B.Berner, G.C. Mazzenga, J.H.Otte, R.J. Steffens, R. H. Juang, and C. D. Elbert, *J. Pharm. Sci.*, 78(1989) 402.

[21] B. Berner, R.H. Juang, and G.C. Mazzenga, *J. Pharm., Sci.,* 78(1989)472.

[22] A.S. Michaels, S.K. Chandrasekaran, and J.E. Shaw, *AIChe J.,* 21(1975)985.

[23] P.S. Campbell and S.K. Chandrasekaran, U.S. Patent, 4,379,454 (1983).

[24] H. Imaizumi, N. Nambu, T. Nagai, *Chem. Pharm. Bull.*, 31(7) (1983) 2510.

[25] A. Burger, R. Ramburger, W. Schmidt, *Pharmazie*, 35(11) (1980) 711.

[26] H. K. Chan, I. Gonda, *Int. J. Pharm.*, 41(1-2) (1988) 147.

[27] K. Kubota, E. H. Twizell, H. I. Maibach, *J. Phar. Sci.*, 83(11) (1994) 1593.

[28] N. E. Variankaval, K. I. Jacob, S. H. Dinh, *Journal of Biomedical Materials Research*, 44 (1999) 397.

[29] N. E. Variankaval, K. I. Jacob, S. H. Dinh, *J. Crystal Growth*, 217 (2000) 320-331

[30] J. Hadgraft, R. H. Guy, Transdermal Drug Delivery: Developmental Issues and Research Initiatives, Marcel Dekker, New York, 1989

[31] F.W.D. Rost, Fluorescence Microscopy, v1, Cambridge University Press 1992,

[32] E.I. Wehry, Effects of Molecular Structure and Molecular Environment on Fluorescence. In: Guilbault, G. G.(ED) Practical Fuorescence: Theory, Methods and Techniques, Ch. 3, pp. 79-136. Marcel Dekker, NewYork, 1973.

[33] E. Heftman, "modern Methods of Steroid Analysis", (Academic Press, New York, 1973).

[34] D.N. Theodorou,, U.W.Suter, *Macromolecules*, 18 (1986) 1467,.

[35] K. Kremer and K. Binder, *Comp. Phys. Repts*., 7 (1988) 259.

[36] . J. Baschnegel, K. Binder, P. Doruker, A. A. Gusev, O. Hahn, K. Kremer, W. L. Mattice, F. Muller-Plathe, M. Murat, W. Paul, S. Santos, U. W. Suter, and V. Triies, *Adv. Polym. Sci.*, 152 (2000) 41.

[37] K. Binder, *Adv. Polym. Sci.*, 112 (1994) 181.

[38] P.E. Rouse, *J. Chem. Phys.*, 21 (1953) 1272.

[39] M. Doi and S.F. Edwards, the Theory of Polymer Dynamics, C;arendon Press, Oxford, 1986,

[40] J. D. Ferry, Viscoelastic Properties of Polymers, Wiley, New York, 1980

[41] D. J. Rigby and R. J. Roe, *J. Chem. Phys.*, 87 (1987) 7285.

[42] D. Brown, J.H. R. Clarke, M. Okuda, and T. Yamazaki, *J. Chem. Phys.*, 100 (1994) 1684, 6011.

[43] J. Baschnagel, K. Binder, W. Paul, M. Laso, U. W. Suter, I. Batoulis, W. Jilge, and T. Bürger, *J. Chem. Phys*., 95 (1991) 6014

[44] K. binder(Ed.) Monte carlo and Molecular Dynamics Simulation in Poymer Science, Oxfors University Press, Oxford, 1995.

[45] P.G. de Gennes, *Macromolecules*, 9 (1976) 587, 594.

[46] I. Carmesin and K. Kremer, *Macromolecules*, 21 (1988) 2819.

[47] h. P. Deutsch and K. Binder, *J, Chem. Phys.*, 94 (1991) 2294.

[48] P.H. Verdier and W.H. Stockmayer, *J. Chem. Phys.*, 36 (1962) 227

[49] P.H. Verdier, *J. Chem. Phys.,* 45(1966)2122

[50] P.G. de Gennes, *Phys. Lett. A*, 38 (1972)329

[51] D.E. Kranbuehl and P.H. Verdier, *J. Chem. Phys.*, 71(1979)2662

[52] P.H. Verdier and D.E. Kranbuehl, *Polymer Preprints (ACS),* 17(2) (1976)148

[53] D.E. Kranbuehl and P.H. Verdier, *Polymer Preprints (ACS)*, 21(2) (1980)1087

[54] N. madras and A.E. Sokal, *J. Stat. Phys.,* 47 (1987)573

[55] P.H. verdier, *J. Comput. Phys.*, 4(1969)204

[56] O. J. Heilmann, *Mat. Fys. Medd. Dan. Vid. Sesk.,* 2(1968)37

[57] F. Geny and L. Monnerie, *J. Polym. Sci. Phys. Ed.,* 17(1979)131

[58] K. Kremer, *Macromolecues*, 16(1083)1632

[59] D. J. Heimann and J. Rotner, *J, Stat. Phys.*, 27(1982) 499

[60] A. Baumgartner, K. Kremer and K. Binder, *Faraday Discuss. Chem. Soc.,* 18(1983)398

[61] A. Sadiq and Y. Khwaja, *Z. Phys. B*, 42(1981)163

[62] Y. Khwaja and A. Sadig, *J. Polym. Sci. Polym. Phys.,* 80(1981)499

[63] A. K. Kron, *Polymer Sci. USSR,* 7(1965)1361

[64] A.K. Kron and O. B. Pitsyn, *Polym. Sci. USSR,* 9(1967)847

[65] A.K. Kron, O. B. Pitsyn, A. M. Skvortsov and A. K. Fedorov, *Molec. Biol.,* 1(1967)487

[66] F. T. Wall and F. Mandel, *J. Chem. Phys.,* 63(1975)4592

[67] F. Mandel , *J. Chem. Phys.,* 70(1979)3934

[68] J.R. Banavar and M. Muthukumar, *Chem. Phys. Lett.*, 93(1982)35

[69] M. Muthukumar, *J. Stat. Phys.,* 70(1983)457

[70] A. Baumgartner and D.W. Heermann, *Polymer,* 27(1986)35

[71] M. Lal, *Molec. Phys.,* 17(1969)57

[72] O.F. Olaj and K.H. Pelinka, *Makromol. Chem.,* 177(1976)3413

[73] B. Mac Donald, N. Jan, D.L. Hunter and M.O. Steinitz, *J. Phys. A,* 18(1985)2627

[74] D.L. Hunter, N. Jan, B. Mac Donald, *J. Phys. A*, 19(1986)L 543

[75] N. Madas and A.D. Sokal, *J. Stat. Phys.,* 50(1988)109

[76] Forrest, B.M.; Suger, U.W. *J.Chem. Phys*., 101 (1994) 2816

[77] O. F. Olaj and W. Lantschbauer, *Makromol. Chem. Phys.*, 15 (1982) 847

[78] M.L.Mansfield, *J. Chem. Phys.,* 77(1982)1554

[79] V. Tikare and J.D. Cawley, *Acta Materialia*, 46(4) (1998) 1333.

[80] D.J. Srolovitz, M.P. Anderson, and P.S. Sahni, *Scripta metall.*, 17 (1983) 241,

[81] N. Metropolis, A.W. Rosenbluth, M. N. Rosenbluth, A. N. Teller, and E. Teller, *J. Chem. Phys*., 21 (1953) 1087.

[82] Y. Limoge, and J. L. Bocquet, *Acta mettall.*, 36(7) (1988) 1717.

[83] I. Gutzow , J. Schmelzer, The Vitreous State, Spinger, 1995.

[84] J. Zeng, K. I. Jacob, V. Tikare, *J. Crystal Growth* 262 (2004) 602-611.

[85] R. B. Potts, T*Proc. Camb. Phil. Soc.*, 48 (1952) 106.

[86] I. Carmesin and Kurt Kremmer, *Macromolecules*, 21 (1988) 2819-2823

[87] P.H. Versier, W. H. J. Stockmayer, *J. Chem. Phys.* 36 (1962) 227

[88] M. Dial, K. S. Crabb, C. C. Crabb, J. Kovac, *Macromolecules*, 18 (1985) 2215

[89] J. P. Downey, C. C. Crabb, C.C.; J. Koveac, *Macromolecules,* 19 (1986) 2203

[90] K. Binder and W. Paul, *J. Poly. Sci: Part B: Poly. Phys.*, 35, (1997) 1-31

[91] D. Brown, J. H. R. Clarke, M. Okuda, and T. Yamazaki, *J. Chem. Phys.*, 100 (1994) 1684, 6011

[92] D. Richchter, R. Butera, L.J. Fetters, J.S. Huang, B. Farago, and B. Ewen, *Macromolecules*, 25 (1992) 6156

[93] N. Madras, A. D. Sokal, *J. Stat. Phys*. 47 (1987) 573

[94] P.E. Rouse, *J. chem. Phys*, 21(1953)1272

[95] M. Doi and S.F. Edwards, The Theory of Polymer Dynamics (Clarendoo, Oxford, 1988).

[96] S.F. Edwards, *Proc. Phys. Soc*. 92 (1967) 9

[97] P.G. De Gennes, *J. Chem. Physics*. (1971)572; Scaling Concepts in Polymer physics(Cornell University, Ithaca, NY, 1979).

[98] H. Wittmann, K, Kremer, K. Binder, *J. Chem. Phys*. 96(8) (1992) 6291-6306

[99] G. L. Flynn, S. H. Yahkowsky, and T. J. Roseman, *J. Pharmaceutical Sciences*, vol 63 No. 4 (1974) 479-510

[100] W. I. Higuchi, *J. Pharmaceutical Sciences*, vo 56, no. 3 (1967) 315-324

[101] T. Higuchi, *J. Pharm. Sci*. 50 (1961) 874

[102] D. E. Wurster, and P.W. Taylor, *J. Pharm. Sci*., 54 (1965) 169

[103] J. G. Wagner, *J. Pharm. Sci*., 50 (1961) 359

[104] W. Reine, et al., *Journal of Controlled Release*, 43 (1991) 497-5505

[105] J. Baschnagel and K. Binder, *Marcromol. Theory. Simul*., 5 (1996) 417-448

[106] T. Holzl, C. mesner, M. Wittkop, S. Kreitmeier, S. Kain, D. Gorritz, *Computational and Theoretical Polymer Science*, 9 (1999) 99-109